Green processes for selective oxidation of petroleum and biomass derived components using novel catalysts

Thesis Submitted to AcSIR for the award of the Degree of

Doctor of Philosophy

in

Chemical Sciences

By

Lakshmiprasad Gurrala

AcSIR No. 10CC11A26028

Under the guidance of

Dr. C. V. V. Satyanarayana

CSIR-National Chemical Laboratory, Pune-411008

सीएसआईआर - राष्ट्रीय रासायनिक प्रयोगशाला
(वैज्ञानिक तथा औद्योगिक अनुसंधान परिषद)
डॉ. होमी भाभा मार्ग, पुणे - 411 008. भारत
CSIR - NATIONAL CHEMICAL LABORATORY
(Council of Scientific & Industrial Research)
Dr. Homi Bhabha Road, Pune - 411 008, India

CERTIFICATE

This is to certify that the work incorporated in this Ph.D. thesis entitled "***Green processes for selective oxidation of petroleum and biomass derived components using novel catalysts***" submitted by **Mr. Lakshmiprasad Gurrala** to Academy of Scientific and Innovative Research (AcSIR) in fulfillment of the requirements for the award of the degree of ***Doctor of Philosophy***, in ***Chemical Sciences***, embodies original research work carried out under my supervision. I further certify that this work has not been submitted to any other University or Institution in part or full for the award of any degree or diploma. Research material obtained from other sources has been duly acknowledged in the thesis. Any text, illustration, table etc., used in the thesis from other sources, have been duly cited and acknowledged.

Lakshmiprasad Gurrala
(Student)

Dr. C. V. V. Satyanarayana
(Supervisor)

Communication Channels
NCL Level DID : 2590
NCL Board No. : +91-20-2590 2000
EPABX : +91-20-2589 3300
: +91-20-2589 3400
FAX
Director's Office : +91-20-2590 2601
COA's Office : +91-20-2590 2660
COS&P's Office : +91-20-2590 2664
WEBSITE
www.ncl-india.org

DECLARATION

I, **Lakshmiprasad Gurrala**, hereby declare that this Ph.D. thesis entitled "***Green processes for selective oxidation of petroleum and biomass derived components using novel catalysts***" was carried out by me for the degree of Doctor of Philosophy in Chemical Sciences under the guidance and supervision of Dr. C. V. V. Satyanarayana, CSIR-National Chemical Laboratory, Pune, India.

I confirm that:

- this work was done wholly by me while in candidature for a research degree at this institution.
- no part of this thesis has previously been submitted for a degree or any other qualification at this institution or any other institution.
- the interpretations put forth are based on my reading and understanding of the original articles and all sources have been duly acknowledged.

Place : PUNE

Date : 20th MARCH 2017

Lakshmiprasad Gurrala

Research Scholar

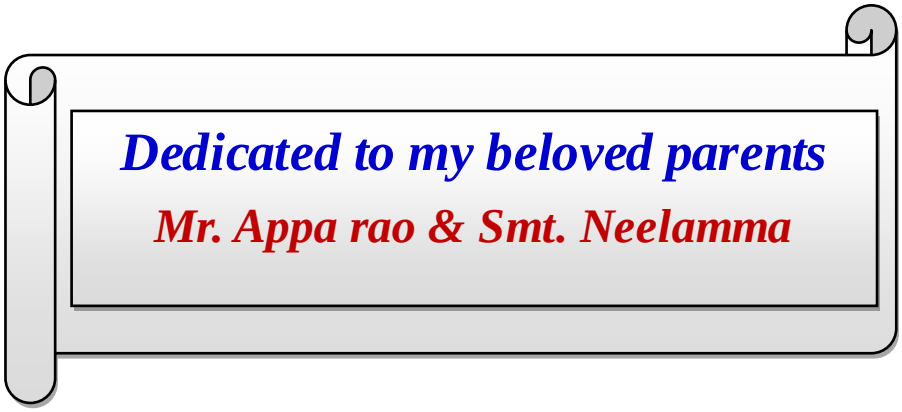

Be the change that you wish to see….. ***-M.K.Gandhi***

Acknowledgements…..

The completion of this thesis is credited to the support and encouragement of numerous people encompassing my family members, friends, colleagues and well wishers. At this point of accomplishment I am privileged to acknowledge all those people who made this thesis possible. It is a pleasant task to reciprocate to the ones who contributed in many ways to the success of this study.

First and foremost, I would like to express my heartfelt and sincere gratitude to my research supervisor **Dr. C. V. V. Satyanarayana** who introduced me to a fascinating realm of chemistry. I am deeply grateful to him for his invaluable guidance and unconditional support. His constant inspiration and constructive criticism helped me enormously to focus my views in proper perspective. His tireless attitude has been an impetus for me throughout the course of study. He gave me the freedom to think and work; and I shall cherish my learning experience under his guidance. I take this opportunity to express my deepest sense of gratitude and respect towards him for guiding me in the right direction throughout the research tenure.

Words fail me when I intend to express my thanks and gratitude to Dr. Gopinath Chinnakonda and Dr. T. Raja for his professional and personal support. I believe the better way of thanking them would be through my future contribution to scientific community.

I extend my sincere thanks to the Director of CSIR-NCL Prof. Ashwini Kumar Nangia, Dr. Sourav Pal (former director) and Dr. D. Srinivas (Chairperson, Catalysis and Inorganic chemistry Division) for providing me the opportunity to accomplish my research work in this prestigious and well-equipped laboratory. My humble thanks to Dr. Sayam S. Gupta, Dr. Paresh L. Dhepe and Dr. N. P. Argade being my DAC members and their constant support and guidance. My heartful thanks are due to Dr. Nandini Devi, Dr. C. P. Vinod, Dr. Umbarkar, Ms. Violet Samuel, Mr. Madhu, Mr. R. K. Jha, Mr. P. Purushothaman and all other scientific and non-scientific staff for their help and support in scientific and technical matters during my tenure as a research student.

My deepest gratitude to my School teachers all who inspired me form the beginning towards the values of education and society, Ms jayashree, Mr. Benjemen, Mr. Kamraj. I would like to remember a person Dr. Nagaraju, the person how inspired for the love of science and looked at my inner potential, without his inspiration I would not be here. I Acknowledge Ms. Aruna who was supported me all the time during my under graduation

college. My teachers at post-graduation college Prof. G. Nageswara Rao, Prof. T. Shiva rao, Prof. A. V. Prasad Rao, Prof. M. S. Prasad Rao, Prof. Ramana, Prof. P. vani and Asst. Prof. Bhasavhai and many more for their inspirational teaching, guidance and blessings.

I extend my sincere thanks to Student Academic Office and catalysis division at CSIR-NCL for their help and support at crucial times. I am grateful to UGC, New Delhi, for awarding the research fellowship and Director, CSIR-National Chemical Laboratory for extending all infrastructural facilities

I have high regard to my seniors Dr. Ganesh Kokate, Dr. Narashima Rao Kanna, Dr. Nishita Lucas, Dr. Reji, Dr. Hanmanth Gurav and Dr. Atul nagpure for their unconditional support and help during my Ph D. Course.

I am indebted to my labmates and colleague Richa, Srikanth, Pranjal, Seema, Dheeran, Vipul, Sivaprasad and my previous labmates Venkatesh, Gajanan, Aditya rao, Lalith, Dr. Mangesh, Dr. Amlan, Jay and Ramana. I sincerely thank all my divisional friends especially Dr. Rajesh, Jijil, Soumya, Leena, Pavan, Dr. Edwin, Devraj (BG), Prabhakar, Dr. Bogesh, Dr. Devadutta, Dr. Unni, Dr. Jobi, Sagar, Ashok, Aswati, Prbhu^2 (K and M), mani, Anish, Vysakh, Sunil, Dr. Shreedala, Anju, yogitha, Prasenjit, Matsagar, Anup, suman, rajendhra and Zinoy for their love and encouragement.

I would like to take this occasion to thank few more friends in and around my P.hD course of time Dr. Swaroop, Dr. Yadagiri, Dr. Sudhakar, Dr. Suneel, Dr. Chandrababu, Dr. Bala, Dr. Manoj, Dr. Rami, Dr. Rambabu, Dr. Chaitanya Kriran, Dr. Venubabu, Dr. Janaki ram, Dr. Nagendra, Dr. Narendra, Dr. Sitaram (Dude), Dr. Chaitanaya krishana, Srinivas (pyridine), Suresh (Bhai), Tarun, Eswar, Satheesh (UoP), Naresh, Dr. Shanthi vardan, Dr. Sathesh Chandra, Dr. Nookaraju, Trinadh, Chaitanya, Innaiah kumar, Hanuman, Kumar Raja (Kura), Naresh (ramudu annaya), Srikanth (Jusi), Swami, Praveen, Pravin shinde, Dr. Wahid, Dr. Manjoor, Ashwani (aunty), Avinash, Vasu, Lenin, Mohan (macha), Subbu, Somen, sarath, Jagadeesh, and all those who are with me and extended their support.

I take this occasion to thank badminton co-players Dr. Sunil, Dr. Vysakh, Kiran (shijju), Zinoy, Dr. rami, Dr. Sudakhar and KuRa darling for those wonder full days to take out the frustration and the all the fun we had whiling playing.

I take this occasion to thank my companions Ashok, Trinadh and Mohan for those unforgettable memories that we had together.

I extend huge thanks to my friends Kumar, Sekhar, Ramesh, Rambo, Rk(Doc), Murali (M^3), Krishna rao, Balu, Uday, Dharma, Hari, Nag (mastaru), Ravi and Santhosh Ch during school, Divya, Mohan (patari), Sagar (darling), Sravan (Nippon), Ramya Sri, Suresh Badi, Sathesh (mayya) and Late. Suresh (Bablu), Amrutha during college, Dr. Ajay, Nagarjuna, gopal (mayya) gowthami, Prasanna, Jagathesh (bava), Kartheek, Kishor (Kis) and Hari (bava) Master's days.

I extend huge thanks few more friends in and around as well as past and present Pooja N, Nivedita, Rajesh, Dr. navneeth, Honey Marry, Vilas, Hari, Mithun, Smitha, Bhagashre, Gauri, Pooja. C and Gopi.

I would like to take this occasion to thank few of my family members who consistently supported me all the time in my up and down of carrier, staring from my father and mother because of their love and moral support I have crossed all the odds that I have faced to reach this stage. The very next I would like to my elder brothers Dhrama and Prem, for their love and care. Kalidas and Simamma I need to specify these names for their love and support. Finally my little brother Praveen (ram), Pradeep (laxman) and my sister Jyothi for their love. Love you all for my life time.

Above all I would like to acknowledge all my family members, teachers, well-wishers, classmates and friends in various stages for their teachings, love, encouragement, kind cooperation and good wishes that I received from them.

Above all, I owe it all to Almighty God for granting the wisdom, health and belief to undertake research work for my thesis and enabling me to its completion.

Lakshmiprasad Gurrala

Table of Contents

List of Figures

List of Schemes

List of Tables

List of Abbreviations

HCN	Hydrogen cyanide
FCC	Fluid catalytic cracking
MC	Mid-Century process
FT	Fischer-Tropsch synthesis
RON	Research octane number
MVK	Mars-Van-Krevelen mechanism
PX	p-Xylene
PTA	Pure terephthalic acid
PET	Polyethylene terephthalate
HMF	5-hydroxy methyl furfural
DMF	Dimethyl furan
TBHP	Tetrabutlyhydroperoxide
OMS	Octahedral molecular sieves
AC	Activated carbon
CNTs	Carbon nanotubes
SWCNTs	single-walled carbon nanotubes
MWCNTs	multi-walled carbon nanotubes
NMC	Nitrogen-doped mesoporous carbon
C_3N_4	Carbon nitrides
g-C_3N_4	Graphitic Carbon nitrides
CNNT	Carbon nitride nano tubes
DP	Deposition-precipitation
XRD	X-ray diffraction
BET	Brunauer-Emmett-Teller
FTIR	Fourier transform infrared spectroscopy
DRIFTs	Diffuse Reflectance Infrared Fourier Transform Spectroscopy
SEM	Scanning electron microscopy
TEM	Transmission electron microscopy

XPS	X-ray photoelectron spectroscopy
ICP-OES	Inductively coupled plasma-optical emission spectrometry
TPD	Temperature programmed desorption
TPR	Temperature programmed reduction
MASNMR	Magic angle spinning Nuclear Magnetic Resonance
DRS UV-Vis	Diffuse Reflectance UV-Vis Spectroscopy
TGA	Thermogravimetric analysis
GC	Gas chromatography
FID	Flame ionization detector
MS	Mass spectrometry
HPLC	High Performance Liquid Chromatography
RID	Refractive index

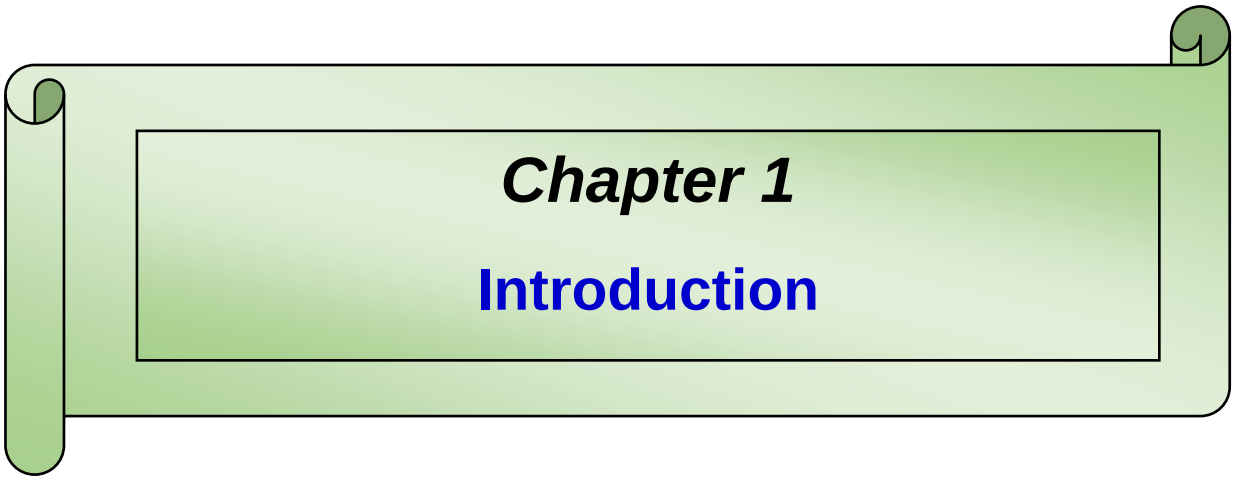
Chapter 1
Introduction

1.1. Introduction

The term 'catalysis' was coined by Swedish chemist J. J. Berzelius for the first time in the first half of the 19th century. He coined the term after the observing a chemical reaction in presence of another material, i.e., catalyst, which does not participate in the reaction.[1-3] When chemical transformation occurs in presence of a catalyst, then the process is called catalytic. Ostwald in 1895 has proposed that *"a catalyst accelerates a chemical reaction without affecting the position of the equilibrium"*.[4] *A catalyst is a substance that decreases the activation energy of a reaction and facilitates the chemical reaction without being consumed in the process"*.[5] The enzymes, which are natural catalysts, are very important for biochemical conversions.

Catalysis plays vital role in everyday life and contributes significantly to the development of society and economy. Catalysis includes processes like, hydrogenation, oxidation, hydrogenolysis, polymerization *etc*. Developing a catalytic process from laboratory scale to industrial scale for manufacturing of various chemicals is of great challenge. Since early 20th century, nitric acid preparation (Ostwald process, 1902),[6] ammonia synthesis (Haber-Bosch process, 1909),[6] methanol synthesis (1923),[6] Fischer-Tropsch synthesis (1925),[6] HCN synthesis,[7] Olefin polymerization (Ziegler Natta polymerization, 1956),[8] desulfurization of petroleum fractions,[9] are some of the important industrial processes. All these catalytic processes contributed to the industrial revolution in 20th century.[4, 10] Thus, the catalytic processes became backbone to the chemical industry contributing significantly to our society. Broadly catalytic processes are involved in three major areas as (i) petroleum refining, (ii) fine chemical preparations and (iii) automotive emission control.

Many catalysts used in these above catalytic processes can be classified into homogeneous and heterogeneous catalytic processes.

1.1.1 Homogeneous catalysis

Homogeneous catalysis can be defined as "a catalytic reaction where the catalyst is in the same phase as the reactants and products". These processes show better selectivity, activity at low temperatures, but are associated with drawbacks like recyclability and solvents that are not environmental friendly.[6]

1.1.2 Heterogeneous catalysis

In a reaction, if the catalyst is in a different phase than that of reactants it is called as a heterogeneous catalyst. Generally, the catalyst is a solid and the reactants can be either gases or

liquids. The catalysis occurs at the interface of two phases typically gas-solid or liquid-solid.[11] Since the catalyst is in different phase than reactant/product, its separation from the final reaction mixture is quite easy. Examples of heterogeneous catalytic systems are cracking, condensation, hydrogenation, dehydrogenation, isomerization, oxidation and alkylation.[10] Hence, development of heterogeneous catalytic processes is important and challenging.[12]

1.2. Sustainable chemical processes and Green chemistry

During industrial revolution, many new catalytic processes were developed. But, little efforts were made towards waste minimization and ensuring sustainability of a process. As a result, plenty of waste was produced by industries, while practicing catalytic processes.[12] This led to environmental damage and also to release of green house gases such NO_x and CO_2 to the atmosphere. This motivated the transition from traditional methods to sustainable processes. Sustainable development is a process for "*Meeting the needs of the present generation without compromising the ability of future generations to meet their own needs"*, provided the natural resources and ecosystem balance out on which the economy and society depend.[13]

Subsequently, with time the concept of sustainability has seen greater attention in development new processes, in which 'Green chemistry' became an integral part. A desired chemical process should eliminate or reduce the hazardous substances. The term 'Green Chemistry' was coined in the early 1990's by Anastas *et al.*,[14] of the U.S. Environmental Protection Agency (EPA). The 12 principles (Fig. 1.1) of green chemistry are given below:

Fig. 1.1 Principles of green chemistry.[14]

The academia and industry have widely recognized and accepted the principles of green chemistry for the sustainable development. Sustainable development can be achieved either by utilization of the renewable or non-renewable resources by using above principles.[12, 14]

1.3. Non-renewable raw materials

A non-renewable material is a natural resource that is utilized faster than it can be re-generated. Fossil fuels (coal, petroleum and natural gas) and nuclear minerals (uranium) are examples of non-renewable materials. Since early 20th century, modern society started using non-renewable sources for several applications. Most important part (84%) of primary energy sources are the carbon based fossil fuels. During 2012, fossil fuel usage for energy production consisted of coal (28%), petroleum (33%), and natural gas (23%).[15]

***Coal*:** It is a combustible black or brownish-black sedimentary rock which contains large quantity of carbon along with some hydrocarbons. The coal is derived from the plants of swampy forests that are buried millions of years ago (Fig. 1.2). The high heat and pressure caused the plants to turned into coal.[16] Coal is categorized into four main types: bituminous, anthracite, lignite and sub-bituminous (Table 1.1).[16] Its energy content depends on the amount of carbon it contains as the heat is generated by its combustion. The type of a coal deposit is determined by its conditions of formation over time.

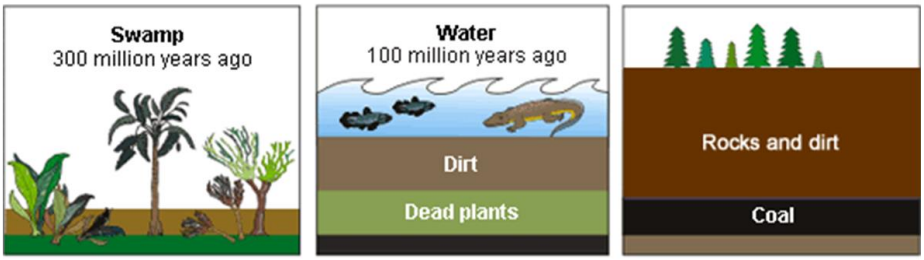

Fig. 1.2 A brief illustration of coal formation.[16]

Table 1.1 Types of coal.[16]

S. No	Type	% of carbon
1	Bituminous	45-86
2	Anthracite	86-97
3	Lignite	25-35
4	Subbituminous	35-45

***Petroleum or Crude oil*:** a mixture of hydrocarbons formed over millions of years ago from animals and plants. The petroleum exists within sedimentary rocks (Fig. 1.3).[17] At an oil refinery crude oil is distilled into various petroleum products. These include gasoline, diesel fuel, jet fuel, heating oil, waxes, lubricating oils, petrochemical feedstocks and asphalt.[17]

***Natural gas*:** It consists mainly of methane, small quantities of liquid hydrocarbons and non-hydrocarbon gases.[18] The remains of animals and plants on decay form thick layers with silt and sand over millions of years. Heat and pressure changed these organic materials into natural gas (Fig. 1.3).

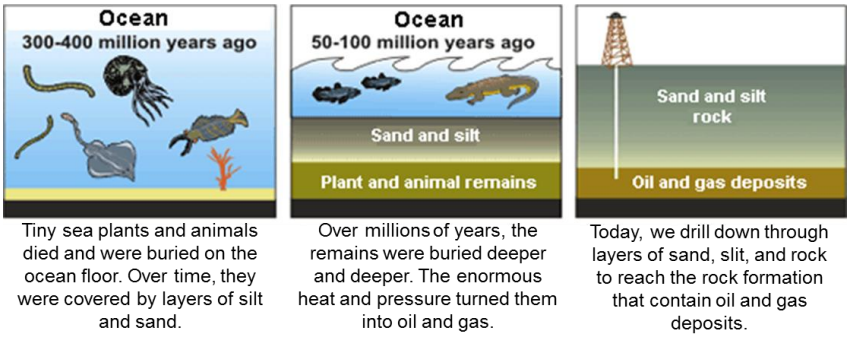

Fig. 1.3 A brief illustration of crude oil and natural gas formation.[18]

***Nuclear power*:** Nuclear energy can be released by nuclear fission and the heat energy generated in the process can be used to produce electricity.[19] Uranium-235 is mostly used for the production of nuclear energy.[19] Nuclear fission is a chain reaction where a neutron hits a uranium atom and splits it to release a large amount of energy as heat and radiation (Fig. 1.4). The neutrons released from the uranium further hit other uranium atoms and the process repeats itself over and over again.[19] These reactions are controlled in nuclear power plant reactors to produce a desired amount of energy which can be converted to electricity.

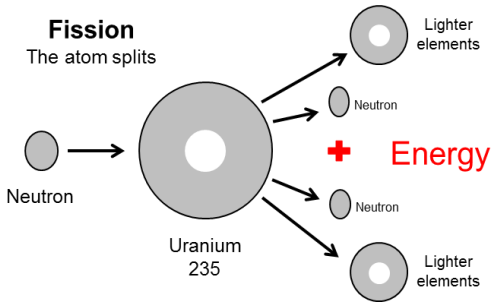

Fig. 1.4 Nuclear fission of uranium.[19]

1.3.1 Petroleum derived chemicals

From the time of invention of combustion engines, transportation has become important. During the 2nd world war there was a huge demand for the transportation fuels and chemicals.[6] Most of them were derived from crude oil. The demand for the petroleum derived chemicals increased through 20th to 21st century. This huge demand for petroleum based chemicals led to the introduction of catalysis or catalytic processes for their production.

Most of the petroleum (84%) is used to get energy-rich fuels, including gasoline, jet fuel, diesel and liquefied petroleum gas (LPG).[15] The remaining 16% of petroleum is used for the production of many chemicals including pharmaceuticals, pesticides, fertilizers and plastics. Present consumption of oil is 84 million barrels (13.4×10^6 m^3) per day, at this rate oil supply will last less than 120 years.[15]

1.3.2. Processes for conversion of petroleum to fuels and chemicals

Fractional distillation is the process for the separation of a mixture of components into its individual components. Chemical components are separated in terms of their boiling range by heating the mixture and by condensation of various vaporized fractions. Generally these components differ by 25 °C in terms of boiling point from each other under atmosphere pressure (Fig. 1.5). If the difference in boiling points is greater than 25 °C a simple distillation is used.

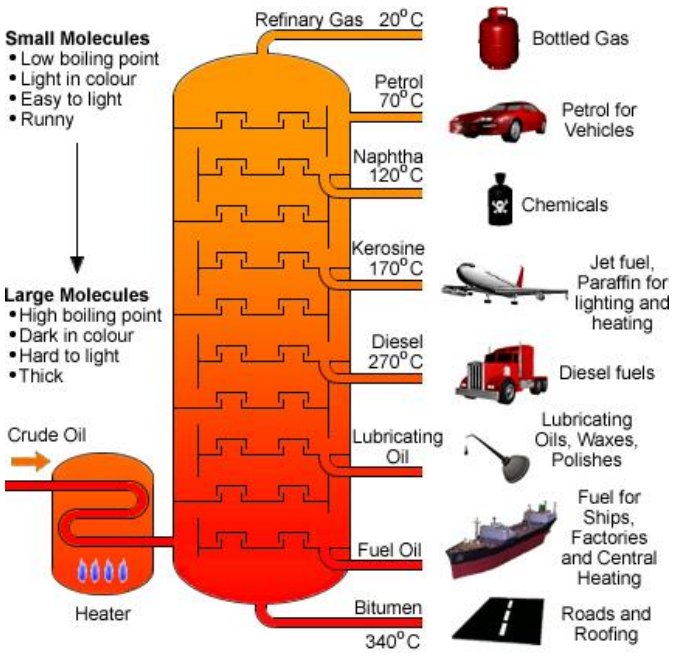

Fig. 1.5 Illustration of crude oil fractional distillation column.[11]

Pictorial representation of fractional distillation is shown in Fig.1.5. Catalysis plays crucial role in the development of efficient processes for upgradation of petroleum feedstock to chemicals and fuels such as gasoline, diesel, fuel oil, jet fuel and lubricants.[6] Most (~60%) of petroleum processes are catalytic.[6, 20] One of these processes is catalytic cracking which has great impact on the economy as it is used to crack heavier crude oils. Fluid catalytic cracking (FCC) process is used to shorten the large and complex molecules to useful fuels.[6]

1.3.2.1 Catalytic cracking

Catalytic cracking is used to downsize heavy petroleum fractions to premium middle distillates. It is one of the most significant technologies developed in 20th century with huge impact on economy. Efficient production of larger fractions of premium fuels with high selectivity and yield was achieved by introducing zeolite as cracking catalyst in the year 1962.[6]

1.3.2.2 Hydrotreating

Catalytic conversions involve the removal of oxygen, nitrogen and organic sulfur from petroleum crudes by hydrogenation of unsaturates at high H_2 pressures involving minor cracking of high molecular hydrocarbons is called as hydrotreating. Hydrotreating capacity has increased since 1970s to get very low sulfur containing fuels to avoid SO_2 emissions to the atmosphere.[6]

1.3.2.3 Hydrocracking

In hydrocracking, polynuclear aromatics are cracked and hydrogenated simultaneously to get low distillates. In hydrocracking, catalyst must be bifunctional, with acid sites to catalyze cracking and metal sites to catalyze hydrogenation. It is necessary to reduce aromatic content in the fuel to increase quality.[21] The production of alkanes from the hydrogenation of the aromatics improves the cetane number which is a measure of the combustion efficiency of diesel fuel.[6]

1.3.2.4. Naphtha reforming

Naphtha with a distillation range of 70-200 °C (C_5-C_{10}), is composed primarily of alkanes and cycloalkanes with small fraction of aromatics. Reforming of naphtha includes conversion of cycloalkanes and normal alkanes to branched alkanes and aromatics to improve octane number.[6]

1.3.2.5. Isomerization

Isomerization of normal alkanes such as butane, pentane and hexane to their branched isomers raises their research octane number (RON). The addition of isomerized components to gasoline results in the increased quality of the fuel.[6]

1.3.2.6. Alkylation

Isobutane is combined with light alkenes, such as propylene, isobutene or butenes from the gas mixture of a catalytic cracker to get high RON fuel components. These high-octane products such as isooctane are used to get high quality gasoline.[6]

1.3.3. Value added chemicals and fuels from petroleum

Petroleum contains C_1-C_{35} hydrocarbons which can be separated and converted through different processes. Some of the important chemicals are benzene, toluene, xylene isomers, toluene and butanes.[22] Catalytic reforming of naphtha results in BTX aromatics (benzene, toluene and the xylene isomers) separated from the catalytic reformates.[6] Schematic illustration of conversion routes of petroleum derivatives is shown in scheme 1.1.[22]

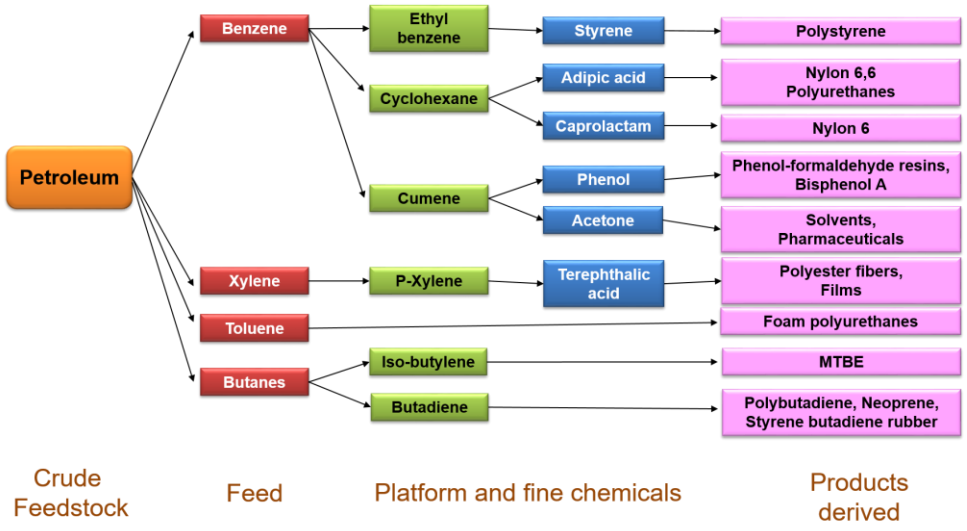

Scheme 1.1 Schematic illustration of conversion routes of petroleum.[22]

1.3.3.1 p-Xylene

p-Xylene is obtained by separation of xylene from C8 cut of reformate. One of the most important application of p-xylene is that it can be converted to pure terephthalic acid (PTA) by selective oxidation. Worldwide production of PTA is approximately 39 million metric tons in 2009, with global demand growing at 7-8%/year during 1999-2009. AMOCO process which is a modified version of Mid-Century (MC) process is widely used for the production of PTA till date. PTA is polymerized with ethylene glycol to from polyethylene terephthalate (PET), a polymer used to make clothing and plastic bottles.

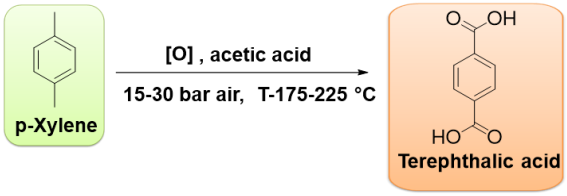

Scheme 1.2 AMOCO process for terephthalic acid production.

1.3.3.2 Benzyl alcohol

Benzyl alcohol is a platform chemical, obtained from toluene, can be used for the synthesis of fine chemicals and used as starting material for the production of many useful products. Benzyl alcohol derivatives include benzyl acetate, benzaldehyde, benzoic acid, benzyl ethers, benzyl benzoate etc., produced through catalytic transformations (Scheme 1.3). A variety of chemicals can be obtained using different chemical transformation like acylation, oxidation, dehydration, dehydrogenation, condensation, hydrogenolysis, hydrogenation, etc. Each and every product obtained from benzyl alcohol has their importance. Among them benzaldehyde is used in many industrial applications. It is an intermediate in the production of fine chemicals, flavors, pharmaceuticals, foods, drinks and cosmetics.

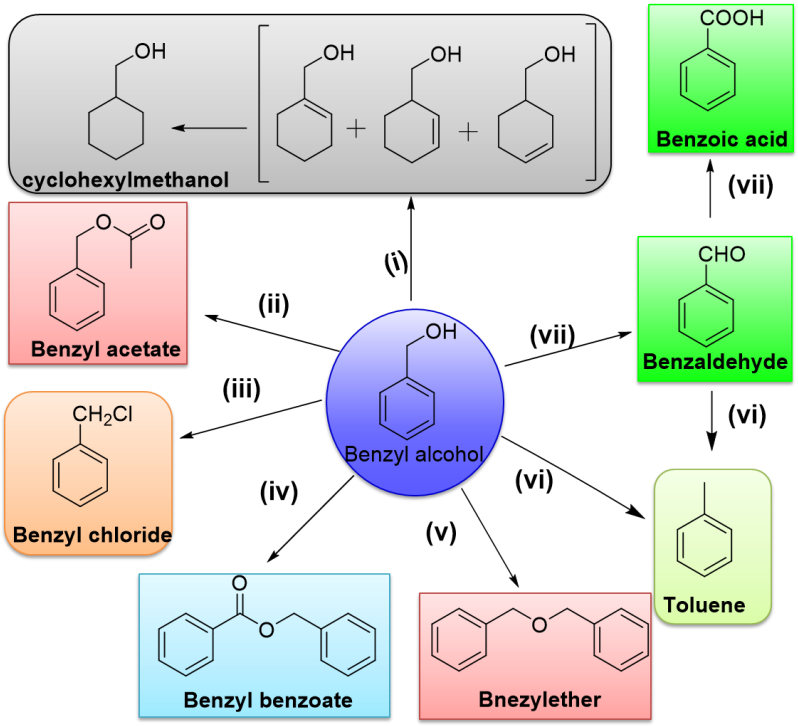

Scheme 1.3 Various products from benzyl alcohol; (i) hydrogenation, (ii) acylation, (iii) chlorination (halogenation), (iv) esterification, (v) etherification, (vi) dehydration and (vii) oxidation.

1.4. Renewable raw materials: Their utility

Biomass is an important source to meet the energy requirements of the society for future generations. Presently, fossil fuels such as petroleum, coal, natural gas and nuclear fuel meets nearly 88% of the world energy demands.[15] However, fossil fuel reserves are limited and there is expected to be 1.1% per annum rise in the use of liquid transportation fuels, 1.0% raise in the consumption of industrial sector, 1.9% per year raise in the natural gas consumption worldwide during 2012 to 2040 (Fig.1.6).[15] Further, the utilization of fossil fuels and their derivatives is associated with a net addition to CO_2 levels in atmosphere. It is predicted that CO_2 emissions will increase from 32.3 to 35.6 and to 43.2 billion metric tons from 2012 to 2020 and by 2040.[15] The rise in CO_2 emissions has a detrimental effect on environment due to global warming and climatic change. These concerns have forced the society to look for alternative sources of energy and chemicals. Renewable sources like, solar, wind, hydropower, biomass and geothermal energies are to be meant for future generations. Hence, it is important to utilize biomass and biofuels as renewable energy sources.

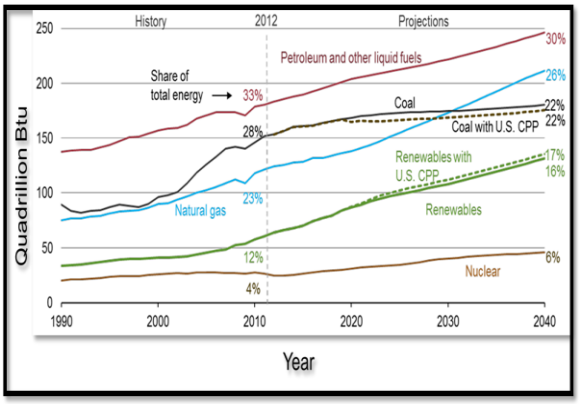

Fig. 1.6 World market for consumption of fuels and energy, 1990-2040.[15]

1.4.1. Biomass valorization

1.4.1.1. Introduction

Effective utilization of renewable resources using advanced technologies is the need of the hour to meet the needs of future generations. Renewable resources include hydropower, wind, solar and biomass etc. Among the renewable resources, biomass is superior as it is the only source that possesses the energy in the form of chemical bonds. The biomass feedstock's can be used for the production of numerous chemicals and fuels.

"*The term biomass refers to non-fossilized and biodegradable organic materials obtained from plants and animals on a renewable basis, that includes waste and residues of wood, agri-cultural crop, aquatic animals and plants, municipal and other waste materials"* (Fig. 1.7).[23] Thus, the availability of biomass is widespread, abundant and also economical.[24] These excellent features make biomass a better and sustainable source for future requirement of chemicals and energy. Biomass is categorized in two categories; (1) edible and (2) non-edible biomass. Edible biomass comprises of cooking oils while non-edible biomass includes agriculture waste etc.

Fig. 1.7 Different sources of biomass.[25]

Among the above, lignocellulosic biomass is of our interest for the production of carbon feed stocks like chemicals and fuels. Lignocellulosic biomass is derived mainly from forestry, agricultural waste and residue. The CO_2 released during the upgradation of renewable com-pounds is utilized for the photosynthesis process to generate biomass (Fig. 1.8).[26] A successful bio-refinery plays an important role in achieving sustainable development goals.

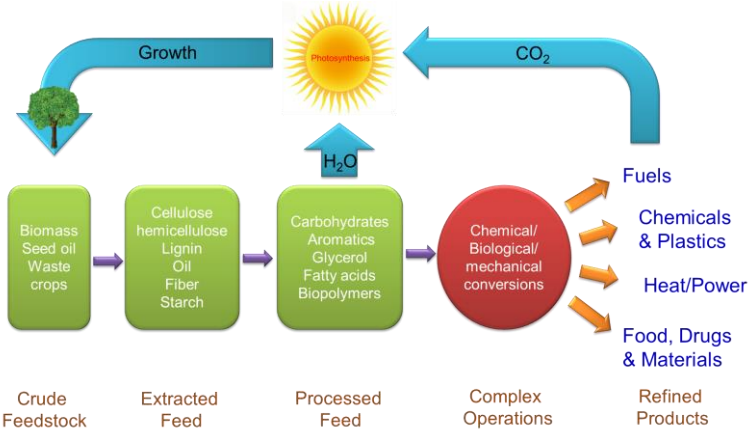

Fig. 1.8 Overview of the processing of crude feedstocks to refined products in a sustainable biorefinery.[26]

1.4.1.2. Composition of lignocellulosic biomass

Lignocellulosic biomass is one of the major promising renewable sources of carbon derived from plants. The conversion of plant lignocellulosic biomass to variety of fine chemicals and fuels in a sustainable way is a great chalange.[26-30] Lignocellulosic biomasses consists of three different fractions: cellulose, hemicellulose and lignin (Fig. 1.9).

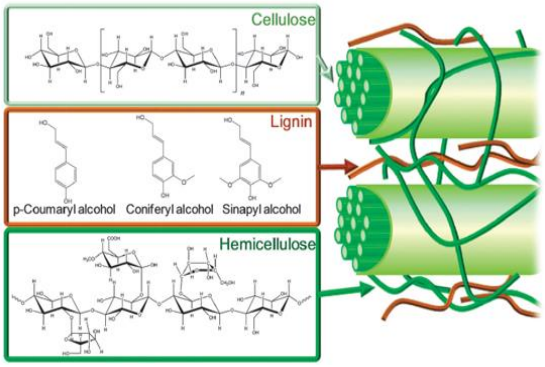

Fig. 1.9 Composition of lignocellulosic biomass.[28]

1.4.1.2.1. Lignin

Major component of lignocellulosic biomass is lignin, which constitutes of 15–30% by weight. It is rich in aromatic functional moieties and contain primarily three monomers (Fig. 1.9).[28] Methoxylated phenylpropane structures such as coniferyl alcohol, sinapyl alcohol and coumaryl alcohol are the building blocks of lignin and it is amorphous in nature.[29] Hemicellulose and cellulose are surrounded by lignin within the plant tissue. The depolymerization of lignin in alkaline-alcohol solutions to isolate the carbohydrate results in alkali lignin (Kraft paper pulping process).[29] Being rich in oxygenated aromatic species, lignin is an ideal feedstock for the production of oxygenated aromatics.

1.4.1.2.2. Cellulose

Cellulose is a polymer of glucose units consists of 30–40% of its weight[28] and it is of β-D-glucopyranose homopolymer linked via β-glycosidic bonds (Fig. 1.9).[28] The degree of polymerization of cellulose varies from source to source; it is approximately 10,000 to 15,000 glucopyranose monomer units for wood and cotton respectively.[31] Glucose monomers are obtained by simple depolymerization of celluloses. Hydrolysis of cellulose from biomass is of great challenge. Partial acid hydrolysis of cellulose gives cellobiose (glucose dimer), cellotriose (glucose trimer) and cello-tetrose (glucose tetramer), while total acid hydrolysis breaks it into glu-

cose.[32] High yields of glucose (>90%) can be achieved through enzymatic hydrolysis of cellulose following biomass pretreatment.

1.4.1.2.3. Hemicellulose

Hemicellulose is an amorphous polymer, constitutes of 15–30% of lignocellulosic biomass, it contains low degree of polymerization and is a branched polymer (branching at every 200 molecules) (Fig. 1.9).[28] Additionally, the structural constituents of the hemicellulose differ from source to source and may consist of pentoses, hexoses and uronic acids.[28] The pentose sugars are xylose and arabinose and hexose sugars are glucose, galactose, mannose, rhamnose, and fucose.[28, 29] Hemicellulose is intercalated to lignin and cellulose strands (Fig. 1.9). Hemicellulose extraction can be achieved through either physical or chemical methods. In general, physical methods, such as steam explosion, hydrolysis under mild conditions using dilute acids produce xylose monomers.[29]

1.4.2. Processes for conversion of biomass to value added chemicals and fuels

1.4.2.1. From ligninocellulosic biomass

Ligninocellulosic biomass can be converted to useful energy and chemicals involving various steps. First step is partial removal of oxygen to reduce the feedstock reactivity. In a second step, it is upgraded to useful chemicals or fuels.[29] The technologies for the transformation of lignocellulosic biomass to generate fuels and chemicals still remain a challenge. Main reason is the structural and chemical complexity of biomass. The lignocellulosic biomass can be directly used for generation of energy and fuels by gasification, pyrolysis/liquefaction and hydrolysis.[29]

1.4.2.1.1. Gasification

Biomass can be treated at high temperatures (>800 °C) to produce synthesis gas (syngas) by gasification. The syngas can be further converted into chemicals and liquid fuels such as methanol, diesel and gasoline by Fischer-Tropsch (FT) synthesis (Scheme 1.4).[29]

1.4.2.1.2. Pyrolysis/Liquefaction

Low-cost liquid fuel can be obtained by pyrolysis/liquefaction of biomass (Scheme 1.4). In this method, biomass is heated in an inert atmosphere at lower temperatures (300-700 °C) to give bio-oil, a dark organic liquid.[33] But this bio-oil consists of a mixture of more than 300 chemicals like aldehydes, ketones, acids, alcohols, esters, sugars and aromatics, which are difficult to separate.[28] Bio-oil contains highly oxygenated products and high content of water (up to

50%) and hence it is considered as poor fuel.[28] High quality of the fuel can be achieved by deoxygenation-hydrogenation in presence of H_2[34] or its conversion to aromatic compounds using zeolite based catalysts.[35]

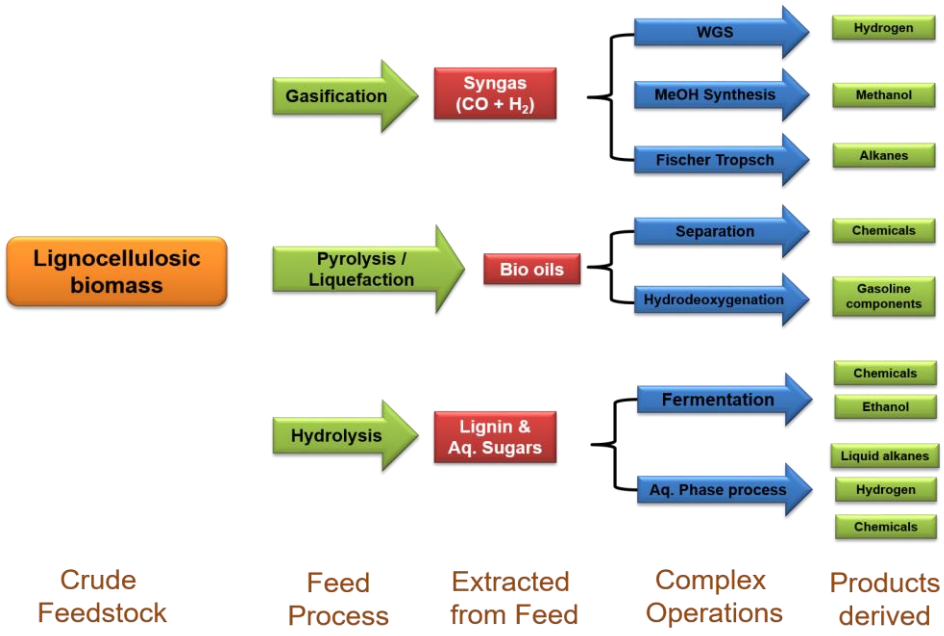

Scheme 1.4 Schematic illustration of conversion routes of lignocellulosic biomass to chemicals and fuels.

1.4.2.1.3. Hydrolysis

Hydrolysis methodology is more beneficial than gasification and pyrolysis. Isolation of sugar monomers to monomers is possible by selective transformations by complex processes from lignocellulosic feedstocks.[29] Isolated sugar monomers can be converted by a variety of catalytic technologies. These sugars can be further upgraded to fine chemicals and fuels *via* various chemical transformations[26, 30] like fermentation and aq. phase reforming (Scheme 1.4).[29]

1.4.2.2. From lignin

Lignin can be used for the production of fuels and chemicals. The treatment of isolated lignin by different methods results in the formation of oxygenated aromatic monomers.[29] Pyrolysis is a method in which a thermal treatment of lignin in the absence of oxygen is carried out, but the amount of product depends on temperature and heating rate. Hydrogenolysis or hydrocracking involves thermal treatment in the presence of hydrogen. In this process cleavage of bonds is assisted by the addition of hydrogen.[29] Hydrogenolysis occurs at low temperatures; hence higher yields of monomeric phenols can be achieved. Hydrolysis is the process in which polymer breaks down to monomeric units by addition of water. Oxidation is the thermal treatment in presence of

O_2, which generally gives aldehydes.[29] Oxidation of lignin gives wide range of products like vanillin, vanillic acid and other carboxylic acids. The chemicals obtained from all these processes and their utilization are represented in Scheme 1.5.

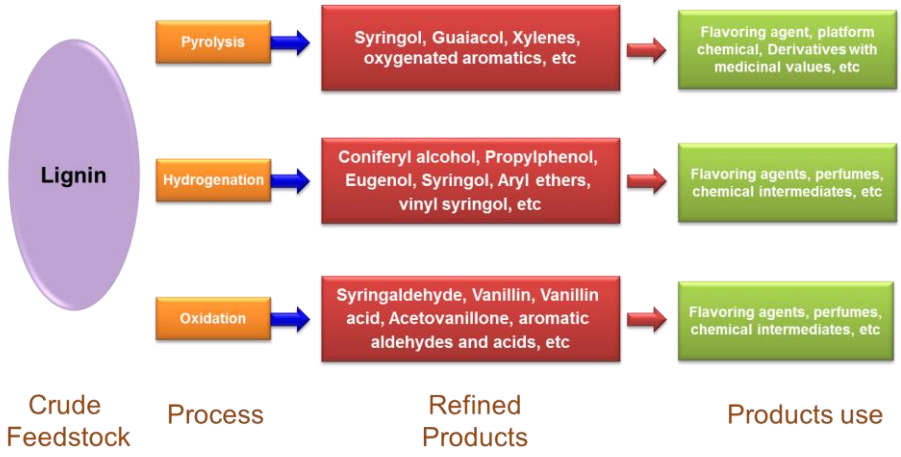

Scheme 1.5 Schematic illustration of **v**alue added chemicals and fuels from lignin.[22]

1.4.2.3. From cellulose and hemicellulose

Cellulose and hemicellulose are highly branched polymers made up of many C_5 and C_6 sugar monomers, which can be used for the production of chemical intermediates and platform chemicals. The cellulose and hemicellulose can be converted into monomers through catalytic processes like, hydrogenolysis, hydrolysis, oxidation and de-polymerization.[29]

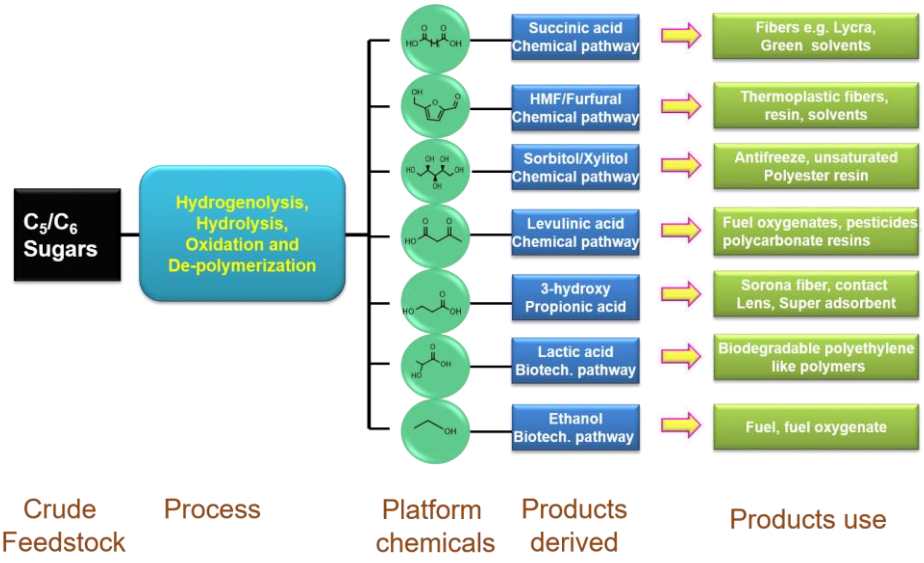

Scheme 1.6 Schematic illustration of value added chemicals and fuels from C5/C6 sugars.[22]

These processes yield a wide variety of platform chemicals like, HMF, furfural, sorbitol, xylitol, levulinic acid and lactic acid etc.[26] These chemicals have applications like production of thermoplastic fibers, resins, solvents, fuel oxygenates, pesticides, solvents, polycarbonate resins and many more.[22] All the processes, the chemicals obtained and their utilization are represented in Scheme 1.6.

1.4.3. Value added chemicals from biomass

Glucose ($C_6H_{12}O_6$) is a hexose monomer of the cellulose and hemicellulose (Scheme 1.7). Glucose has many applications such as in fermentation and pharmaceutical industries as direct and indirect source.[22, 29] It is one of the raw material used in the generation of high value platform bio-based chemicals such as 2,5 furan dicarboxylic acid, glucaric acid and sorbitol identified by U.S. Department of for their high importance.[22] Glucose is produced by simple hydrolysis of cellulose or oligomers of glucose (cellobiose and maltose etc.).

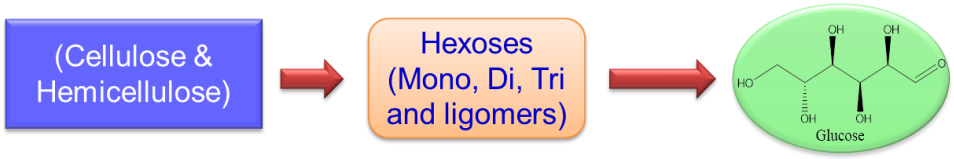

Scheme 1.7 Formation of glucose from biomass-derived compounds.

1.4.3.1. Glucose as platform chemical

Glucose can be converted to many useful chemicals by different chemical transformations. According to Werpy and Peterson, glucose derivatives include gluconic acid, glucaric acid, sorbitol, adipic acid, fructose and 5-hydroxymethy furfural, etc. These are produced through catalytic transformations (Scheme 1.8).[26] These can be obtained using different chemical transformation like oxidation, dehydration, reforming, reduction, fermentation (biochemical paths) etc.[26] Oxidation of glucose gives gluconic acid, which is further oxidized to glucaric acid which in turn can be selectively hydrogenated to adipic acid. Adipic acid is a monomer for the synthesis of nylon 66 etc.[22] Selective hydrogenation of glucose gives sorbitol and on dehydration it forms isosorbide at low operating cost. The isosorbide is used as a monomer for the polymer synthesis. The major applications of it are copolymer with PET like polymers such as polyethylene isosorbide terephthalates for the use in bottle production.[22] Dehydration of glucose to HMF followed by its hydrogenation yields dimethyl furan (DMF), a transport fuel with good fuel characteristics.[29]

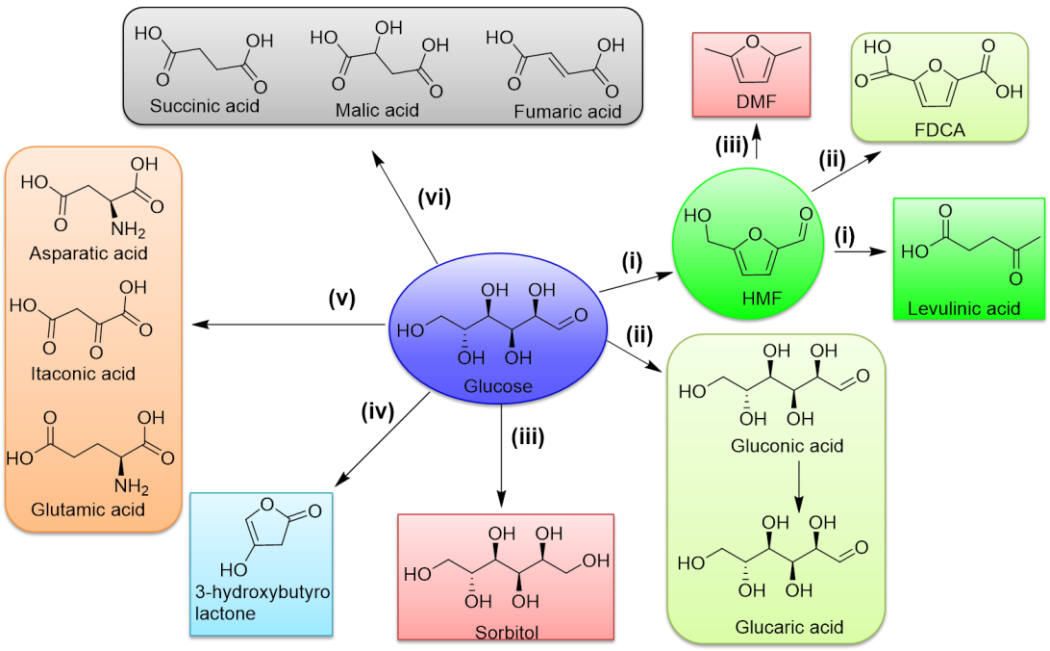

Scheme 1.8 Synthetic routes from glucose to various chemicals through (i) dehydration, (ii) oxidation, (iii) hydrogenation, (iv) fermentation & oxidation, (v) fermentation (vi) fermentation & Krebs Pathway.[31]

1.5. Selective catalytic oxidations in chemical manufacture

Catalytic oxidation reactions are among the oldest and commercially important. More than half of the commercial chemical production involves oxidation step as part of their synthesis. Most monomers used to produce fibers, plastics and other polymer products are produced via selective oxidation of hydrocarbons. Some topics of catalytic selective organic oxidations are included in the *handbook of Heterogeneous Catalysis*.[11] Some industrial important oxidation processes are also listed in Table 1.2.

Table 1.2 Some industrially important oxidation processes.[11]

Entry	Name of processes	Reactant	Product	Catalyst
1	Sulfuric acid production	SO_2	SO_3	V/K sulfate on silica
2	Nitric acid production	NH_3	HNO_3	90%Pt & 10% Rh
3	HCN production	NH_3	HCN	90%Pt & 10% Rh
4	Formaldehyde	CH_3OH	HCHO	Fe-Mo oxide
5	Ethylene oxide	Ethylene	Ethylene oxide	Ag catalyst
6	Ammoxidation	Propylene	Acrylonitrile	Bi-Mo catalyst
7	Ammoxidation	propane	Acrylonitrile	V or Mo catalyst
8	Selective oxidation	n-butane	Maleic anhydride	V-Phosphate

1.6. Selectivity in catalytic oxidation

Selectivity is an important aspect in catalytic oxidation. It is defined as the ratio of the desired amount of product formed to the sum of the total products obtained in a particular reaction. Generally oxidation reactions are classified into three categories, viz., (i) Regioselective, (ii) Chemoselective and (iii) Stereoselective.

Regioselectivity refers to the oxidation of one functional group in the presence of the same functional group present at a different location in an organic molecule (Scheme 1.9).

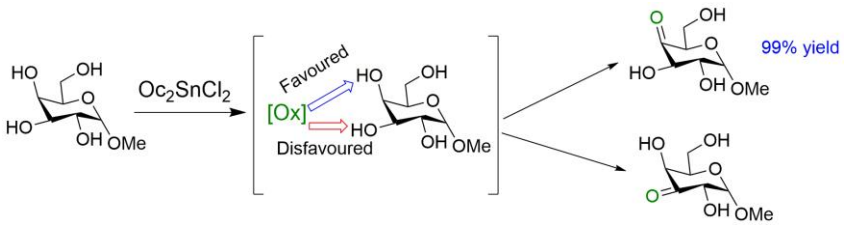

Scheme 1.9 Regioselective oxidation of carbohydrates.[36]

Chemoselectivity of the oxidizable functionalities has been key issue in the field of heterogeneous catalysis. It is important when one functional group has to be selectively oxidized in a molecule which contains more than one functional group (Scheme 1.10).

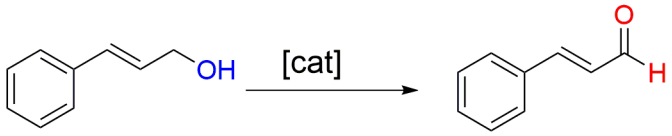

Scheme 1.10 Chemoselective oxidation of alcohol to carbonyl compounds.[37]

Stereoselectivity is related to the formation of one stereoisomer selectively. If the stereoisomers are enantiomers then such transformation is known as enantioselective oxidation (Scheme 1.11).

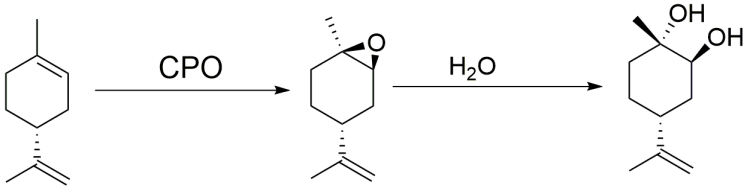

Scheme 1.11 Stereoselective oxidation of *R*-(+)-limonene in the absence of KCl.[38]

1.7 Oxidants used in chemical transformations

In case of an oxidation, there should be an oxygen donor for the reaction to proceed. Oxygen donors are classified as organic and inorganic oxygen donor sources. Organic oxygen do-

nors are compounds like tetrabutlyhydroperoxide (TBHP). Some of the inorganic oxygen donors are H_2SO_4, HNO_3, ClO_4^- (perchlorate), MnO_4^- (permanganate), H_2O_2, O_3, O_2, etc. Some inorganic oxidants have been used in industrial processes. However, use of H_2SO_4 and HNO_3 is environmentally harmful. Uses of environment friendly (green) oxidants that generate minimum amount of waste have been given more importance in the catalytic applications. The extent of harmfulness depends on the by-products released from the oxidant. Table 1.3 lists the most commonly used oxidants with amount of oxygen and by-products they generate.

Table 1.3 Common oxidants used.

S.No	Oxidant	% of active oxygen	By-product
1	Oxygen	100	Nil
2	Hydrogen peroxide	47	H_2O
3	Ozone	33.3	O_2
4	N_2O	36.4	N_2
5	Perchlorate (ClO_4^-)	21.6	Cl^-
6	$(CH_3)_3COOH$ (TBHP)	17.8	$(CH_3)_3COH$
7	H_2SO_4	16.3	HSO_3
8	HNO_3	25.3	NO_2
9	C_6H_5IO (PhIO)	7.3	C_6H_5I

From a sustainability point of view, an oxidative process should address the following criteria, (i) providing highest percentage of active oxygen, leading to greater atom economy;[39] (ii) avoid formation of toxic and difficult to eliminate by-products; (iii) should be abundantly available at low cost. O_2 is the most environmental friendly due to its 100% atom economy. It can preferably be used in industrial applications to reduce waste. Many processes employ H_2O_2, as water is the by-product, but the production cost of H_2O_2 is very high compared to O_2.

Reactive oxygen species that are observed in commonly used oxygen and hydrogen peroxide (Figure 1.10) are (i) superoxide radical, (ii) peroxide anion, (iii) hydroxyl radical and (iv) hydroxyl anion. Superoxide ($O_2^{\bullet -}$) is obtained by addition of electron to molecular oxygen (O_2), resulting in one unpaired electron over the molecule, making it highly reactive. When superoxide accepts one more electron, it is reduced to peroxide (O_2^{2-}). Hydrogen peroxide generates hydroxyl ion (OH^-) by accepting an electron. Thus hydroxyl radicals ($OH^{\bullet}$) are formed by homolytic cleavage of hydrogen peroxide.

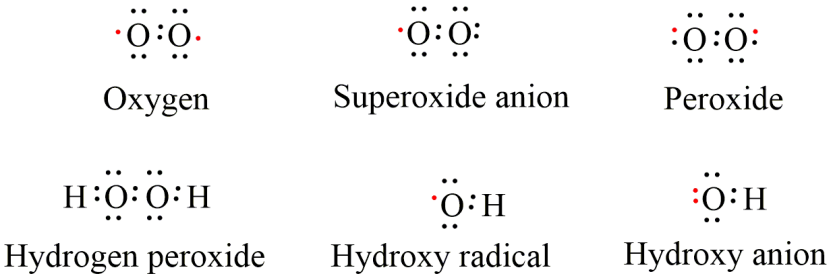

Fig 1.10 Active oxygen species

1.8. Introduction to porous materials

Materials containing pores are called as porous materials. The skeletal portion of the material is often called the "matrix" or "frame". A skeletal material is usually a solid, but structures like foams are referred to as porous. The properties like electrical conductivity, tensile strength and permeability can be obtained from the respective properties of its constituents. Porous materials can be classified in to three types, based on their pore size (average diameter of pore). They are (a) microporous, (b) mesoporous and (c) macroporous.

a) Microporous: Materials that contain average pore size <2 nm.

b) Mesoporous: Materials that contain pores in the range of 2-50 nm.

c) Macroporous: Materials that contain pores in the range of >50 nm.

Mesoporous materials have a high impact with pore size in the range of 2-50 nm, as kinetic radii of most organic molecules fall in that range facilitating their catalytic transformations. In catalytic processes, catalysts having properties like adsorption-desorption and diffusion corresponding to the reactant molecule play a key role. The catalysts with suitable morphology having these properties show better activity.

1.8.1. Porous Mn oxides materials

Mixed valent manganese oxides having a general formula A_xMnO_2 are categorized as microporous tunnel structures. The building block of this tunnel structure is MnO_6 octahedra. The sharing of octahedral corners or edges results in chains which are cross-linked to build one-dimensional (1D) tunnels. To maintain charge balance and to support the framework, some cations reside in these pores. Porous manganese oxide structures can be described as a components of B and P building blocks: B (birnessite, $(Na_{0.3}Ca_{0.1}K_{0.1})(Mn^{4+},Mn^{3+})_2O_4$ 1.5 H_2O), and P (pyrolusite, MnO_2), where B the edge-sharing and P represents corner-sharing mode of the octahedral

building blocks.[40] The size and shape of tunnels is differentiated as ramsdellite (2 × 1), hollandite (2 × 2), romanechite (2 × 3), todorokite (3 × 3) and synthetic $Rb_{27}MnO_2$ (2 × 5). RUB-7 (2 × 4).[41, 42] Cations and water molecules present in the tunnels stabilize the tunnel structure, which results in pore size distributions.[41]

Fig. 1.11 Tunnel sizes of various OMS materials (Mn porous materials).

1.8.2. Porosity

From the studies of size and shape of the tunnels, broad pore size distributions are observed in OMS materials, as shown in Figure 1.11. For example, OMS-1 has tunnel size of ~6.9 Å, with diagonal distance of the tunnel being ~9.6 Å, while OMS-2 has tunnel size of ~4.6 Å.[43]

1.8.3. Todorokite

Todorokite (OMS-1) is one of the main Mn minerals deposited in ocean Mn nodules. Todorokite occurs with plate type or fibrous morphologies, that support a tunnel or layer-type structure and it is extracted as major mineral from many terrestrial Mn deposits.[44] For many years the crystal structure of todorokite was a subject of considerable conjecture and controversy. The tunnel structure of todorokite was confirmed by high resolution TEM images, which illustrate that tunnels are constructed of triple chains of MnO_6 octahedra. These synthetic materials are octahedral molecular sieves (OMS) consisting of manganese oxide octahedra linked by edges and vertices. A synthetic todorokite has molecular formula of $Mg^{2+}_{0.98\text{-}1.35}\,Mn^{2+}_{1.89\text{-}1.94}\,Mn^{4+}_{4.38\text{-}4.54}\,O_{12}\cdot 4.47\text{-}4.55\,H_2O$ with a 3 X 3 manganese octahedral unit of pore diameter 6.9 Å.[43]

1.8.4. Hollandite

The hollandite structure is constructed of double chains of edge-sharing MnO_6 octahedra, which are linked in such a way as to form tunnels with square cross sections, measuring two octahedra on a side (Fig. 1.11.). The tunnels are partially filled with large uni- or di-valent cations and in some cases, water molecules. The charges on the tunnel cations are balanced by substitution of lower valence cations [e.g., Mn (III), Fe (III), Al (III), etc.] for some of the Mn (IV). Hollandite minerals can be major phases in the oxidized zones of Mn deposits and important ores.

The different minerals in the hollandite group are defined on the basis of the predominant tunnel cation: hollandite (Ba), cryptomelane or OMS-2 (K), coronadite (Pb), and manjiroite (Na). Natural specimens having end-member compositions are unusual and chemical analyses show a wide range of tunnel cation compositions. Consistent with their chain structure, they typically are found as fibrous crystals, usually in compact botroyoidal masses. Cryptomelane has a tunnel size of 4.6 X 4.6 Å.[43]

Mixed valency of OMS type manganese makes it a semiconductor and a good oxidation catalyst. The average manganese oxidation state is reported in the range of 3.4 to 3.9 due to the presence of a mixture of Mn^{4+}, Mn^{3+} and Mn^{2+} ions. The water and cation positions in the tunnels of todorokite were predicted by Rietveld method using powder X-ray diffraction data.[45] Low valence cations Ni (II), Mn (III), and Mg (II) substitute for Mn (IV) charges in the tunnel cations.[46] OMS have been used as supports as well as a catalyst for many transformations.[47] The presence of Mg^{2+} in the tunnel imparts basicity to the material and framework substitution of OMS is of great interest.[48]

1.9. Carbon materials, nitrogen-doped carbon and carbon nitride

If we look at our surroundings, it is realized that a greater part of the material is based on carbon. Amorphous carbon, tetrahedral carbon, diamond-like carbon, fullerenes, CNx, graphene, carbon nanotubes; the list of new or different structures based on carbon is growing each year due to the extensive research and discovery of new carbon based materials

1.9.1. Different structures of carbon materials

Carbon is one of the most abundant elements in nature. There are several allotropes of carbon depending on hybridization and bonding. Some allotropes of carbon like diamond and graphite occur naturally and are known from ancient times. Carbon nanomaterials and its allotropes provide a wide range of useful properties pertaining to high tensile strength, high BET surface area, chemical and thermal stability making them very fascinating materials to a broad range of applications. Graphite and amorphous carbon are the two most common allotropes.

1.9.1.1. Amorphous carbon

Amorphous carbon does not have any crystalline structure (Fig. 1.12a).[49] This carbon is highly disordered with no structural integrity. The disorder permits it to have many available bonds and because of that more complex carbon based structures can be constructed. The true

amorphous carbon has localized π electrons and bonds formed in it are inconsistent in lengths compared to any other allotrope of carbon.[49]

1.9.1.2. Graphite

Graphite is a crystalline form of carbon and is most stable in standard conditions. Carbon with sp^2 hybridization forms graphite (arranged in hexagonal sheets). Carbon atoms are arranged in a honeycomb lattice in each layer with carbon-carbon sp^2 bond length of 0.142 nm and the spacing between these carbon layers is 0.335 nm (Fig. 1.12b).[50] The layers are bonded through weak Van der Waals forces, allowing layers of graphite to be easily separated or to slide past each other. There are two forms of graphite namely alpha and beta.[51] The alpha form of graphite possess hexagonal lattice with ABAB stacking sequence of the layers whereas beta form has rhombohedral lattice with ABCABC stacking sequence of the layers. The beta form is unstable and converts into alpha when heated above 1300 °C.

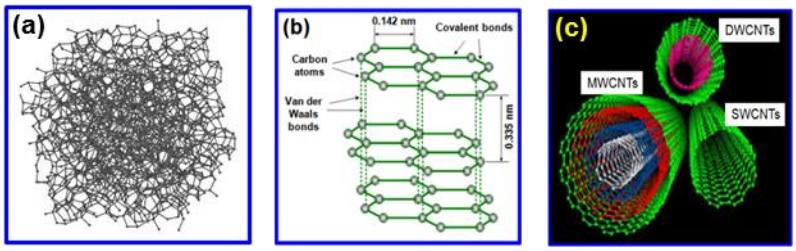

Fig. 1.12 Structure of (a) amorphous carbon, (b) graphite and (c) carbon nanotubes.

1.9.1.3. Activated carbon

Activated carbon is a crude form of graphite which is different from graphite by containing an imperfect random structure and with high porosity and broad range of pore sizes.[52] Hence, it has large surface area, often more than 1000 m^2/g, thus having strong physical adsorption forces. Chemical treatment can amplify the adsorption properties. Activated carbon is a carbon synthesized from carbonaceous materials like wood, peat, nutshells, coconut husk, coir, coal and petroleum pitch. It can be produced *via* physical (steam) activation or chemical activation.

1.9.1.4. Carbon nanotubes

Carbon nanotubes (CNTs) are the members of carbon family, CNTs can be formed by one-atom-thick sheets of carbon, called graphene, which rolled up into a cylinder (Fig. 1.12c).[53] Carbon with sp^2 hybridization will form carbon nanotubes (long hollow tubes of carbon). These graphene sheets are wrapped at specific and distinct angles. CNTs can be categorized into two

types: single-walled carbon nanotubes (SWCNTs) and multi-walled carbon nanotubes (MWCNTs).

1.9.2. Nitrogen-doped carbons

In carbon materials, it is the long- and short-range coordination and sequencing of carbon atoms that decide the electrical properties and their potential for different chemical processes.[54] Graphitic carbon materials have been extensively employed as catalyst supports for anchoring metal nanoparticles in various industrial applications. However, metal nanoparticles supported on carbon materials easily leach out during catalytic processes because of weak interaction between metal nanoparticle and carbon surface. Doping carbon with hetero atoms, like phosphorus and nitrogen as electron donors or boron as an electron acceptor, into carbon matrix strengthens the interaction between the carbon surface and the metal nanoparticles (Fig. 1.13).[55] The most common dopant in carbon materials is nitrogen, which transforms the material significantly to more stable form. Additionally, N-doping improves the carbon-metal nanoparticles binding interaction and also amplifies the number of chemically active sites. This can be witnessed by increased metal dispersion, much better resistance to metal sintering and coarsening and enhanced catalytic performance.[56] Therefore, N-doped carbon materials are considered as good supports to stabilize and activate metal nanoparticles.

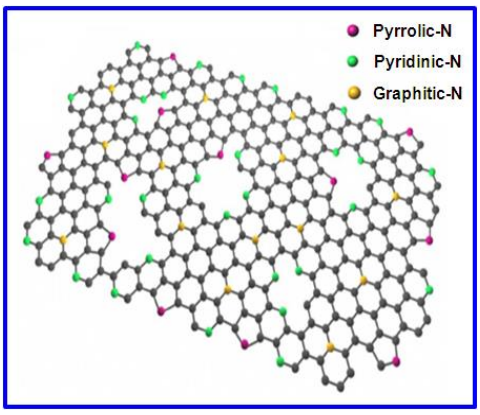

Fig. 1.13 Schematic view of the N-doped carbon showing different types of N atoms.

1.9.3. Carbon nitride

Carbon nitrides are compounds of carbon and nitrogen as the backbone forming elements. The binary carbon nitride with the formula C_3N_4 is still an elusive monomer compound. Carbon nitride exists in five different crystalline structures, which were described by Teter and

Hemely as shown in Figure 1.14. All the carbon nitrides are derived from either triazine or heptazine (tri-s-triazine) units. These exhibit different degrees of condensation, physical and chemical properties. The detailed structures of these materials have been examined and the mechanical, electrical and optical properties were studies. Hardness value of carbon nitride (CN*x*) is in 10-40 GPa range based.[57-59]

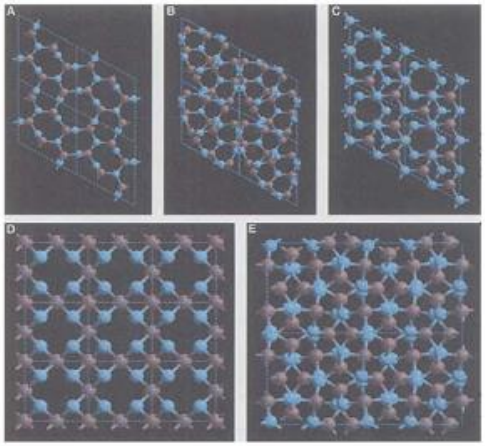

Fig. 1.14 Different types of C_3N_4 (A) β-C_3N_4, (B) α- C_3N_4, (C) graphitic-C_3N_4 (D) pseudo cubic-C_3N_4 and (E) cubic-C_3N_4, viewed down the [001] axis. The carbon and nitrogen are depicted as gray and blue spheres.

The synthesis and characterization of g-C_3N_4 is a challenging task and different experimental attempts have been made to synthesis g-C_3N_4. The possible building block, tri-s-triazine (heptazine) ring is structurally related to the hypothetical polymer melon.[60-64] Recent studies show the triazine-based monomer formation of g-C_3N_4 is energetically favoured,[65] trigonal nitrogen atoms results in tri-s-triazine rings. However triazine building blocks further condense to form allotrope g-C_3N_4. Recent work has shown that the pyrolysis of melamine dicynamide, and cynamide yields a melon polymer built up to from melem units.[66] The energy diagram for the synthesis of carbon nitrides from cyanamide as starting precursor is outlined in Fig. 1.15.[67]

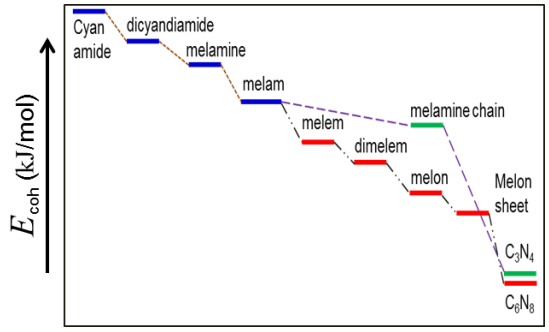

Fig. 1.15 Calculated energy diagram for the synthesis of C_3N_4.[67]

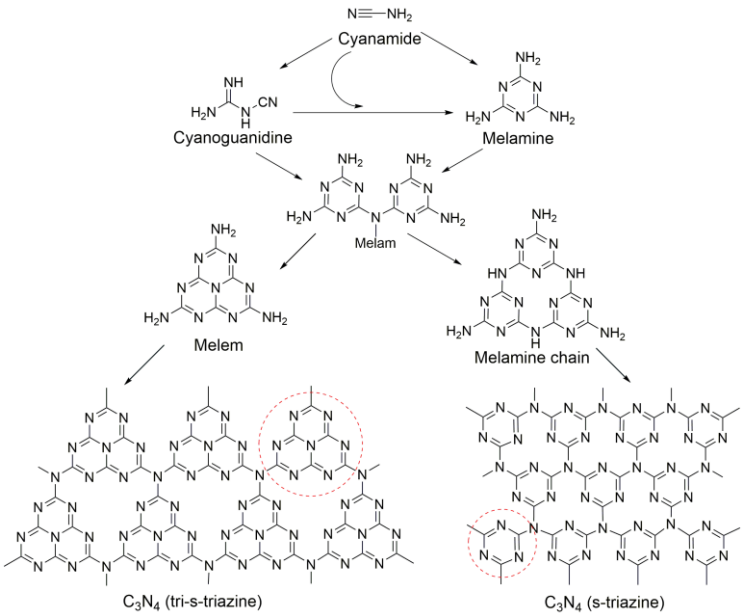

Fig. 1.16 Reaction pathways for the formation of potential allotropes of g-C_3N_4 from cyanamide.[66]

Melamine is formed from cyanamide via dicyandiamide. Further condensation can then proceed via the triazine route (dashed-line) to C_3N_4 or melam can form melem and then follow the tri-s-triazine route (dash-dot line) to form C_6N_8 (Fig. 1.16).

1.10. Metal oxides

Bulk oxide catalysts in pure or mixed form are either amorphous or polycrystalline materials. There are two characteristics of metal oxides that distinguish them from corresponding metals. The first one is the absence of metal-metal bonds and the second is non-zerovalent metal. Three key concepts that describe oxides are (i) oxidation state of metal at the surface, (ii) coordination environment of surface atoms and (iii) redox properties of the oxides. Metal oxides are widely used as catalysts as well as catalyst supports. Metal oxides generally belong to one of the structural classes of corundum, rock salt, wurzite, spinel, perovskite and rutile structures.[68] The corundum, the rutile and the spinel structures are made up of layers of close packed oxygen ions. When these oxide layers are stacked on top of the other in ABABAB sequence, the resulting structure is called hexagonal close packing (hcp) and it forms the basis for the corundum and the rutile structures. If the sequence of the layers is ABCABCABC then the resulting structure is called cubic close packing (ccp) and it forms the basis for the spinel structure. Metal oxide surfaces are more complex in their structure and are highly heterogeneous. Metal oxide surfaces exhibit red-ox properties and also have both basic and acidic characters based on their composition.

These properties are important for catalytic reactions. For example, silica-alumina catalyst is used for cracking of petroleum and bismuth molybdate for ammoxidation of propylene to give acrylonitrile. Rhenium oxide (Re_2O_7) supported on alumina is used for olefin metathesis.

1.10.1 Red-ox properties of metal oxides

In catalytic oxidation, oxide catalysts have to undergo oxidation-reduction cycles. In selective oxidation reactions, gaseous O_2 reacts with substrate to form oxygenates or water. The introduction of oxygen into reactant molecule can take place in two ways, (i) The electrons may be transferred to adsorbed oxygen to form the species like O^-, O_2^{2-} and O_2^-, which on incorporation of oxygen in to a product molecule and its subsequent desorption returns to the solid; (ii) direct incorporation of lattice oxygen of the oxide into product molecule, while the site of adsorped molecule on oxide and incorporated lattice oxygen into the molecule may be different. The migration of oxide ion between these two sites would occur, which is referred to as Mars-Van-Krevelen mechanism.

Some of the important factors that influence the redox cycle during the oxidation reactions are metal-oxygen bond strength, presence of cation vacancies, ability to form shear structures, optimal density of active oxygen, acid base properties, electron binding energy of lattice oxygen and the crystallographic plane.[69]

1.10.2. Acid-base properties of metal oxides

The exposed anion and cation on surfaces of oxides have been described as acid-base pairs.[70] In a metal oxide system, Brønsted or Lewis base site is oxide ion and Lewis acid sites is metal cation. Hydroxyl groups bound at certain oxide surfaces may exhibit considerable Brønsted acidity. Charge imbalance and/or coordination changes caused by incorporation of a second cation results in strong Brønsted acidity in mixed oxides rather than pure oxides. Exposed unsaturated coordination of cations may act as acceptors for free electron pairs of adsorbed species. The acidic strength of metal oxides depends on the charge and size of the cations, both of which may vary with the oxidation number of the cation. In general, according to the concept of hard and soft acids, cations of higher oxidation are harder. For cations in the same group with same oxidation state, those in later period are softer. Harder cations are smaller and polarizable. This will adsorb hard bases stronger than soft or polarisable bases. Surface hydroxyl groups may act as Brønsted acid sites, which may dissociate to protonate-adsorbed bases. The resultant con-

jugate acid and bases are stabilized on the surface by electrostatic interaction with each other and with oxide.

1.10.3. Spinel

The spinel structure is named after the mineral $MgAl_2O_4$ and the general composition is AB_2O_4. The O_2^- ions form an fcc lattice with cubic structure (Figs. 1.17 & 1.18). The cations occupy 1/2 of the octahedral sites and 1/8 of the tetrahedral sites and there are 32 O^- ions in the unit cell. There are two types of cubic building units inside a big fcc lattice, with A-atom in tetrahedral and B-atom in octahedral positions. The spinel structure is very flexible with respect to the incorporated cations. In a tetrahedral site, the interstitial position is in the center of tetrahedra formed (Fig. 1.19). In octahedral position the interstitial site is the space between 6 regular atoms that form octahedra (Fig. 1.20)

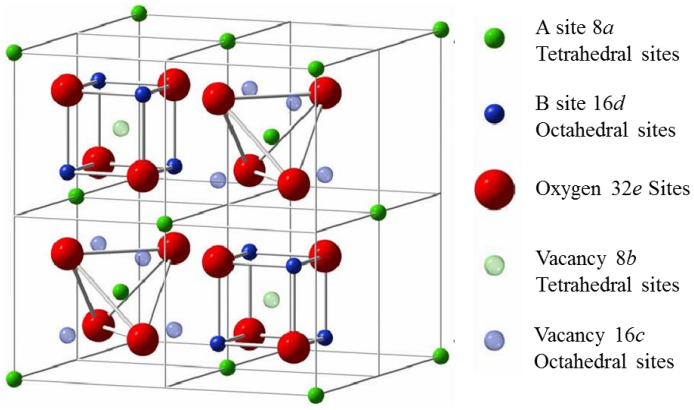

Fig.1. 17 AB_2O_4 spinel structure.

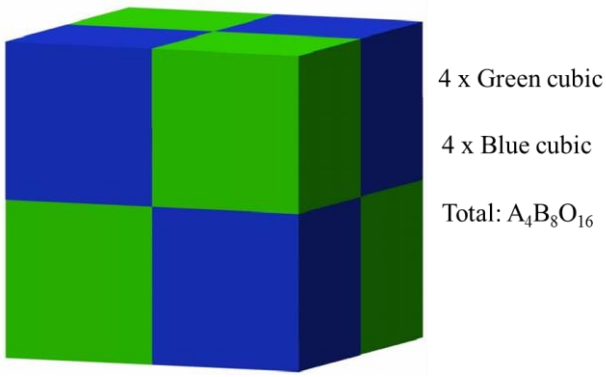

Fig. 1.18 Distribution of the primitive unit cubic in spinel.
(same color refers to the same ion-distribution.)

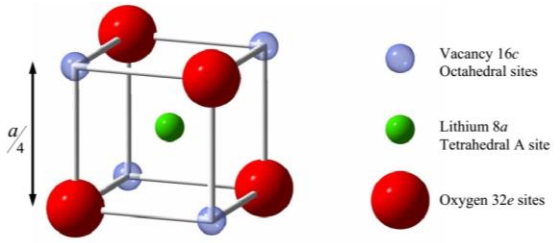

Fig. 1.19 Schematic illustration of lattice surrounding and nearest neighbors for the tetrahedral A sites.

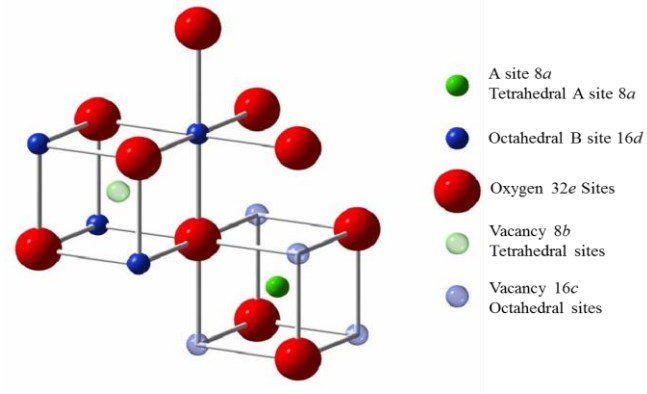

Fig. 1.20 Schematic illustration of lattice surrounding and nearest neighbors for the octahedral B sites.

1.10.3.1 Copper-manganese oxides

Hausmannite, Mn_3O_4 exhibits a normal spinel structure in cubic form containing Mn^{2+} in tetrahedral site and Mn^{3+} in octahedral site. A series of manganites of the general composition AMn_2O_4 with A = Mg, Cd, Fe, Co, Ni or Cu were found to be spinel type. A spinel is considered as a unit cell of 32 oxygens in 'A' sites with tetrahedral coordination, and 16 metal ions in 'B' sites with octahedral coordination with the oxygen. The structure and oxidation states of the components of copper manganite are difficult to determine. Copper-manganese oxide catalysts are used as oxidation catalysts, with an aim to replace precious metals.[71] The amorphous $CuMn_2O_4$ is a powerful oxidation catalyst, that can catalyze oxidation of CO to CO_2 near room temperature and combustion of several organic compounds in a temperature range of 200-500 °C).[72] These oxides were also used for the catalytic oxidation of ammonia and other gas species.[73] Recently, oxidation of p-cresol was also reported by using copper manganese oxides supported on activated carbon.[74]

1.11. Objectives and organization of the thesis

This thesis describes the preparation, characterization and catalytic activity in selective oxidation of petroleum and biomass derived components to value added chemicals. The research investigations are aimed at development of processes for the production of chemicals with high selectivity and in reasonably good yields. The investigation of relationship between the structure of the catalysts such as textural and chemical properties and their catalytic activity were studied for all the processes undertaken during this study. The thesis is divided into six chapters. A brief description of the contents of each chapter is given below.

Chapter 1: Introduction

This chapter provides a general introduction to catalysis, renewable and non-renewable sources of fuels and chemicals, information on various support materials, metal oxides, etc. It also describes uses of these materials as catalysts for the production of fine chemicals and fuels that have potential applications. A brief introduction to the catalytic processes involved in obtaining chemicals and fuels from petroleum feedstock and biomass is also given in this chapter. There is also discussion on some industrial applications of oxidation catalysis in this chapter. A brief over view of the selective oxidation of hydrocarbons and its importance in the synthesis of industrially important organic chemicals and intermediates is provided in addition to a brief introduction to oxidants used in these processes.

Chapter 2: Synthesis of catalysts and their characterization

This chapter provides information on catalyst preparation methods and various characterization techniques used to evaluate these catalyst materials. The characterization studies of catalyst materials was carried out using powder X-ray diffraction, BET surface area measurement, FT-IR, MASNMR, DRS UV-Vis, temperature programmed reduction (TPR), temperature programmed desorption (TPD) of NH_3 and CO_2, TGA, ICP-OES, XPS, etc. For each technique, theory and experimental procedures have been described.

Chapter 3: Selective oxidation of p-xylene to terephthalic acid over CNNT using molecular O_2

A brief literature review of oxidation of p-xylene (PX) to pure terephthalic acid (PTA) is given in the beginning of this chapter. Subsequently, detailed characterization of CNNT catalysts using XRD, SEM and TEM to investigate their structure and morphology is discussed. XPS has

been utilized to investigate the environment of nitrogen present in CNNT and how this influences the selective oxidation activity. Subsequent discussion is focused on finding process conditions that can provide maximum yields of PTA in the absence of an external initiator.

Chapter 4: Vapor phase oxidation of benzyl alcohol over Manganese based oxides in presence of molecular O_2

The selective oxidation of benzyl alcohol is an important reaction to get benzaldehyde, which is an important chemical intermediate particularly in pharma industry. This chapter deals with systematic study of selective oxidation of benzyl alcohol using copper and manganese containing spinel type mixed metal oxides as catalysts. These oxides were synthesized using established procedures and characterized for their textural and structural characteristics. They were employed for selective oxidation of benzyl alcohol using a fixed bed reactor. Optimum conditions for getting high benzaldehyde yields were established for continuous production of benzaldehyde. The presence of copper in the catalyst was found to play a key role by bestowing catalytic activity. Thus, this work has to led to the development of a robust catalytic process for continuous manufacture of benzaldehyde.

Chapter 5: Selective oxidation of biomass-derived compounds over supported metal catalysts using molecular O_2

This chapter starts with an introduction to selective oxidation of biomass based feedstocks such as glucose. Further, a detailed literature review of the oxidation of glucose to gluconic acid (GA) and glucaric acid (GCA) was discussed. The work in this chapter deals with the selective oxidation of glucose to GA, and GA to GCA over supported metal catalysts using molecular O_2. This chapter is divided into two parts. Part 5A deals with selective oxidation of glucose to GA on supported Au catalysts. Part 5B deals with selective oxidation of GA to GCA using Pt supported catalysts.

In Part 5A has detailed discussion on the utility of 2wt% Au on OMS-1 for selective glucose oxidation to gluconic acid. High GA selectivity (95%) under mild reaction conditions (70 °C, 5 bar O_2) was observed at 100% conversion of glucose. The catalysts with different precious metals were evaluated for glucose oxidation using O_2 as oxidant. Our investigations show that Au/Mg-OMS-1 catalysts does not need addition of external base for the reaction. Effect of reaction conditions like temperature, catalyst weight, Au content, O_2 pressure and duration of the re-

action were studied. The catalyst was successfully recycled 5 times. At the end, conclusions were drawn based on the catalytic studies and their correlation with the characterization results.

Part 5B contains discussion on highly dispersed Pt on K-OMS-2, which shows remarkable catalytic activity for oxidation of GA. Among other precious metals such, Pt shows remarkable activity for this reaction. Effect of reaction parameters like temperature, catalyst weight, Pt content, O_2 were investigated to optimize the GCA yield. Our investigations show that Pt/K-OMS-2 catalyst is active and selective for GCA formation in the absence of external base. The basicity of K-OMS-2 support facilitates the adsorption of GA and thereby improves catalytic activity. The conclusions drawn from these studies are included at the end of each section.

Chapter 6: Summary and conclusions

This chapter summarizes results of all the above chapters with a reference to conclusions drawn from each of the investigations. The reaction results correlated with characterization data also find mention in this chapter. This chapter also discusses salient features of results of the investigations conducted with regard to various catalysts used for selective oxidations of petroleum and biomass-derived compounds. At the end, it includes some suggestions for further research in the area of selective oxidation of petrochemicals and biomass derived components.

1.12. References

1. Green Stanley Joseph, *Industrial Catalysis*. Macmillan Company: New York, 1928.
2. Jöns Jacob Berzelius, *Årsberättelse om framstegen i fysik och kemi*. Royal Swedish Academy of Sciences: 1835.
3. Jöns Jacob Berzelius; Henrik Gustaf Söderbaum; Kungl Svenska vetenskapsakademien, *Jac. Berzelius travel notes*. P.A. Norstedt & söner: Stockholm, 1903.
4. Davis B. H.; Ertl G.; Knözinger H.; Weitkamp J. (Eds.), *Handbook of Heterogeneous Catalysis*. VCH: Weinheim, 1997; Vol. 1.
5. Bowker M., *The Basis and Application of Heterogeneous Catalysis*. Oxford Science Publications: Oxford Chemistry, Primers, 1998.
6. Calvin H. Bartholomew; Robert J. Farrauto, *Fundamentals of Industrial catalytic processes*. 2 ed.; John wiley & Sons.
7. Andrussow L., *Angew. Chem.* **1935,** 48, 593–595.
8. Thomas E. Nowlin; Robert I. Mink; Yury V. Kissin, Supported Magnesium/Titanium-Based Ziegler Catalysts for Production of Polyethylene. In *Handbook of Transition Metal Polymerization Catalysts*, Ray Hoff; Mathers, R. T., Eds. 2010.
9. Gary J. H; Handwerk G. E., *Petroleum Refining Technology and Economics (2nd ed.).* Marcel Dekker, Inc.: 1984.
10. Hagen J., *Industrial Catalysis: A Practical Approach*. 2 ed.; Wilwy-VCH: Weinheim, 2006.
11. Ertl G.; Knozinger H.; Schuth F.; Weitkamp J., *Handbook of Heterogeneous Catalysis*. Wiley-VCH: Weinheim, 2008; Vol. 1.
12. Gadi Rothenberg, *Catalysis concepts and Green applications*. Wiley-VCH Verlag GmbH & Co. KGaA: 2008.
13. Brundtland C. G., *Our Common Future, The World Commission on Environmental Development*. Oxford University Press: Oxford, 1987.
14. Anastas P.; Warner J. C., *Green Chemistry: Theory and Practice*. Oxford University Press: Oxford, 1998.
15. Doman Linda E. International Energy Outlook 2016: World energy demand and economic outlook *Periodical* [Online], May 11, 2016. http://www.eia.gov/forecasts/ieo/.
16. Ayaka Jones. International Energy Outlook 2016: Coal *Periodical* [Online], May 11, 2016. http://www.eia.gov/energyexplained/index.cfm?page=coal_home.

17. Laura E. Singer. International Energy Outlook 2016: Oil *Periodical* [Online], May 11, 2016. http://www.eia.gov/energyexplained/index.cfm?page=oil_home.

18. Victoria Zaretskaya. International Energy Outlook 2016: Natural Gas *Periodical* [Online], May 11, 2016. http://www.eia.gov/energyexplained/index.cfm?page=natural_gas_home.

19. Nancy Slater-Thompson. International Energy Outlook 2016: Nuclear *Periodical* [Online], May 11, 2016. http://www.eia.gov/energyexplained/index.cfm?page=nuclear_home.

20. National Research Council, Panel on New Directions in Catalyst Science and Technology. In *Catalysis look to future*, National Academy Press: Washington, DC, 1992.

21. Stanislaus A; Copper B. H, *Catal. Rev.-Sci. Eng.* **1994,** 36, 75-123.

22. Werpy T.; Petersen G. *Top Value Added Chemicals from Biomass: Vol. 1-Results of Screening for Potential Candidates from Sugars and Synthesis Gas*; Report No. NREL/TP-510-35523; National Renewable Energy Laboratory, CO, 2004.

23. Pandey A., *Handbook of plant based biofuels*. CRC Press/Taylor & Francis: Boca Raton, 2008.

24. He R. H.; Ye P.; English B. C.; Satrio J. A., *Bioresour. Technol.* **2009,** 100, 5305.

25. Biomass Innovation Center: Fueling growth through clean technology. http://www.biomassinnovation.ca/biomassandbioenergy.html

26. Juben N. Chheda; George W. Huber; James A. Dumesic, *Angew. Chem. Int. Ed.* **2007,** 46, 7164 – 7183.

27. Pierre Y. Dapsens; Cecilia Mondelli; Javier Perez-Ram´ ırez, *ACS Catal.* **2012,** 2, 1487−1499.

28. David Martin Alonso; Stephanie G. Wettstein; James A. Dumesic, *Chem. Soc. Rev.* **2012,** 41, 8075–8098.

29. David Martin Alonso; Jesse Q. Bond; James A. Dumesic, *Green Chem.* **2010,** 12, 1493–1513.

30. Michele Besson; Pierre Gallezot; Catherine Pinel, *Chem. Rev.* **2014,** 114, 1827−1870.

31. O'Sullivan A. C., *Cellulose* **1997,** 4, 173.

32. Hsu T. A.; Ladisch M. R.; Tsao G. T., *Chem. Technol.* **1980,** 10, 315.

33. Mohan D.; Pittman C. U.; Steele P. H., *Energy Fuels* **2006**, (20), 848.

34. Elliott D. C., *Energy Fuels* **2007,** 21, 1792.

35. Carlson T. R.; Vispute T. P.; Huber G. W., *ChemSusChem* **2008,** 1, 397.

36. Wataru Muramatsu, *Org. Lett.* **2014,** 16, 4846−4849.

37. Lidia De Luca; Giampaolo Giacomelli; Porcheddu, A., *Org. Lett.* **2001,** 3, 3041-3043.

38. Sergio Aguila; Rafael Vazquez-Duhalt; Raunel Tinoco; Manuel Rivera; Gina Pecchia; Joel B. Alderete, *Green Chem.* **2008,** 10, 647–653.

39. Gilbert D. L., *Oxygen and Living Processes. An Interdisciplinary Approach*. Springer Verla: NewYork, 1981.

40. Post J. E.; Bish D. L., *Modern Powder Diffraction, eds.* Mineral. Soc. of Am.: Washington, DC, 1989.

41. Stephanie L. Brock; Niangao Duan; Zheng Rong Tian; Oscar Giraldo; Hua Zhou; Steven L. Suib, *Chem. Mater.* **1998,** 10, 2619-2628.

42. Steven L. Suib, *Accounts of Chemical Research* **2008,** 41, 479-487.

43. Steven L. Suib, *Annu. Rev. Mater. Sci.* **1996,** 26, 135-51.

44. Burns R. G.; Burns V. M., *In Marine Manganese Nodules*. Elsevier, Amsterdam: 1977.

45. Post J. E.; Bish D. L., *Am. Mineral.* **1988,** 73, 861.

46. Ostwald J., *Mineral. Mag.* **1986,** 50, 336.

47. Nishita L.; Narasimha R. K.; Atul S. N.; Ganesh, K.; C., S., *J. Chem. Sci.* **2014,** 126, 403-413.

48. Nicolas-Tolentino, E.; Zheng-Rong, T.; Hua, Z.; Guanguang, X.; Steven, L. S., *Chem. Mater.* **1999,** 11, 1733-1741.

49. Robertson J., Amorphous carbon. *Advance in physics* **1986,** 35, 317-374.

50. Pierre Delhaes, *Graphite and Precursors*. Gordon and Breach Science: The Netherlands, 2001.

51. Lipson H.; Stokes A. R., *Nature* **1942,** 149, 328.

52. Harry Marsh; Rodríguez-Reinoso, F., *Activated Carbon*. Elsevier Ltd: 2006.

53. Mildred S. Dresselhaus; Gene Dresselhaus; Avouris, P., *Carbon Nanotubes: Synthesis, Structure, Properties, and Applications*. Springer-Verlag Berlin Heidelberg: 2001; Vol. 80.

54. Geim A. K.; Novoselov K. S., *Nat. Mater.* **2007,** 6, 183.

55. Zhou Y. K.; Neyerlin K.; Olson T. S.; Pylypenko S.; Bult J.; Dinh H. N.; Gennett T.; Shao Z. P.; O'Hayre R., *Energy Environ. Sci.* **2010,** 3, 1437.

56. Lei Z. B.; An L. Z.; Dang L. Q.; Zhao M. Y.; Shi J. Y.; Bai S. Y.; CaoY. D., *Microporous Mesoporous Mater.* **2009,** 119, 30.

57. Sjöström H.; Stafström S.; Boman M.; Sundgren J.-E., *Phys. Rev. Lett.* **1995,** 75, 1336

58. Gago R.; Jiménez I.; Cáceres D.; Agulló-Rueda F.; Sajavaara T.; Albella J.M.; Climent-Font A.; Vergara I.; Räisänen J.; Rauhala E., *Chem. Mater.* **2001,** 13, 129.

59. Kohzaki M.; Matsumuro A.; Hayashi T.; Muramatsu M.; Yamaguchi K., *Thin Sol Films* **1997,** 239, 308.

60. Franklin E. C., *J. Am. Chem. Soc.* **1922,** 44, 486.

61. Gmelin L., *Ann.Pharm.* **1835,** 15, 252.

62. Von Liebig J., *Ann. Chem. Pharm.* **1850,** 50, 337.

63. Von Liebig J., *Ann. Chem. Pharm.* **1850,** 72, 257.

64. Sehnert J.; Baerwinkel K.; Senker J., *J. Phys. Chem. B.* **2007,** 111, 10671.

65. Kroke E.; Schwarz M.; Horath-Bordon E.; Kroll, B. N. P.; Norman A.D., *New J. Chem.* **2002,** 26, 508.

66. Yong Wang; Xinchen Wang; Markus Antonietti, *Angew. Chem. Int. Ed.* **2012,** 51, 68-89.

67. Arne Thomas; Anna Fischer; Frederic Goettmann; Markus Antonietti; Jens-Oliver Mu ¨ller; Robert Schlogl; Johan M. Carlsson, *J. Mater. Chem.* **2008,** 18, 4893–4908.

68. Wang Z. L.; Kang Z. C., *Functional and Smart Materials: Structural Evolution and Structure Analysis*. Springer: 1998.

69. Sheldon R. A.; Van Santen R. A., Catalytic Oxidation: Principles and Applications. *World Scientific* **1995**, 53.

70. Burwell R. L. Jr.; Haller G. L.; Taylor K. C.; Read J. F., *Adv. Synth. Catal.* **1969,** 29, 1.

71. Morales M. R.; Barbero B. P.; Cadus L. E., *Appl. Catal. B: Environ.* **2006,** 67, 229.

72. Veprek S.; Cocke D. L.; Kehl S.; Oswald H. R., *J. Catal.* **1986,** 100, 201.

73. Wollner A.; Lange F.; Schmelz H.; Knozinger H., *Appl. Catal. A* **1993,** 94, 181.

74. Wang F.; Guan-yu Yang; Zhang W.; Wen-hai Wu; Xu J., *Chem. Comm.* **2003,** 10, 1172.

Chapter 2

Synthesis of Catalysts and their Characterization

2.1. Introduction

Synthesis of novel materials, their characterization and evaluation as catalysts are important aspects in any heterogeneous catalysis investigation. The aim of characterizing any catalyst material is to know its composition, crystalline phase and its purity, crystallinity and crystallite size, surface structure and its textural properties. Characterization of acidity, basicity and the nature of active (metallic) sites is essential to correlate catalytic activity with its properties. This chapter outlines the basic theory and principles of various characterization techniques used for catalyst materials such as X-ray diffraction (XRD), BET surface area analyser, temperature programmed reduction (TPR), temperature programmed desorption (TPD) of a probe molecule (NH_3-TPD and CO_2-TPD), NMR, FTIR, DRS UV-Vis, thermogravimetric analysis (TGA), X-ray photoelectron spectroscopy (XPS), inductively coupled plasma-optical emission spectroscopy (ICP-OES), scanning and transmission electron microscopy (SEM and TEM). The structure-activity relationship can be better understood by these techniques, which finally helps to design and improve the catalyst performance for various applications.

2.2. Catalyst preparation

2.2.1. Preparation of CNNT

CNNT was synthesized according to reported literature.[1] In a typical synthesis, 13.5 g of melamine was dissolved in 600 mL of ethylene glycol in a 5 L beaker using overhead stirrer for 2 h; to get saturated solution of melamine. To it, 1800 mL of HNO_3 (0.12 M) was added dropwise for 6 h and the obtained precipitate was filtered, washed with ethanol and dried at 60 °C for 10 h. The solid is melamine fiber, which was subsequently crushed to get its powder. This fiber was sintered in air (50 mL/min) flow at desired temperatures. The synthesis procedure is systematically illustrated in Scheme 2.1**.** The samples are designated herein as CNNT@*x*@*y*, where *x* denotes the sintering temperature and *y* denotes the sintering time. On the other hand, the bulk g-C_3N_4 was prepared as per procedure reported in literature at 520 °C.[2] In the synthesis of bulk g-C_3N_4, melamine was heated above its sublimation temperature, while for the synthesis of CNNT protonated melamine was heated at its sublimation temperature.

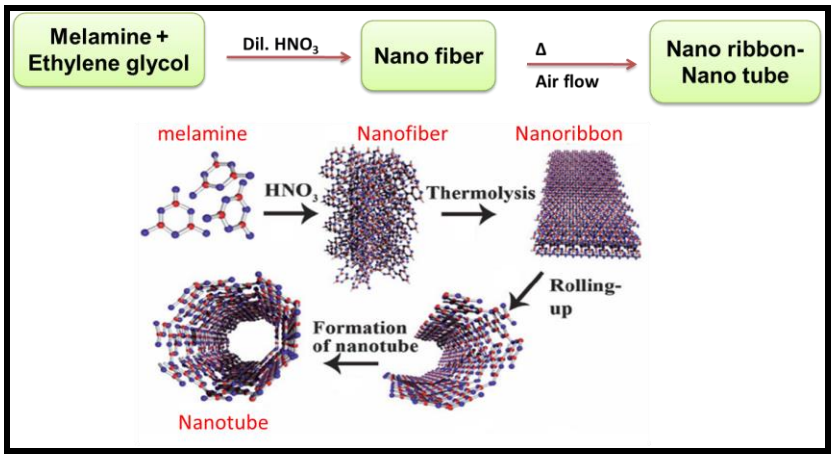

Scheme 2.1 Schemetic illustration for synthesis of CNNT.

2.2.2. Preparation of spinel type oxides by co-precipitation method

Cobalt and copper doped–manganese mixed oxides, $M_xMn_{3-x}O_4$ with x = 0.25, M=Co or Cu, were co-precipitated by KOH using dilute acetate solutions of Cu, Co and Mn as per procedures given in earlier reports.[3] In a typical synthesis for the preparation of 5 g of $Co_xMn_{3-x}O_4$ with x = 0.5, stoichiometric quantities of Mn (II) and Co (II) acetate (14.67 and 1.35 g) solutions (0.1 M) were precipitated using 0.2 M KOH solution. Metal salt solutions and precipitating agent were added simultaneously, under vigorous stirring; by maintaining a pH of ~10.5. The obtained precipitate was filtered and washed with distilled water (DW) until the pH of filtrate is ~7.5. The solid sample obtained was dried at 100 °C for about 10 h and calcined at 500 °C with for 6 h. The elemental analysis of the oxide samples was carried out using ICP-OES. Similar procedure was adopted for the preparation of copper containing spinel $Cu_xMn_{3-x}O_4$ with x = 0.25.

For the preparation of Mn_2O_3, similar procedure as described above was followed. The precipitate was dried and calcined at 600 °C for 6 h in a static furnace, while raising the temperature @ 5 °C/min.

2.2.3. Synthesis of Todorokite (Mg-OMS-1)

Mg-OMS-1 was prepared by a double aging process, as per the literature in a four step process with some modifications.[4]

(i) Preparation of Na-Birnessite

Three solutions were prepared for subsequent mixing. Solution-A was made using of $Mn(OAc)_2{\cdot}4H_2O$ (19.6 g) and $Mg(OAc)_2{\cdot}4H_2O$ (3.4 g) in 140 mL of DW, solution-B was made

by dissolving 50 g of NaOH in 160 mL of DW and a solution C was prepared using 4.8 g of $KMnO_4$ in 140 mL of DW. Solution B was taken in a 1000 mL single neck round bottom flask, to which A was added dropwise under vigorous stirring, to get slurry of Mn and Mg hydroxides. To it, solution C was added dropwise under vigorous stirring to obtain a brownish black suspension of MnO*x*. The suspension was aged with stirring for 2 days and subsequently aged without stirring for 2 days at 40 °C. Well-crystallized solid was filtered, washed till filtrate pH reached 9.5. The solid obtained was dried at room temperature to get Na-birnessite.

(ii) Stabilization of Na-Birnessite to Na-Buserite

The metastable Na-birnessite was transferred to a 1000 mL beaker filled with 800 mL of distilled water (DW), aged for 2 days under mild stirring at room temperature (RT). The solid product obtained was filtered; a part was dried at RT used for characterization studies, while the rest of the wet solid sample was used for ion-exchange.

(iii) Ion-exchange of Na-Buserite to Mg-Buserite and subsequent conversion to Mg-Todorokite

40 g of stabilized Na-buserite was ion-exchanged with a solution of $MgCl_2 \cdot 6H_2O$ (200 mL, 0.4 M) by stirring the mixture at room RT for 12 h. The filtered solid was dispersed in 750 mL of DW and filled in 1000 mL teflon lined autoclave and heated under autogenous pressure at 150 °C for 2 days to get Mg-OMS-1. The Autoclave was cooled to RT; solid product was filtered and washed with DW until the pH of the filtrate is neutral, dried at 100 °C for 12 h.

2.2.3.1. Loading of metal on the Mg-OMS-1 support

The metal containing catalyst was prepared by deposition-precipitation method.

Deposition-precipitation

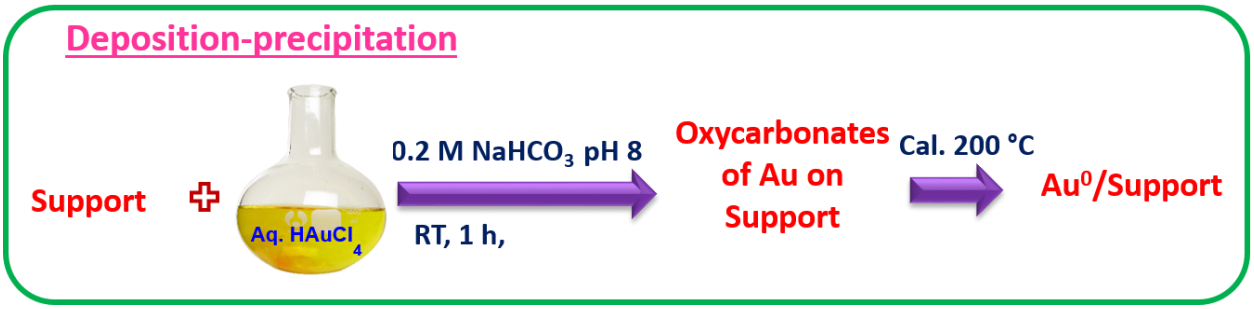

Scheme 2.2 Schemetic illustration for synthesis of Au supported catalyst by deposition-precipitation method.

2.2.3.1.1. Preparation of 2wt% Au/Mg-OMS-1 and other precious metal catalysts

The Au metal was loaded on to Mg-OMS-1 by deposition-precipitation method. In a typical synthesis, the desired amount of metal solution ($HAuCl_4$, Au content is 7.5 mg/mL) was taken in 20 mL of DW, to this required amount of support was added and stirred for 30 min. To this, 0.2 M $NaHCO_3$ solution was added drop wise under stirring to reach pH of 8.5 and the dispersed solid was stirred for 60 min at RT, filtered, washed, dried at 60 °C for 6 h and calcined at 200 °C for 3 h. The resulting catalyst is named as 2wt% Au/Mg-OMS-1.

Other precious metals (Ru, Pd, Pt) were deposited on to Mg-OMS-1 by adopting the above procedure by using appropriate precious metal salts and metal deposited were reduced using Aq. $NaBH_4$. The resulting catalyst are named as 2wt% Ru/Mg-OMS-1, 2wt% Pd/Mg-OMS-1 and 2wt% Pt/Mg-OMS-1 respectively.

2.2.4. Preparation of 2wt% Au catalysts on other supports

2wt% of Au metal containing catalysts supported on oxides like Al_2O_3, MnO_2, hydrotalcite (3:1) (HT) and MgO were prepared by simple deposition-precipitation method by adopting the procedure given in section 2.2.3.1.1. The resulting catalysts are named as 2wt% Au/Al_2O_3, 2wt% Au/MnO_2, 2wt% Au/HT (3:1) and 2wt% Au/MgO respectively depending on the support.

2.2.5. Synthesis of K-OMS-2 (Hollandite)

Hollandite octahedral molecular sieve (K-OMS-2) was prepared as per the literature reported.[5] In a typical synthesis, solution A was prepared using $MnSO_4 \cdot H_2O$ (8.8 g) in 30 mL of water and 3 mL concentrated HNO_3, solution B was prepared using $KMnO_4$ (5.89 g) in 100 mL of water. Solution "B" was added to solution "A" slowly under stirring conditions and refluxed at 100 °C for 24 h. The product obtained was filtered, washed, and dried at 100 °C.

2.2.5.1. Preparation of 2wt% Pt/K-OMS-2

2wt% of Pt containing K-OMS-2 was prepared by wet impregnation method. In a typical synthesis, the desired amount of metal solution (Aq. H_2PtCl_6) was taken in 20 mL of DW, to which requried amount of the support was added and stirred for 2 h at 70 °C. Subsequently, it was cooled to RT and metal was reduced using Aq. $NaBH_4$ (5 eq to metal). After stirring the dispersed solid for 30 min, it was filtered, washed and dried at 60 °C for 6 h. The resulting catalyst is named as 2wt% Pt/K-OMS-2.

2.2.5.2. Preparation of 2wt% Au /K-OMS-2 and 2wt% Au /H-OMS-2

For the preparation of 2wt% Au containing H-OMS-2, we have prepared H-OMS-2 initially. One gram of K-OMS-2 was added to 60 mL 1 M solution of HNO_3 and this mixture was stirred for 3 h at 70 °C. After cooling to RT, the solution was filtered and dried at 100 °C.

2wt% of Au metal was loaded onto K-OMS-2 and H-OMS-2, by adopting the privous described procedure in section 2.2.3.1.1 The resulting catalysts are named as 2wt% Au/K-OMS-2 and 2wt% Au/H-OMS-2.

2.3. Techniques used for characterization of catalysts

Characterization of the above synthesized materials would help to understand the physico-chemical properties of the catalysts in a better way, so that materials can be designed to meet the requirements. The following write-up gives a brief account of the theory and principles of various characterization techniques applied for the current study. The detailed procedure used for each experimental technique is also described.

2.3.1. Powder X-ray diffraction (XRD)

X-ray powder diffraction is used as the main characterization technique for any material. The detailed information about the theory of X-ray diffraction of powder materials can be found in books by Azaroff and Burger.[6, 7] X-rays are electrically neutral, the frequency of range lies in the range of 0.04 to 1000 Å. An atomic distance lies in the range of ~1.5 Å, hence X-rays with only shorter wavelengths (from few Å to 0.1 Å) are used for diffraction applications. The diffraction involves the interaction of the incident monochromatic X-rays (like Cu Kα) with the atoms of a periodic lattice in the materials. The ordered interfere constructive scattering is observed by atoms according to Bragg's law (Fig. 2.1).[8]

$$n\lambda = 2\ d\ \sin\theta;\ n = 1, 2, 3, \qquad (2.1)$$

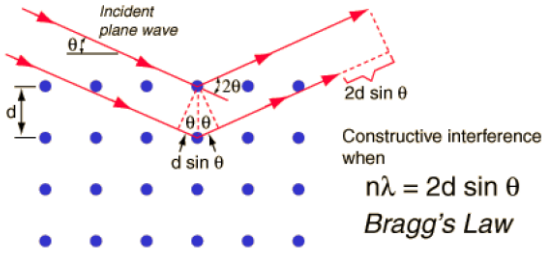

Fig. 2.1 Principle of Bragg's law.

Where, n is integer called order of reflection, λ is wavelength of the X-rays, d is distance between two lattice planes in the crystal and θ is the angle between the incoming X-rays and the reflecting lattice plane. The lattice spacing (d) can be obtained from Bragg's equation, which is characteristic of a particular material. This law relates the wavelength (λ) of electromagnetic radiation to the lattice spacing (d) and the diffraction angle (θ) in a crystalline material.

Width of the diffraction peaks indicate the dimension of the reflecting planes. It is well-known that the width of a diffraction peak increases when the crystallite size is reduced. Hence, XRD patterns can be used for the estimation of an average crystallite size of small crystallites using XRD line broadening technique with the help of Scherrer formula (Equation 2.2).[9]

$$t = 0.9\lambda/\beta \, Cos\theta \qquad (2.2)$$

Where, t is the thickness of the crystallites (Å), β is the full width at half maxima of the diffraction peak, λ is the wavelength of X-rays, and θ is the diffraction angle. XRD patterns of all the samples reported in this thesis were collected using Rigaku Miniflex diffractometer operating at 15 mA and 40 kV. The spectra were scanned in the 2θ range of 5-90° in 0.02° steps using CuKα (= 1.5406 Å) radiation, with a scintillator counter at a scanning rate of 4° min^{-1}.

High temperature XRD measurements were made using PANalytical X'pert Pro dual goniometer operating at 30 mA and 40 kV. The spectra were scanned using Cu Kα (λ= 1.5406 Å) radiation and a Ni filter. Data was recorded in the 2θ range of 5-90° in 0.02° steps using a flat holder in Bragg-Brentano geometry.

2.3.2. N_2 Physisorption studies

BET Surface area measurement

Surface area and porosity are important characteristic of a catalyst that influence its activity. In 1938, Brunauer, Emmett and Teller[10] developed most common accepted technique for measuring the surface area of materials by considering the multilayer adsorption of adsorbate molecules on the surface. The most commonly used technique for determining surface area is the so-called BET method, which has some limitations. Its assumptions are (i) adsorption energy remains constant from zero coverage to full coverage for the primary layer of the adsorbate and each of the layers above; (ii) there are no inter molecular interactions, though they attract and retain molecules striking them from the gas phase (iii) enthalpy of adsorption is the same for any layer other than the first (iv) a new layer can be initiated before the one under formation is

completed. Multilayer adsorption isotherm points are transformed using the linear version of the BET equation (Equation 2.3):

$$p/V(p°-p) = 1/cVm + [(c-1)/cVm]\ (p/p°) \quad (2.3)$$

Where $p°$ is saturation vapor pressure of the adsorbate at the experimental temperature, p is adsorption equilibrium pressure, Vm is volume of adsorbate required for monolayer coverage, V is volume of gas adsorbed at pressure p, and c, a constant that is related to the heat of adsorption and liquefaction. A linear relationship between $p/V(p°/p)$ and $p/p°$ is required to obtain the quantity of N_2 adsorbed. This linear portion is restricted to a limited portion of the isotherm, generally between 0.05-0.3. The monolayer volume, Vm is given by 1/(S+I), where S is the slope and is equal to $(c-1)/cVm$ and I is the intercept and is equal to $1/cVm$. The surface area of the catalyst (SBET) is related to Vm by Equation 2.4.

$$SBET = (Vm/22414)\ Na\ \sigma \quad (2.4)$$

Where Na is Avogadro number and σ is mean cross sectional area covered by one adsorbate molecule. The σ value generally accepted for N_2 is 0.162 nm^2. The BET surface area of the catalysts was determined by N_2 physisorption at liquid nitrogen temperature (-196 °C) using a Quantachrome Autosorb iQ surface area analyzer employing the standard multi-point BET analysis method.

Fig. 2.2 Quantachrome Autosorb IQ instrument used for N_2 physisorption.

Pore size distribution and pore volume measurement

Pore size distribution and pore volume were obtained by measuring the volume adsorbed at different $p/p°$ values and by applying different methods. The pore size distributions are calculated by the BJH model, while the pore volume was estimated by measuring the volume of

gas adsorbed at *p/p°* of 0.998. The BJH method was developed by Barrer, Joyner and Halenda to describe the adsorption-capillary condensation process in the mesopores of materials. This method[11] gives the distribution of pore volume against the pore size. In the capillary condensation region (*p/ps* > 0.4), a pressure increase causes an increase in the thickness of the adsorbed layer on the pore walls and capillary condensation in pores having a core size *rc* defined by Kelvin Equation 2.5:

$$\ln (p/p_{s)} = -(2\gamma w_m \cos\theta)/(RTr_c) \quad (2.5)$$

Where, r_c represents the radius of the cylindrical pores; the distance between walls for slit shaped pores; γ, the surface tension; w_m, the molar volume and θ, the contact angle. This equation allows the contribution of the thickness of the adsorbed film to the total adsorption to be calculated and then the core volume. The core volume can be converted into the pore volume and the core size into the pore size.

2.3.3. Temperature programmed methods

Temperature programmed desorption (TPD), temperature programmed reduction (TPR), and temperature programmed oxidation (TPO) are called as temperature programmed methods. They typically involve monitoring surface or bulk processes when temperature is increased at a programmed rate. Continuous analysis of the gases after interaction with the solid as a function of temperature is done. Instrumentation for temperature-programmed investigations consists of a reactor charged with the catalyst in a furnace that can be temperature programmed and change in concentration of gas passed through the sample is measured by thermal conductivity detector (TCD) (Fig. 2.3). The detailed information about the theory and experimental procedure of these programs can be found in 'Handbook of heterogeneous Catalysis'.[12]

Fig. 2.3 Micromeritics Autochem 2920 used for TPD and TPR studies.

2.3.3.1. Temperature programmed reduction (TPR)

The TPR is a technique used for the characterization of supported metals/metal oxide catalysts. This technique gives quantitative and qualitative information about the number of reducible species present in the catalyst and reveals the temperature at which the reduction occurs.[13] TPR profiles were obtained using a Micromeritics Autochem 2920 equipped with a TCD detector. The samples were pretreated in high-purity (99.98%) argon (20 $mL.min^{-1}$) at 300 °C for 3 h. After cooling to ambient, argon was replaced with a 5% H_2 in argon mixture, and the catalyst was heated up to 800 °C at a heating rate of 5 °C/min. The flow rate of H_2-Ar mixture used for this purpose was 30 $mL.min^{-1}$. The water produced during the reduction step was condensed and collected in a cold trap immersed in a slurry of isopropanol-liquid nitrogen mixture. The change in H_2 concentration at the outlet was monitored quantitatively by a thermal conductivity detector (TCD) that was calibrated before the study.

2.3.3.2. Temperature programmed desorption (TPD) of CO_2 and NH_3

Temperature programmed desorption is a simple technique used for estimation of the acidity and basicity of solids, in terms of their strength and concentration. TPD of NH_3 is used for characterization of the acid sites while TPD of CO_2 is used for characterization of the basic sites of the catalyst. By measuring the quantity and strength of the acidic/basic sites, the catalyst performance can be correlated. The catalyst surface is contacted with the probe molecule (NH_3/CO_2), which is adsorbed onto the surface either by chemisorption, physisorption or by the formation of chemical bonds, that minimizes the energy of the species. Desorption is carried out by raising the temperature linearly with time in presence of a steady stream of inert carrier gas. When the thermal energy overcomes the activation energy, the bond between the adsorbate and adsorbent breaks and the adsorbed species is desorbed. If sites with different strengths of acidity/basicity are present, desorption of adsorbate species takes place at different temperatures. The amount of desorbed species at different temperatures is proportional to the number and strength of active sites. The common probe molecules for determination of acidity are ammonia, methylamine, pyridine, trimethyl amine, dimethyl amine, n-butyl amine etc. The common probe molecules that are used to study basicity are carbon dioxide and sulfur dioxide which are acidic in nature.

The basicity and acidity of the catalysts was investigated by temperature-programmed desorption of CO_2 and NH_3 (CO_2/NH_3-TPD) using a Micromeritics Autochem-2920 instrument. For TPD run, around ~100 mg of sample was activated at 400 ºC under He flow (30 mL.min^{-1}) for 30 min. Subsequently, the temperature was brought down to 50 ºC and CO_2 was adsorbed by exposing the samples to a stream of 10% CO_2 in He (30 mL.min^{-1}) for 30 min. The temperature was then raised to 100 ºC and flushed with He (30 mL.min^{-1}) for 30 min at 100 ºC to remove the physisorbed CO_2. The desorption of CO_2 was carried out in He flow (30 mL.min^{-1}) by increasing the temperature to 500 ºC at 5 ºC.min^{-1}, while the amount of CO_2 desorbed was estimated quantitatively by TCD, which was calibrated before the TPD study. Similar procedure was adopted for NH_3-TPD and the amount of NH_3 desorbed were monitored quantitatively by TCD, which was calibrated before the TPD study.

The temperature-programmed desorption of O_2 was investigated by using a Micromeritics Autochem-2920 instrument. Before TPD run, around ~100 mg of sample was activated at 400 ºC under He flow (30 mL.min^{-1}) for 30 min. Subsequently, the temperature was brought down to 300 ºC and O_2 was adsorbed by exposing the samples to a stream of 10% O_2 in He (30 mL.min^{-1}) for 30 min. The temperature was then brought down to 100 ºC and flushed with He (30 mL.min^{-1}) for 30 min at 100 ºC. The desorption of O_2 was carried out in He flow (30 mL.min^{-1}) by increasing the temperature to 500 ºC at 5 ºC.min^{-1}, while the amount of O_2 desorbed was estimated quantitatively by TCD.

2.3.4. IR spectroscopy

Infrared spectroscopy is the most important of the modern spectroscopic techniques that has found profound applications in the field of catalysis. The basic principle of this technique is the fundamental vibrations and associated rotational-vibrations of a sample. The mid-infrared region of 4000–400 cm^{-1} is mostly used for these studies. The change in vibrational energy in molecules or in solid lattices by the absorption of photons, results in change in dipole moment. The intensity of the infrared band is proportional to the change in dipole moment. A variety of IR techniques have been used to get information on the surface chemistry of different solid materials. With respect to the characterization of solid catalysts, two techniques i.e., the transmission/absorption and the diffuse reflection techniques (DRIFT) are mostly used.[14-18] It is therefore a useful tool to identify phases that are present in the catalyst or its precursor stages, the

adsorbed species, adsorption sites and the way in which the adsorbed species are chemisorbed on the surface of the catalyst.[19, 20]

FTIR procedure

Spectra can be measured in the transmission/absorption mode. The sample consists typically of 10-100 mg of catalyst, pressed into a disc of approximately 1 cm^2 and a few tenths of a millimeter thickness. The Fourier transform-infrared spectra of the catalysts reported here were recorded on Bruker Tensor 27 FT-IR spectrometer at ambient conditions. The spectra were recorded using thin discs made by pressing the mixture of catalyst sample (~1 mg) and KBr (~99 mg).

DRIFT procedure

In diffuse reflectance mode, samples can be measured by simply loading the sample in the sample holder. The principle of this technique is diffuse reflectance or absorbance by a solid sample. The infrared absorption spectrum is described by Kubelka Munk function (Equation 2.6).[21, 22]

$$F(R\infty) = (1-R\infty)2/2R\infty = K/S \quad (2.6)$$

Where, K is the absorption coefficient, which is a function of the frequency ν, while S is the scattering coefficient and R_∞ is the reflectivity of a sample of infinite thickness, measured as a function of ν. The DRIFT spectra of the catalysts reported here were recorded on Bruker Tensor 27 FT-IR spectrometer at with Harrick DRIFT mode.

2.3.5. UV-visible diffuse reflectance spectroscopy (UV-Vis DRS)

UV-Vis DRS is a suitable technique for studying solid catalysts.[14] Diffusion reflectance spectroscopy is a technique based on the interaction of light in the ultraviolet (UV), and visible (Vis) regions with the sample. This interaction of light results in excitation in the electron from ground state to its high energy state (Fig. 2.4). The difference in the energy between molecular bonding, non-bonding and anti-bonding orbitals ranges from 125-650 kJ/mole. DRS is particularly a suitable technique for studying the transition metal ions because it measures both their d-d transitions and charge transfer bands. Good reviews are available to give a background of DRS technique.[14, 23]

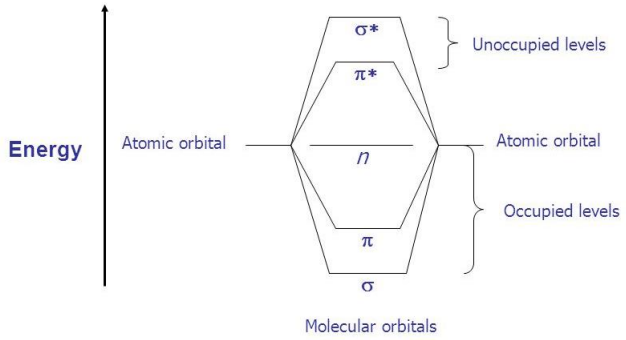

Fig. 2.4 Observed electronic transitions: graphical representation.

In a DRS spectrum the ratio of the light scattered from infinitely thick layer and the scattered light from an ideal non-absorbing reference sample is measured as a function of the wavelength λ. The illumination of powdered samples by incident radiation leads to diffuse illumination. The incident radiation can undergo partial absorption and scattering. The diffuse reflectance can be calculated using Equation 2.7.[23]

$$-dI/k\rho\, dS = I - (j/k) \qquad (2.7)$$

Where *I* is the incident light intensity of a given wavelength, *dI/dS* is the change of the intensity with the path length *dS*, ρ is the density of the medium, *k* is attenuation coefficient corresponding with the total radiation loss due to absorption and scattering, j is the scattering function. For this study, DRS UV-visible spectra were recorded on Shimadzu UV-2700 spectrophotometer in diffuse reflectance mode in the 200-800 nm range at room temperature.

2.3.6. Nuclear Magnetic Resonance spectroscopy (NMR)

Nuclear Magnetic Resonance (NMR) spectroscopy gives information on the interaction of a nucleus having a nuclear spin quantum number, I, greater than zero with an external magnetic field. This is used to obtain physical, chemical and structural information about molecules due to the chemical shift of the nuclei present in the sample. The chemical shift gives information on the local environment of a nucleus. The chemical shift is measured relative to that of a reference compound and is expressed in ppm with respect to the resonance frequency of the reference compound.[24, 25]

The interaction of nuclear spin with an externally applied magnetic field of strength Bo occurs in only 2I+1 ways, either with or against the applied field Bo. For a single nucleus with I=1/2 and positive γ, only one transition is possible between the two energy levels. The

energetically preferred orientation has the magnetic moment aligned parallel with the applied field (spin m = +1/2) and is often given the notation α, whereas the higher energy anti-parallel orientation (spin m = -1/2) is referred to as β.

The angular velocity of the spinning nucleus is given by the expression:

$$\omega_o = \gamma Bo \quad (2.8)$$

Where ω_o is the precession rate which is also called the Larmor frequency. The magnetogyric ratio (γ) relates the magnetic moment μ and the spin number I for a specific nucleus.

In magic angle spinning nuclear magnetic resonance (MASNMR), the angle θ with respect to the external magnetic field is considered, as at this angle aniosotropy of interactions is minimal. At this angle $3\cos^2\theta-1 = 0$, i.e. θ = 54.74°. Hence this technique is known as magic angle spinning (MAS).[25] In case of CPMAS NMR, cross polarization (CP) is involved between protons and the carbons in the molecule, in addition to MAS.

^{13}C and ^{15}N CPMAS NMR spectra of melamine and catalysts were recorded at room temperature using JEOL (JNME-ECX Series) spectrometer operating at 400 MHz. For recording the ^{13}C and ^{15}N MAS NMR spectra, the samples were filled into zirconia rotors with 4mm diameter and mounted in a standard double-resonance MAS probe. The signals were referenced to adamantane (^{13}C) and glycine (^{15}N), respectively. Rotation frequencies of 8 kHz were chosen. A ramped cross-polarization sequence was employed to excite both ^{13}C and ^{15}N nuclei via the proton bath where the power of the 1H radiation was linearly varied about 70%.

2.3.7. Thermogravimetric analysis (TGA)

Thermogravimetry (TG) is a technique which measures the change in mass of a material as a function of temperature and time in a controlled manner.[26, 27] (i) The variation in mass can either be a loss or gain of mass by the materials as a function of temperature at subjected atmosphere. It is ideally used to assess volatile content, degradation characteristics, and thermal stability. (ii) Differential thermal analysis measures temperature difference (ΔT) between a sample and reference material during heating (iii) Differential scanning calorimetry (DSC), measures the differential heat flow between a sample and reference material during heating.[28]

In the present work, thermogravimetry measurements of the samples were performed with a Mettler Toledo TGA/SDTA 851 apparatus. The analyses were carried out in air (40

mL.min^{-1}) at a heating rate of 5 °C min^{-1} from 30 °C to 800 °C or 1000 °C using about 10-15 mg of sample in an alumina crucible. Calcium oxalate was used to calibrate the instrument.

2.3.8. Inductively coupled plasma-optical emission spectrometry (ICP-OES)

ICP-OES is one of the most powerful and popular analytical tools for the determination of trace elements. It was developed by Fassal at Iowa state university in US and by Greenfield at Albright & Wilson, in the UK Ltd in the mid 1960s.[29] This technique uses the inductively coupled plasma to generate excited atoms and ions, which emits radiation at characteristic wavelength of the element involved (Fig. 2.5).[29] The concentration of the element within the sample is indicated by the intensity of emitted radiation. The liquid and gas samples may be injected directly into the instrument, while solid samples require extraction or acid digestion so that the analytes will be present in a solution. The sample solution is converted in to an aerosol and directed into the central channel of the plasma. At its core, the inductively coupled plasma (ICP) sustains a temperature of approximately 10,000 K, so the aerosol is quickly vaporized.

Sufficient energy is normally available in order to convert the atoms to ions and subsequently promote the ions to excited states. Both the atomic and ionic excited state species may then relax to the ground state *via* emission of photons. Thus the wavelength of the photons can be used to identify the elements from which they originated. The total number of photons is directly proportional to the concentration of the originating element in the sample. Sample introduction in ICP-OES instrument is depicted in Fig. 2.5.

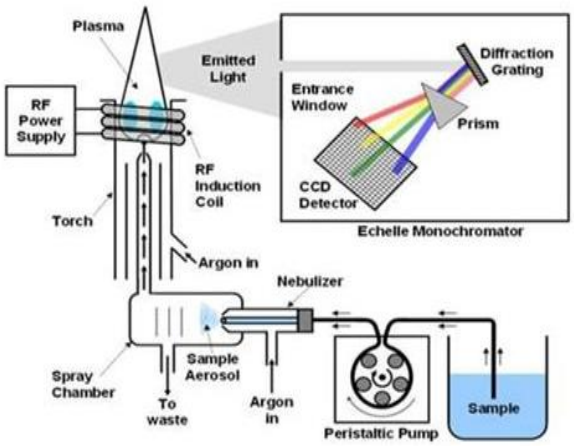

Fig. 2.5 Schematic illustration of sample introduction to ICP-OES.

ICP-OES analysis was carried out using a Spectro Arcos instrument equipped with the Winlab software (FHS-12). Standard solutions containing different elements were used for the calibration purpose. The solid samples were digested with aqua-regia before ICP-OES analysis.

2.3.9. X-ray photoelectron spectroscopy (XPS)

XPS is one of the most frequently used techniques in catalysis for surface analysis. X ray photoelectron spectroscopy was developed by Kai Siegbahn (Nobel prize winner, 1981) and his co-workers at Uppsala University, Sweden. This technique is based on the phenomena of photoelectric effect discovered by Heinrich Hertz and explained later by Albert Einstein.[30, 31] It is a widely used technique for finding chemical information of various material surfaces, information likes elemental composition, the oxidation state of elements, chemical bonding and in favorable cases the dispersion of one phase over another. The sample surface is irradiated with X-rays and the emitted photoelectrons are measured. When an atom absorbs a photon of energy hν, a core or valence electron with binding energy Eb is ejected with kinetic energy Ek:

$$Ek = h\nu - Eb - \varphi \quad (2.9)$$

Where, h is Planck's constant, ν is the frequency of the exciting radiation, Eb is the binding energy of the photoelectron relative to the Fermi level of the sample and φ is the work function of the spectrometer. The emitted photoelectrons have different kinetic energies that are characteristic of the emitting atoms and their bonding states. XPS is a surface-sensitive technique because the electrons whose energies are analyzed in XPS arise from a depth of no greater than about 5 nm.

The shape of the peaks and the binding energy can be slightly changed by the chemical state of the emitting atom. Chemical shifts are typically in the range of 0-3 eV.[32] The stimulating X-ray sources being usually Al Kα (1486.6 eV) or Mg Kα (1253.6 eV). The XPS spectrum is usually a plot of the intensity of photoelectrons versus binding energy. An experimental problem in XPS is that electrically insulating samples may charge during measurement, as photoelectrons leave the sample. Due to the positive charge on the sample, all XPS peaks in the spectrum shift by the same amount to higher binding energies. Calibration for this effect is generally done by using C1s binding energy (284.5 eV) from carbon contamination, which presents on most of the catalysts.[33-38]

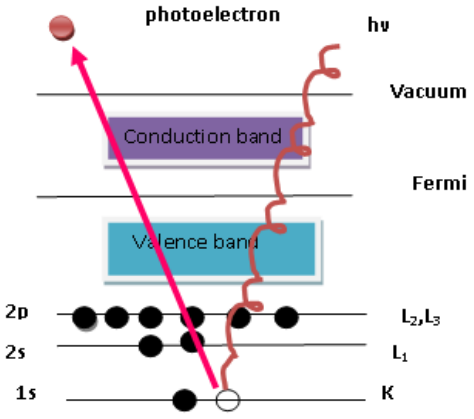

Fig. 2.6 Principle of XPS.

XPS measurements were carried out using a Lab based APPES unit equipped with VG scienta R 3000 HP electron energy analyzer, X-ray core level spectra are recorded with Al Kα radiation (hν = 1486.6 eV). The base pressure in analyzing chamber was maintained at 3–6 x 10^{-10} mbar. The peak corresponding to carbon 1s at 284.5 eV was taken as reference in estimating the binding energy values of various elements in the catalyst.

2.3.10. Electron microscopy

The electron microscopy has many variants. In this section, we deal only with scanning electron microscopy (SEM) and transmission electron microscopy (TEM). The SEM is very useful for the examination of physical characteristics of the sample, like size and shape of the crystals/particles in the material. On the other hand TEM is useful to study the nano structure of the material along with the metal particle distributions.

2.3.10.1. Scanning electron microscopy (SEM)

The scanning electron microscope (SEM) produces images by detecting secondary electrons which are emitted from the surface due to excitation by the primary electron beam. High-energy beam of electrons focused in a raster scan pattern, with detectors building up an image by mapping the detected signals with beam position. It is a simple technique to investigate the morphological characteristics of the samples. A probe of electrons (5-50 eV) is scanned over a sample surface that emits either secondary or back-scattered electrons which are detected as a function of the position of the primary beam. The interaction between the incident electrons with the atoms in the sample produces different types of signals, which carry detailed information

about the sample surface topography and the composition of the sample.[39] A major advantage of SEM is that bulk samples can also be directly studied by this technique.

The SEM images of the samples were studied using a Field emission scanning electron microscope of Nova Nano SEM 450. The samples prepared by dispersing them ultrasonically in isopropyl alcohol, transferring a portion of it on silicon wafers which were dried and subjected to gold coating in vacuum

2.3.10.2. Transmission electron microscopy (TEM)

Transmission electron microscopy (TEM) involves a high voltage electron beam emitted by a cathode and directed by magnetic lenses. The electron beam that has been partially transmitted through a very thin (and so semitransparent for electrons) specimen carries information about the structure of the specimen. This is followed by imaging and angular distribution analysis of the forward scattered electrons (unlike SEM where backscattered electrons are detected) and energy analysis of the emitted X-rays.[40] The spatial variation in this information (the "image") is then magnified by a series of magnetic lenses until it is recorded by hitting a fluorescent screen, photographic plate or light sensitive sensor such as a CCD (charge-coupled device) camera. The image detected by the CCD may be displayed in real time on monitor of a computer.

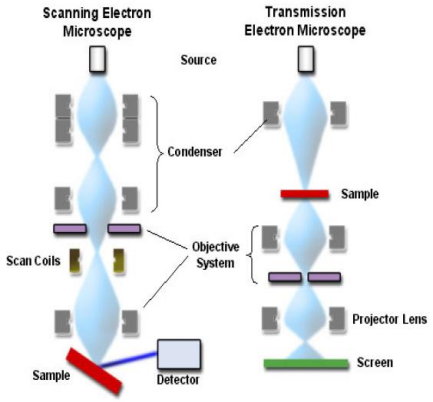

Fig. 2.7 Alignment of SEM and TEM instruments.

The TEM images of the samples were collected using a FEI Technai TF-30 and T-20 instrument operating at 300 kV and 200 kV. The samples for TEM measurement were prepared by placing a droplet of the highly diluted suspension of the sample in 2-propanol on a carbon-coated copper grid (mesh 200) and allowing it to dry at room temperature. The difference in the alignment of the SEM and TEM is depicted in Fig. 2.7.

2.4. References

1. Jun Gao; Yong Zhou; Zhaosheng Li; Shicheng Yan; Nanyan Wang; Zhigang Zou, *Nanoscale* **2012,** 4.
2. Yan S. C.; Li Z. S.; Zou Z. G., *Langmuir* **2009,** 25, 10397-10401.
3. Satyanarayana Reddy A.; Chinnakonda S. Gopinath; Satyanarayana Chilukuri, *J. Catal.* **2006,** 243, 278–291.
4. Jian L.; Qiuhua Z.; Aimin H.; Oscar G.; Steven L. S., *Inorg. Chem.* **1999,** 38, 6106-6113.
5. Roberto N. DeGuzman; Yan-Fei Shen; Edward J. Neth; Steven L. Suib; Chi-Lin O'Young; Steven Levine; John M. Newsam, *Chem. Mater.* **1994,** 6, 815-821.
6. Azaroff L. V.; Burger L E., *The power method in X-ray Crystallography,*. McGraw-Hill: New York, 1985.
7. Ertl G.; Knozinger H.; Schuth F.; Weitkamp J., *Handbook of Heterogeneous Catalysis*. WILEY-VCH Verlag GmbH & Co.: New York, 1985.
8. Cullity B. D.; Stock S. R., *Elements of X-ray diffraction*. 3 ed.; Prentice Hall: 2001.
9. Henry N. F. M.; Lipson J.; Wooster W. A., *The interpretation of X-ray diffraction photographs*. Macmillan and Co Ltd.: London, 1951.
10. Brunauer S.; Emmett P. H.; Teller E., *J. A. Chem Society* **1938,** 60, 309.
11. Leofanti G.; Padovan M.; Tozzola G.; Venturelli B., *Catal. Today* **1998,** 41, 207.
12. Daniele A. M. M.; Baiker A., *J. Catal.* **1983,** 83, 323.
13. Delgass W. N.; Haller G. L.; Kellerman R.; Lunsford J. H., Spectroscopy in Heterogeneous Catalysis. In Academic Press: New York, 1979.
14. Fierro J. L. G.; Fierro i. J. L. G., *Spectroscopic Characterization of Heterogeneous Catalysis Part B*. Elsevier: Amsterdam, 1990.
15. Coudurier G.; Lefebvre F.; Imelik B.; edrine J. C., *Catalyst Characterization: Physical Techniques for Solid Materials.* Plenum Press: New York, 1994.
16. Knozinger H.; Brongersma H.H.; Santen R. A. V., *Fundamental Aspects of Heterogeneous Catalysis Studied by Particle Beams*. Plenum Press.: New York, 1991.
17. Wendlandt W. W.; Hecht H. G., *Reflectance Spectroscopy*. Plenum Press.: New York, 1968.
18. Thomas J. M.; Terasaki O.; Gai P. L.; Zhou W.; Gonzalez-Calbet J., *Acc. Chem. Res.* **2001,** 34, 583.
19. Eischens P.; Pliskin W. A., *Adv. Catal.* **1958,** 10.

20. Kubelka P.; Munk F., *Z. Tech. Phys.* **1931,** 12, 593.

21. Kortum P.; Braun W.; Harzog C., *Angew. Chem. Int. Ed.* **1963,** 2, 333.

22. Weckhuysen B. M.; Schoonheydt R. A., *Catal. Today* **1999,** 49, 441.

23. Schoonheydt R. A.; Delanny F., *Diffuse Reflectance Spectroscopy: Characterization of Heterogeneous Catalysts*. Marcel Dekker Inc.: 1984.

24. Keeler J., *Understanding NMR Spectroscopy*. John Wiley & Sons.: 1995.

25. Wind R. A.; Popov A. I.; Hallenga K., *Modern NMR Techniques and Their Application in Chemistry*. Marcel Dekker, Inc.: New York, 1991.

26. Wendlandt W. W., *Thermal Methods of Analysis*. John Wiley: New York, 1964.

27. Duval C.; Oesper R. E., *Inorganic Thermogravimetric Analysis*. Elsevier: Amsterdam, 1963.

28. Kluwer M. B., *Introduction to Thermal Analysis Techniques and applications*. 2 ed.; Academic pubishiers: 2001.

29. Boss C. B.; Fredeen K. J., *Concept, Instrumentation and Techniques in Inductively Coupled Plasma Optical Emission Spectrometry*. 2 ed.; Perkin-Elmer: Norwalk, CT, 1997.

30. Carlson T. A., *X-ray Photoelectron Spectroscopy, Dowden*. Hutchinson & Ross: Stroudsburg, PA, 1978.

31. Briggs D.; Seah M. P., *Auger and X-ray Photoelectron Spectroscopy*. 2 ed.; Wiley: New York, 1990; Vol. 1.

32. Niemantsverdriet J. W., *Spectroscopic methods in Heterogeneous catalysis*. VCH: Weinheim, 1993.

33. Delgass W. N.; Hughes T. R.; Fadley C. S., *Catal. Rev.* **1970,** 4, 179.

34. Egelhoff W. F. Jr., *Surface Science Reports* **1987,** 6, 253.

35. Moretti G.; Ertl G.; Knozinger H.; Weitkamp J., *Handbook of Heterogeneous Catalysis*. Wiley-VCH: 1997; Vol. 2.

36. Mathew T.; Shiju N. R.; Sreekumar K.; Rao B. S.; Gopinath C. S., *J. Catal.* **2002,** 210, 405.

37. Goldstein J. I.; Yakowitz H., *Practical Scanning Electron Microscopy*. Plenum Press: New York, 1975.

38. Fadley C. S.; Brundle C. R.; Baker A. D., Electron Spectroscopy: Theory, Techniques and Applications. In Academic Press: New York,, 1978.

39. Lawes G., *Scanning Electron Microscopy and X-Ray Microanalysis*. John Wiley and Sons Ltd.: Chichester, 1987.

40. Fryer J. R., *Chemical Applications of Transmission Electron Microscopy*. Academic Press: San Diego, 1979.

Chapter 3

Selective oxidation of p-Xylene to Terephthalic acid over CNNT using molecular O_2

3.1. Introduction

The oxidation of hydrocarbons using green oxidants such as O_2 or Air has immense importance in the synthesis of a broad range of chemical intermediates and products using petroleum based feedstocks.[1] One of the important challenge in this regard is the production of pure terephthalic acid (PTA) from p-xylene (PX) using a greener route. PTA is a chemical intermediate mainly used in the synthesis of polyethylene terephthalate (PET), which can be used for making films, fibers and resins.[2, 3] Some part of the PTA is also used in the manufacture of liquid crystal polymers, terephthaloyl chloride, cyclohexanedimethanol, plasti-cizers and co-polyester ether elastomers. Worldwide manufacture of PTA was approximately 39 million metric tons in 2009, with a global demand growth at 7-8% an year during 1999-2009.[4] It is produced mostly through AMOCO process, which is a modified Mid-Century (MC) process.[5] The two step process involves metal acetate salts of Co, Mn and HBr as catalysts with acetic acid as solvent in the temperature range of 175-225 °C at 15-30 bar pressure of air as the oxidant.[6] Though the present production of PTA through MC-AMOCO process is well established, it has many disadvantages, viz., (i) catalyst is homogeneous that encounter separation problems, (ii) uses corrosive solvent (acetic acid), (iii) involves two-steps (oxidation followed by hydrogenation) and (iv) use of inorganic initiator (HBr) that results in production of unwanted and harmful byproduct CH_3Br. These drawbacks throw a research challenge to develop a green route to the synthesis of PTA that can be translated into a commercial process.

3.2 Literature reports on the synthesis of PTA from PX

To overcome the above cited problems and to develop a green route for the synthesis of PTA, some research groups were focused on using organic initiator N-hydroxyphthalimide (NHPI) with homogeneous catalysts like NHPI-Co-Mn,[7-11] NHPI-O_2/HNO_3 in ionic liquids,[12] guanidine/Co-Mn-Br,[13] Mn(III) Schiff base complex[14] and metalloporphyrin[15] without any initiator. The PX oxidation has been studied on different supported heterogeneous oxide systems like metal oxides,[16] Cobalt(III) complex on SBA-15,[17] silica supported chromium Schiff base complex,[18] zeolites encapsulated metal complex,[19] Co-Mn nanoparticles immobilized on a modified bentonite,[20] CeO_2 containing oxygen vacancies,[21] $(La,Sr)_{0.5}(Mn,Co)_{0.5}O_{2.38}$ perovskite with oxygen deficiency,[22] along with use of different kinds of organic or inorganic initiators. The kinetic studies reveal that the rate of oxidation of PX to p-toluic acid (TA) is directly proportional to the concentration of PX (first order) while the TA oxidation to PTA is first order

with respect to the catalyst content.[23] Lumped kinetic model (Scheme 3.1) is widely adopted for the liquid phase oxidation of PX to PTA. The reaction kinetics have been extensively investigated by using homo- or heterogeneous catalytic systems.[4, 23-27] Walt Partenheimer *et al.* has shown that the catalytic activity of the catalyst for the synthesis of PTA is pH dependent.[28]

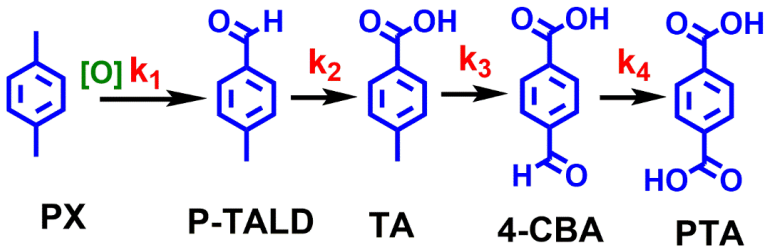

Scheme 3.1. Schematic illustration of Lumped kinetic scheme model for the formation of terephthalic acid from p-xylene via intermediates.

Poliakoff and co-workers extensively studied PTA synthesis in supercritical water in a continuous process, in which water was used alternative to acetic acid. The scope of the reaction system is limited because of reaction conditions employed (T=374 °C, *P*>221 bar, at critical point of water).[29-33] Some research groups tried to modify the reaction conditions in such a way that high yields of PTA under supercritical water is obtained.[34, 35] The influence of N_2/CO_2 along with O_2 as oxidant using Co/Mn/Br catalyst system has been studied by Xiaobin Zuo *et al.*[36] The presence of N_2/CO_2 reduces the burning of solvent and increases the purity of PTA through efficient conversion of intermediates at lower temperatures.[36] Subramaniam and co-workers have developed a spray process[37] for the production of PTA in a greener route that reduces CO_2 emissions, resulting in very low (<25 ppm) impurity of 4-carboxy benzoic acid (4-CBA). This spray process involves the addition of CO_2 and O_2 while using a traditional catalyst system (Mn-Co-Br).[4, 23, 37] John W. Frost and coworkers have demonstrated bio-based production route to PTA from acrylic acid and isoprene derived from biomass. A solvent-free reaction involves cyclo addition of acrylic acid and isoprene with $TiCl_4$ (2 mol %) at room temperature.[38]

Despite all the above research, one major problem is the separation of products after the reaction, since 4-CBA and PTA have similar properties and miscible with one another; hence it is difficult to separate 4-CBA from PTA. Some researchers have tried to separate 4-CBA and PTA on the basis of their solubility and recrystallization, which in turn will rise the PTA cost but can eliminate the second step (hydrogenation of 4-CBA) in the traditional (AMOCO) process.[39,

[40] The above discussion shows that there is still scope for the development of a more efficient process for the production of PTA using a green route.

In this study, we have investigated the activity of metal-free carbon nitride nanotubes (CNNT) as heterogeneous catalyst for the activation of SP^3 C-H bond of PX. Catalytic oxidation of PX to PTA was systematically studied by using molecular oxygen and a noncorrosive solvent in the absence of any external initiator. Different reaction parameters were optimized to maximize the PX conversion to PTA. The catalysts were subjected to detailed characterization to correlate with catalytic activity.

3.3. Synthesis and characterization of CNNT catalysts

3.3.1. Experimental procedures

3.3.1.1. Materials

All the chemicals employed in this study were reagent grade and used without further purifications. p-Xylene, p-toluic acid, p-tolualdehyde, and 4-carboxybenzoic acid were procured from Sigma-Aldrich, USA. Terephthalic acid, ethylene glycol, acetone (HPLC grade), methanol (HPLC grade), formic acid, NaOH, NHPI, NHSI and HNO_3 were sourced from Merck, India. All the chemicals used as received without any further purification.

3.3.1.2 Synthesis of CNNT catalysts

In a typical synthesis for CNNT, saturated solution of melamine was prepared in ethylene glycol. To this HNO_3 (0.12 M) was added dropwise to obtain melamine precipitate, which was filtered, washed with ethanol and dried at 60 °C for 10 h. The solid is melamine fiber, which was crushed and heated to desired temperatures in the presence of air (50 mL/min). The duration of heating was varied. The samples are designated as CNNT@*x*@*y*, where *x* denotes the sintering temperature and *y* denotes the sintered time. For further details on CNNT synthesis, section 2.2.1 may be consulted.

3.3.1.3. Evaluation of catalysts

Oxidation reactions were carried out in a 50 mL Parr autoclave (4848 controller). In a typical reaction, required quantity of p-xylene was taken in 20 mL of solvent and to it freshly activated catalyst was added. The reaction was conducted at desired temperature with continuous stirring (1000 rpm). When the reaction mixture reached around 30 °C below desired reaction temperature, O_2 was slowly introduced into the autoclave thus preventing the rapid raise of

temperature, as PX to PTA reaction is highly exothermic. On reaching reaction temperature, O_2 was bubbled into the reaction mixture to replenish the oxygen consumed during the reaction. At the end of reaction, the reaction mixture was cooled to room temperature, part of it (~0.5 mL) was filtered using nylon 0.22 µm filter and analyzed using a GC (Agilent 7890A) equipped with flame ionization detector (FID) and HP-5 capillary column (50 m length, 0.32 mm diameter). Product identification was done using authentic standards and by using GC-MS (Agilent GC-78908). To the rest of the reaction mixture, desired amount of 0.7 M NaOH and methanol (7:3) were added to make up the solution to 50 mL. From this solution, 1 mL was diluted to 25 mL with methanol; which was analyzed using HPLC, equipped with UV detector and C18 column (4.6 × 100 mm, 3.5 micron). Methanol + water mixture was used as mobile phase at a flow rate of 0.4 mL min^{-1}. All the products were identified and compared with authentic standards. Subsequently, autoclave was washed with 0.7 M NaOH in methanol to remove any residual products before the next reaction.

3.4. Results and discussion

3.4.1. Catalyst characterization

3.4.1.1. X-ray diffraction (XRD)

X-ray diffraction (XRD) pattern of various samples is shown in Fig. 3.1. The diffraction profiles show the transformation of melamine into CNNT via melamine fiber formation through protonation of amine groups during the first step followed by sintering of melamine fiber (Fig. 3.1a). Fig. 3.1b shows the difference in the structure of bulky g-C_3N_4[41] and CNNT[42] by the formation of tri-s-triazine ring and s-triazine ring, respectively. The intense peak of CNNT at 2θ = 27.4° with a d value of 0.3277 nm is closely compared to the characteristic peak of 002 plane of bulky g-C_3N_4 (d = 0.3269),[43-45] pure graphite units (d = 0.353 nm)[45] and crystalline graphite (d = 0.335 nm)[44, 45] which resemble interplanar stacking peak of aromatic rings of carbon. The peaks at 2θ = 17.4° (d = 0.49) and 2θ = 13.0° (d = 0.691) assigned to CNNT and g-C_3N_4 respectively are closely related to the distances of s-triazine (ca. 0.47nm)[46] and tri-s-triazine (ca. 0.73 nm)[45] rings based carbon nitride.

Further, we have also studied the effect of sintering temperature at two different hold times (90 and 60 min) on the formation of CNNT, these results are given in Fig. 3.1c and 3.1d. From the XRD pattern of Fig. 3.1c, it is clear that the crystallinity of the material has decreased

with increasing sintering temperature. As a result, broadening of the (002) plane was observed at higher temperature. The peak corresponding to 2θ value 17.4° (d = 0.49), attributed to the formation of s-triazine rings has disappeared at higher temperatures. These findings clearly show the formation of s-triazine ring structure, which is a building block for the formation of CNNT, is temperature dependent. Similar observations were made in the case of samples sintered at different temperatures, but for a lower duration of 60 min time (Fig. 3.1d).

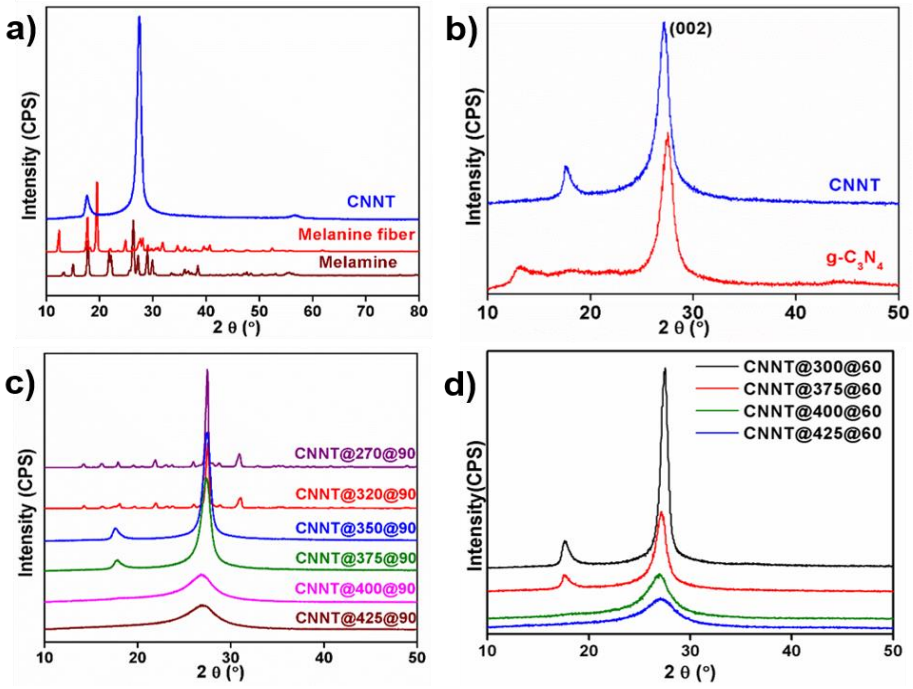

Fig. 3.1 XRD profiles of (a) melamine, melamine fiber and CNNT, (b) CNNT and g-C_3N_4, (c) CNNT prepared at different sintering temperatures with 90 min hold time and (d) CNNT prepared at different sintering temperatures with 60 min hold time.

3.4.1.2 N_2-Physisorption and chemical composition

BET surface area of CNNT catalysts was studied using N_2 physisorption (Table 3.1). No specific trend was observed, as values of all the samples are very close. The relative intensity of peak corresponding to (002) plane (2θ=27.4°) reduced for the samples heated for longer time at the same temperature. To understand it better, we have compared the peak intensities at 13° (1st peak) relative to 27.4° peak and found that CNNT@350 for 60 min has a higher intensity ratio (Table 3.1). Elemental analyses of all the materials are given in Table 3.1. Even the nitrogen to carbon ratio is also high for this sample.

Table 3.1 Structural and textural characteristics of CNNT materials and their chemical composition.

S No.	Catalyst	BET surface area	% weight loss[#]	From XRD			Elemental analysis (wt. %)			N to C ratio
				Area		Ratio of peak-1 to peak-II	C	H	N	
				Peak-I 2θ=13°	Peak-II 2θ=27.4°					
1	Melamine fiber	-	-	-	-	-	19.0	3.5	53.9	2.8
2	CNNT@270@90	-	32.0	-	-	-	19.8	3.5	55.6	2.8
3	CNNT@320@90	-	43.4	-	-	-	21.7	3.5	57.5	2.6
4	CNNT@350@90	7	50.7	956	7582	0.13	27.9	3.2	59.5	2.1
5	CNNT@375@90	6	54.7	700	7018	0.10	28.2	2.9	61.6	2.2
6	CNNT@400@90	6	59.7	-	6533	0	32.1	2.4	62.3	1.9
7	CNNT@425@90	7	64.6	-	8671	0	32.7	2.2	62.2	1.9
8	CNNT@350@60	7	49.4	1250	8862	0.14	25.1	3.0	56.8	2.3
9	CNNT@375@60	6	50.8	873	18492	0.05	27.1	2.8	58.1	2.1
10	CNNT@400@60	7	52.0	-	12488	0	30.8	2.5	59.7	1.9
11	CNNT@425@60	7	59.5	-	10194	0	31.7	2.2	61.2	1.9
12	g-C_3N_4 @ 550 °C	8	76.6	-	-	0	34.6	1.6	58.5	1.7

[#] Weight loss measured by the initial and final weight of the material before and after subjected to Sintering.

3.4.1.3. Thermogravimetric analysis (TGA)

TGA spectra of melamine fiber heated in air flow is given in Fig. 3.2a. Three distinct

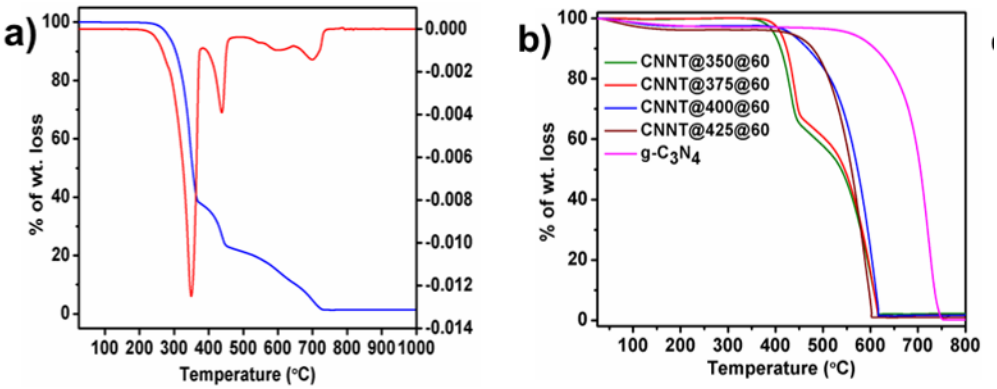

Fig. 3.2 TGA of (a) Melamine fiber and (b) Different samples in presence of air.

weight losses centered around 350, 440 and ~600 °C were seen, which may be assigned to the decomposed products of carbon and nitrogen in the form of CO_2 and NH_3 at different

temperatures.[47] TGA of various samples studied in the presence of air is shown in Fig. 3.2b. The plots show that all catalysts are stable up to 400 °C in the presence of air. In case of samples CNNT@350 and CNNT@375, there is a weight loss centered at 425 °C, which is due to secondary condensation of s-triazine rings to tri-s-triazine rings, which is not observed in case of CNNT@400, CNNT@425 and g-C_3N_4.[41]

3.4.1.4. FTIR spectroscopy

Infrared spectroscopy was employed to study the transformation of melamine into CNNT via melamine fiber (Fig. 3.3a). The characteristic spectrum of CNNT was found to be similar to that reported in the literature.[43, 48, 49] We observed multiple bands characteristic of s-triazine ring in the range of 1400-1600 cm^{-1} for quadrant stretching, overlapped by a strong NH_2 deformation band and double semi-circle stretchings.[48] The band at 800 cm^{-1} was assigned to the out-of-plane ring bending by sextants in all stages of formation of the material (Fig. 3.3a and 3.3b).[43, 49] Further, the bands in 1000-1400 cm^{-1} region are attributed to the C–N stretching, while the peak at 1315 cm^{-1} is characteristic of C−N stretch in the 3-fold N-bridge linking the triazine rings, [43, 48, 49] the bands in 1600-1700 cm^{-1} region are assigned to C=N stretching and bands in 3000-3500 cm^{-1} range are assigned to N−H stretching's.

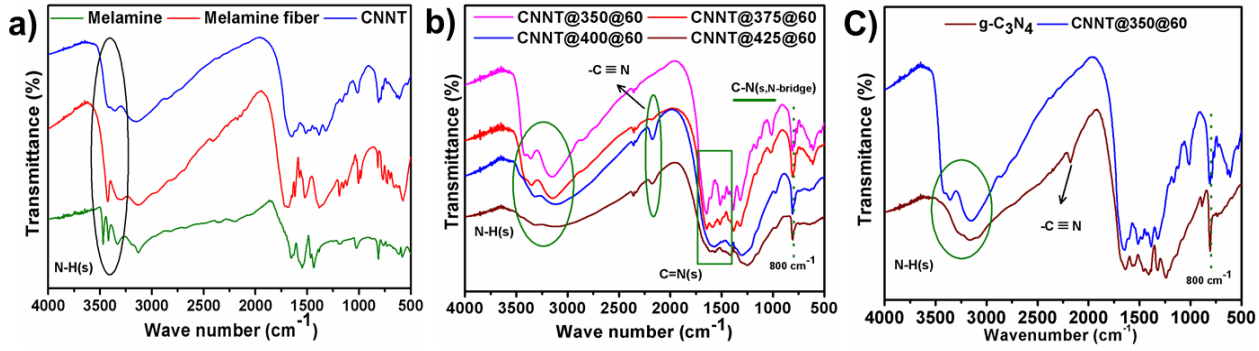

Fig. 3.3 FTIR spectra of (a) Melamine, melamine fiber and CNNT, (b) CNNT at different temperatures, (c) CNNT@350 heated for 60 min and g-C_3N_4.

In Fig. 3.3b, the broadening of bonds was clearly seen at higher temperatures, which corresponds to N−H, C−N and C=N bonds (3000-3500, 1000-1350 and 1400-1650 cm^{-1}). This may be due to decrease in the number of bonds related to N−H, C−N and C=N stretchings, respectively. Even the intense bands at 1020 and 1160 cm^{-1} corresponding to C−N(s) have diminished at higher temperatures, so it may be seen that the structural morphology has changed from s-triazine to tri-

s-triazine at higher temperatures. Similar kind of broad bands were observed in g-C_3N_4 belonging to tri-s-triazine building blocks, as shown in Fig. 3.3c.[41] The bands in 2100-2200 cm^{-1} region are associated with cyano or azide group (−C≡N or −N−N≡N) and cumulated double bond (–N=C=N– or >C=C=N−) which were observed in the sample prepared at higher temperatures. These functional groups act as chromophores leading to change in color of the sample from white to light yellow at higher temperatures (Fig. 3.4). The band near 2172 cm^{-1} usually appears as a result of degradation of triazine ring (to cyano group (−C≡N) at higher temperatures to form melem (tri-s-triazine).[43, 44, 50, 51]

Fig. 3.4 Photograph of the catalyst with different sintered temperatures.

3.4.1.5. DRS UV-Vis spectroscopy

Figure 3.5a shows UV-Vis spectra at various stages of CNNT preparation, compared with the spectra of bulk g-C_3N_4. Melamine shows the characteristic absorption of π-π* and n-π* at 247 and 298 nm, respectively. However absorption at 261 nm for CNNT and g-C_3N_4 were assigned to π-π* transition[41, 43, 48, 49, 51] which lies in the range of π-π* transition for 1,3,5-triazine compounds. Additionally, strong absorptions at 297 and 375 nm correspond to the n-π*

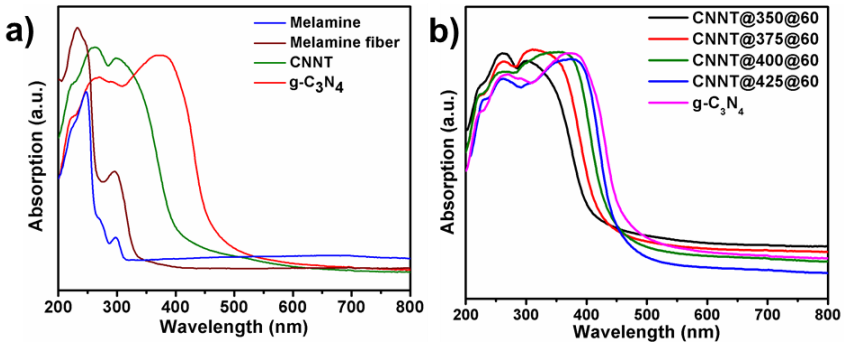

Fig. 3.5 UV-Vis spectra of (a) melamine, melamine fiber, CNNT and g-C_3N_4 and (b) UV-Vis spectra of CNNT at different sintering temperatures and g-C_3N_4.

transition of CNNT and g-C_3N_4 respectively.[48] The characteristic n-π* in case of g-C_3N_4 is towards lower energy. When we look at Fig. 3.5b the absorption correspond to n-π* has

relatively shifted from higher to lower energy with increasing sintering temperature of melamine fiber (from 297 to 372 nm), while absorption intensity corresponding to π-π* has decreased. This shift in the absorption of n-π* in CNNT eventually matches with the value of g-C_3N_4 with increasing sintering temperature. Similar trend was observed in FTIR studies reported earlier (Fig. 3.3b). Hence, it is clear evidence for the formation of tri-s-triazine rings from s-triazine at higher sintering temperatures.

3.4.1.6. X-ray photoelectron spectroscopy (XPS)

X-ray photoelectron spectroscopy (XPS) was used to investigate the types of nitrogen in these nitrogen and carbon containing frameworks. Generally, peaks corresponding to C 1s, N 1s and O 1s binding energies can be seen in the spectra (Fig. 3.6a). The N 1s spectra (Fig. 3.6b) are curve-fitted corresponding to four peaks with binding energies at 398.7, 399.9, 401.1 and 404.1 eV. These were assigned to graphitic nitrogen (C-N=C, **N1**), nitrogen coordinated trigonally to planar carbon atoms (N-C, **N2**), nitrogen belonging to amino groups (C_2-NH and C-NH_2, **N3**) and quaternary nitrogen (**N4**) respectively.[45, 51, 52]

Table 3.2 Different types of nitrogen in relative ratios from XPS.

Catalyst	Type of nitrogen (%)			
	N1	N2	N3	N4
CNNT@350@60	68.6	27.8	3.5	0
CNNT@375@60	68.6	26.9	4.4	0
CNNT@400@60	70.4	23.3	6.1	0
CNNT@425@60	68.9	21.6	9.4	0
g-C_3N_4 @ 520 °C	65.3	18.8	10.4	5.3

The above results shows evidence for the existence of graphite-like sp^2 bonded structure in these materials. The ratios of different nitrogen as shown in Table 3.2; demonstrate that there is an increase in the N3 nitrogen with increasing temperatures as a result of the formation of tri-s-triazine from s-triazine, which resulted in decrease in N2 nitrogen. The C 1s spectra (Fig. 3.6c) are curve-fitted into three peaks with binding energies at 284.6, 286.0 and 288.2 eV assigned to surface adsorbed carbon (**C1**), carbon associated with amino groups (C_2-NH and C-NH_2, **C2**) and graphitic carbon (C-N=C, **C3**), respectively.[52]

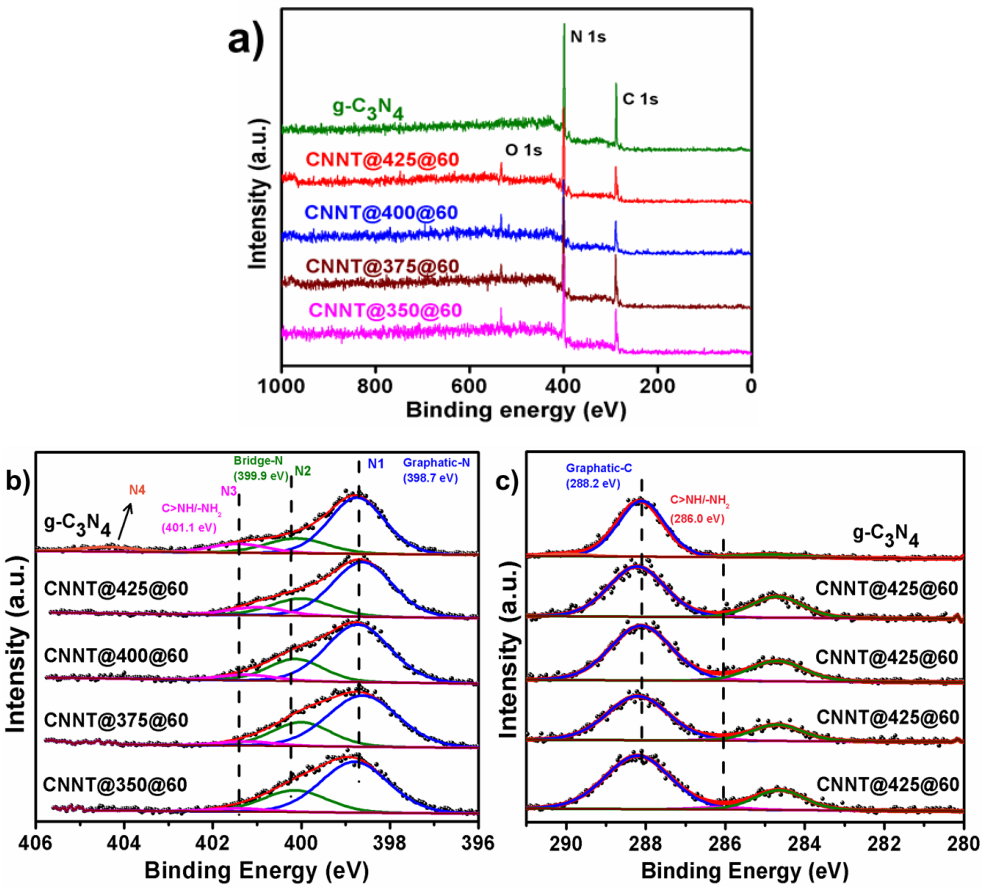

Fig. 3.6 XPS of various samples; (a) General XPS scan, (b) XPS of nitrogen 1s and (c) XPS of carbon 1s.

3.4.1.7. Nuclear magnetic resonance (NMR) spectroscopy of CNNT

Figure 3.7 shows ^{13}C CPMAS NMR spectra of all the samples. It is known that the melamine (s-triazine ring) has three sp^2-hybridized carbons with identical chemical environment[48, 53, 54], while melem (tri-s-triazine ring) has sp^2-hybridized carbons with two different chemical environments (see insert in Fig. 3.7a).[53-55] The ^{13}C spectra of melamine show chemical shift value at 168.0 ppm, while the sintered samples show a peak at 164.9 ppm pointing towards shielding in the s-triazine base polymeric network for the samples prepared at 350 °C, along with a shoulder (158.4 ppm) attributed to change in the chemical environment of carbon due to polymerization. A shift was observed of shoulder peak going from lower to higher temperatures during its formation (158.4 to 156.9 ppm). In case of g-C_3N_4, which is formed out of the tri-s-triazine polymeric network, has two types of chemical environments (164.78 and 156.5 ppm). Hence, this study clearly follows the changes in the carbon environment of the samples heated at different temperatures. It also shows that there is a change in the monomeric unit from s-triazine

to tri-s-triazine with increasing sintering temperature. The deshielded carbons are considered as more electrophilic than the shielded carbons. Similarly, deshielding was also observed in case of nitrogen atoms for the samples prepared at higher temperature as shown in Fig. 3.7b.

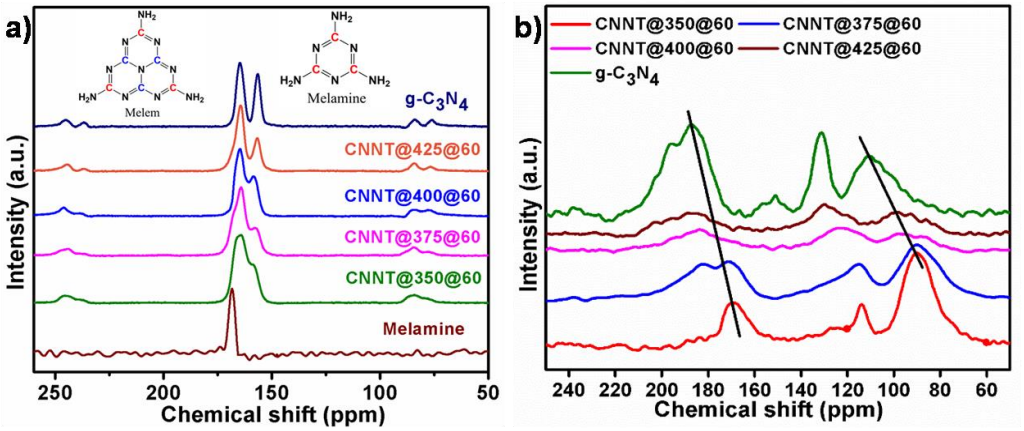

Fig. 3.7 CPMAS NMR of melamine and samples heated at different temperatures. (a) ^{13}C and (b) ^{15}N.

3.4.1.8. Scanning Electron Microscopy (SEM) of CNNT

Morphology of catalysts prepared at 350 and 400 ^{o}C were studied using FE- SEM and the results are given in Fig. 3.8. It was observed that there is a change in morphology of the

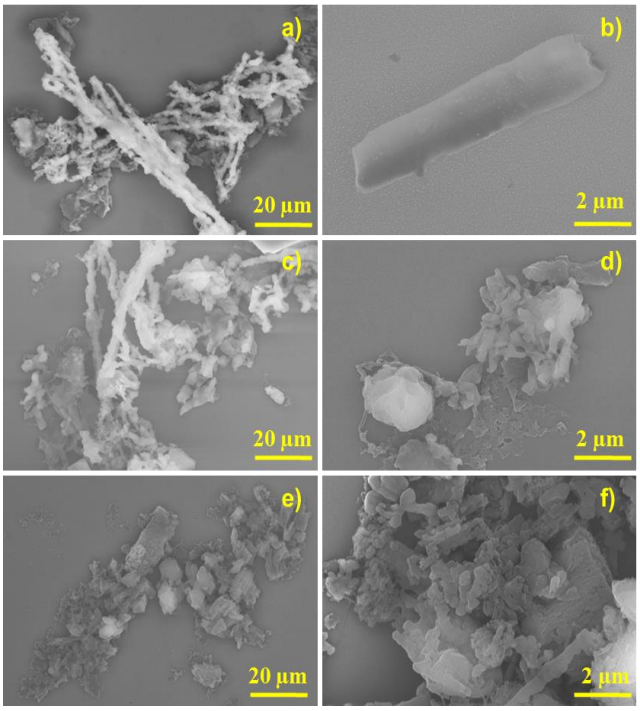

Fig. 3.8 SEM images of fresh catalyst; CNNT@350@60 (a,b); CNNT@400@60 (c,d) and g-C_3N_4 (e,f).

samples (CNNT@350 to CNNT@400) prepared at two temperatures. The bulk g-C_3N_4 has sheet/plates like morphology (Fig. 3.8e-f), while the CNNT@350 shows tubular morphology, probably due to s-triazine rings (Fig. 3.8a-b).[42] Whereas, on increasing the temperature for formation of catalyst, this morphology was changed slightly from tube to sheet form as may be observed in Fig. 3.8c-d. This may be due to secondary condensation as discussed in the TGA section. As a result, formation of the tri-s-triazine ring from triazine may lead to the opening of tube to sheet form due to changes in thermodynamic conditions.

3.4.2. Catalytic activity of CNNT

The CNNT catalysts were evaluated in liquid phase using a batch reactor for selective oxidation of p-xylene under various experimental conditions to check their activity and selectivity with respect to temperature, solvent, catalyst amount and O_2 pressure.

3.4.2.1. Effect of solvent

The influence of solvent on the catalytic activity in PX oxidation was investigated over CNNT@350@60 catalyst at 170 °C under 10 bar O_2 pressure (Fig. 3.9).

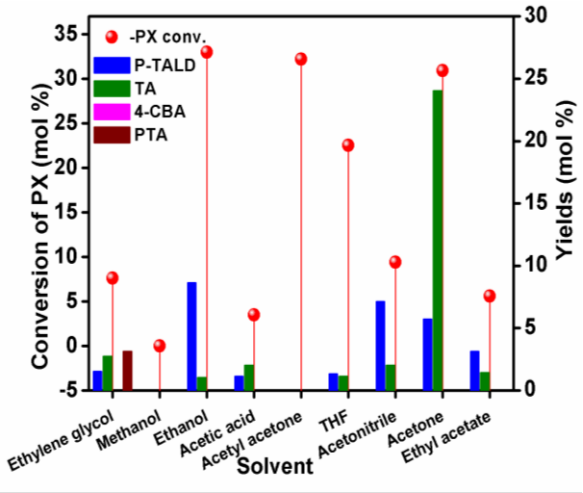

Fig. 3.9 Effect of solvent on oxidation of p-xylene.

Reaction conditions: PX (10 mmol); catalyst (CNNT@350@60) 50 mg; solvent (18.5 mL); temperature (170 °C); oxygen pressure (10 bar); reaction time (6 h).

Solvents of different chemical nature like protic solvents (methanol, ethanol, ethylene glycol and acetic acid) and aprotic-polar solvents (acetone, ethyl acetate, acetonitrile, THF and acetyl acetone) were used to find out the suitable solvent for the reaction. It was found that the

catalyst dissolves when protic solvents like ethylene glycol, methanol and acetic acid are employed. Ethylene glycol and acetic acid show poor activity. In ethanol, PX conversion of 33 mol% with yields of 8.6 mol% p-Tolualdehyde (P-TALD) and 1 mol% of p-toluic acid (TA) were obtained. It was observed that the ethanol participates in the reaction resulting in unwanted by-products (ethyl ester and ethyl ethers), thereby lowering the selectivity of desired products. Aprotic-polar solvents such as THF and acetyl acetone also competed with PX substrate for active sites and resulted in side reactions. Among the other aprotic polar solvents; acetonitrile, acetone and ethyl acetate were found to be relatively better without giving any unwanted by-products compared to the solvents used above. Among these solvents, acetone was found to be the best with PX conversion of 30.9 mol% with TA and P-TALD yields of 24.1 and 5.7 mol% (Fig. 3.9). Based on these results acetone was chosen as the solvent of choice for further investigations.

3.4.2.2. Comparison of various catalysts

Various CNNT catalysts sintered at different temperatures were evaluated and compared with g-C_3N_4 (Table 3.3). It was observed that g-C_3N_4 shows lower activity than CNNT and among the CNNT catalysts activity reduced when sintered at high temperatures. As discussed in characterization sections, structural changes occur when samples are sintered at higher than a desired temperature, leading to changes in properties of the materials. This led to reduction in the activities of the catalysts. It is also to be noted that there is no formation of PTA under the reaction conditions studied. Hence, the reaction conditions have to be further optimized with respect to temperature, O_2 pressure, reaction time *etc* using CNNT@350@60 catalyst.

Table 3.3. Product distribution for oxidation of PX using different catalysts.[a]

Entry	Catalyst	Conv. (mol%)	Yield (mol%)			
			P-TALD	TA	4-CBA	PTA
1	CNNT@350@60	30.9	5.7	24.1	0	0
2	CNNT@375 @60	20.1	6.2	13.9	0	0
3	CNNT@400 @60	17.7	6.0	11.5	0	0
4	CNNT@425 @60	10.4	5.5	3.5	0	0
5	g-C_3N_4	11.1	5.0	3.9	0	0
6	No catalyst	4.5	3.3	<1	0	0

[a] Reaction conditions: PX (10 mmol); catalyst (50 mg); acetone (18.5 mL); temperature (170 °C); oxygen pressure (10 bar); reaction time (6 h). P-TALD = p-Tolualdehyde. TA = p-Toluic acid. 4-CBA = 4-Carboxybenzoic acid. PTA = Pure terephthalic acid.

3.4.2.3. Effect of temperature

Influence of reaction temperature was studied using CNNT@350@60 catalyst. Reaction got initiated at temperatures ≥140 °C, while no reaction occurred below this temperature even after 6 h. This shows that there is a threshold energy required for the reaction to occur. Increase in the temperature led to a linear increase in PX conversion.[15] But, the PTA formation occurred only at high temperatures in the 190 - 200 °C zone, when maintained for 6 h (Fig. 3.10).

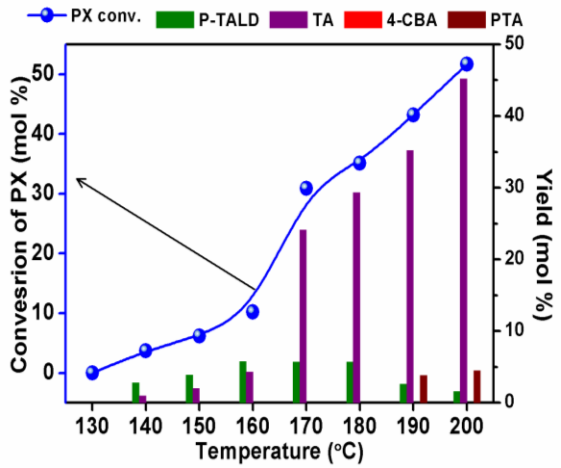

Fig. 3.10 Effect of temperature on selective oxidation of p-xylene.

Reaction conditions: p-Xylene (10 mmol); catalyst (CNNT@350@60, 50 mg); acetone (18.5 mL); O_2 pressure (10 bar); reaction time (6 h).

These findings clearly show that the threshold energy required for the activation of PX is reasonably lower, as it has an electron donating -CH_3 group, to give P-TALD. But, much higher activation is required for the formation of PTA, as it has to form via the activation of toluic acid (TA), which has an electron withdrawing group (-COOH). This reduces the activity of methyl group of TA. At higher reaction temperatures (>190 °C), solvent (acetone) also participates in the reaction resulting in the formation of impurities like acetic acid by C-C bond cleavage. Hence, the reaction should not be conducted at higher temperatures. Further studies were carried out at a temperature of 170 °C while varying other reaction parameters for the optimization.

3.4.2.4. Effect of oxygen pressure

Effect of oxygen pressure was systematically investigated at reaction temperature of 170 °C. Gradual increase in the PX conversion was observed with increase in O_2 pressure (Fig. 3.11).[27] The PTA formation was observed only at high O_2 pressures in the region of 15-20 bar.

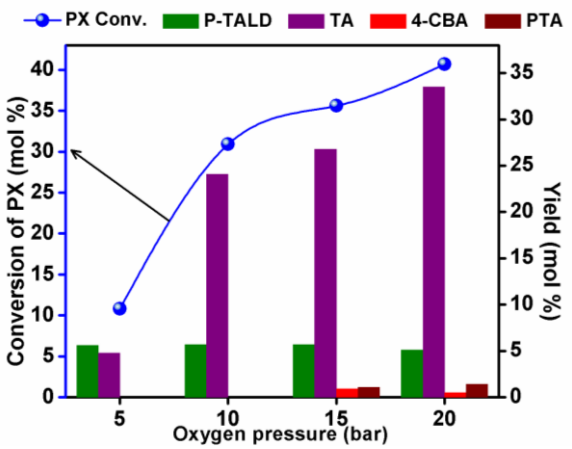

Fig. 3.11 Effect of oxygen pressure on p-xylene oxidation.

Reaction conditions: p-Xylene (10 mmol); catalyst (CNNT@350@60, 50 mg); acetone (18.5 mL); reaction time (6 h); temperature (170 °C).

The O_2 pressure has a profound influence on PX conversion and product formation. As per reports by Raghavendrachary *et al*., "The rate of oxidation of TA to PTA (secondary oxidation) is proportional to the square root of O_2 partial pressure".[23] which shows that oxidation in secondary step increases at high O_2 partial pressure. This can be clearly seen in the region of 15-20 bar (Fig. 3.11). Thus increase in the O_2 pressure has a positive effect on the reaction. Possibly, this effect of increased O_2 pressure on the rate of reaction is due to increased solubility of O_2, which may be readily available for the reaction. It is also to be noted that the solubility of oxygen in acetone is high when compared with other solvents employed in this study.[56, 57]

3.4.2.5. Effect of catalyst amount

Different catalyst contents were used in the reaction to find its influence on PX conversion and product yields. It was found that there is a rise in the PX conversion from 40.7 to 70.4 mol% with an increase in the catalyst amount from 50 to 100 mg, with PTA yield of 22.1 mol% for 100 mg of catalyst (Fig. 3.12). But, a further increase in the catalyst amount to 150 and 200 mg resulted in a drop in the conversion of PX and in lower PTA yields. The decrease in the PX conversion was due to the formation of acetic acid in good concentration from acetone at high catalyst contents, and the formation of acetic acid might have led to the solubility of catalyst, as discussed earlier with regard to solvent effect on this reaction.

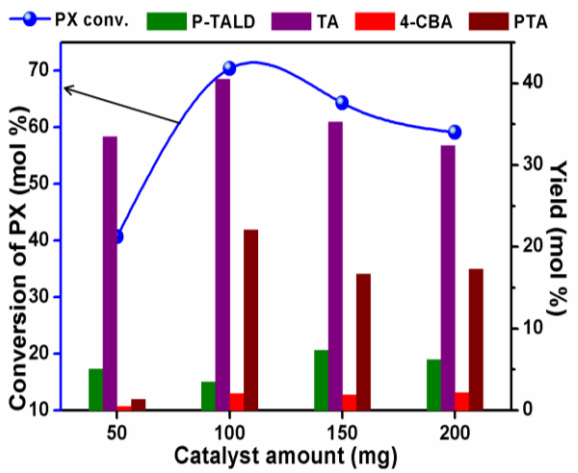

Fig. 3.12 Effect of catalyst amount on p-Xylene oxidation.

Reaction conditions: p-Xylene (10 mmol); CNNT@350@60 catalyst; acetone (18.5 mL); O_2 pressure (20 bar); reaction time (6 h); temperature (170 °C).

3.4.2.6. Time on stream study of PX oxidation

Considering the influence of all the above discussed parameters, time on stream study of the CNNT@350@60 catalyst was investigated. As shown in Fig. 3.13, linear increase (17.4 to 94.5 mol%) in the PX conversion was observed with increasing reaction time (from 3 h to 12 h).

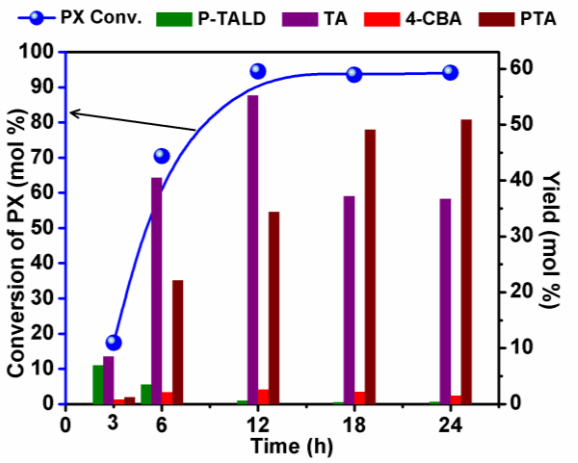

Fig. 3.13 Time on stream study on p-Xylene oxidation.

Reaction conditions: p-Xylene (10 mmol); catalyst (CNNT@350@60, 100 mg); acetone (18.5 mL); oxygen pressure (20 bar); temperature (170 °C).

Conversion remained same thereafter up to 24 h (94.1 mol%). However, the yield of PTA has increased from 34.4 to 50.9 mol%, with simultaneous decrease in the TA yield from 55.2 to 36.7 mol%. After 12 h on stream, TA was 55.2 mol% while PTA was 34.4 mol%, the later increased

by 14.7 mol% on prolonging the reaction for further 6 h, with a simultaneous reduction in TA yield. Since the formation rate of TA from PX is high when compared to the rate of formation of PTA from TA, longer durations are required to for achieving high yields of PTA. In the beginning, PX is the only substrate molecule that competes for the active catalytic sites. But, with the reaction proceeding further, formation of other products like P-TALD, TA and 4-CBA also compete for the active sites along with PX, resulting in a reduced rate of reaction for PTA. As discussed earlier, the activation energy required for TA conversion is much higher than that required for activation of PX. The oxidation of PX to TA is a 4 step reaction involving three intermediates (Scheme 3.1).The rate of lumped reaction is pseudo-first-order and the rate constants for each step decreased in the following order: k2 (TALD - TA) > k4 (4-CBA - TA) > k1 (PX - TALD) > k3 (TA - 4-CBA). These reported results are in good agreement with our experimental observations.[27]

3.4.2.7. Recyclability of the CNNT catalyst

The recyclability of the CNNT@350@60 catalyst was investigated by repeating the PX oxidation reaction multiple times with the same catalyst (Fig. 3.14), as per the procedure describe below.

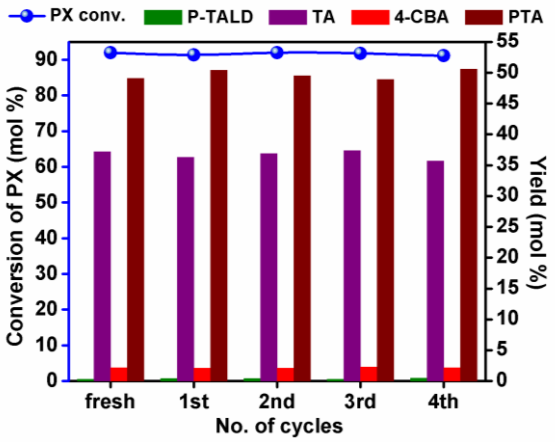

Fig. 3.14 Recyclability study in oxidation of PX to PTA over CNNT@350@60.

Reaction conditions: mole to wt. ratio of PX to catalyst (0.1); solvent (acetone, 18.5 mL); O_2 pressure (20 bar); temperature (170 °C); time (18 h).

After each reaction run, 0.5 mL of the reaction mixture was filtered using nylon 0.22 µm filter and injected into GC-FID. To the rest of the reaction mixture, desired amount of NaOH and

methanol (7:3) was added and filtered. The solution obtained was diluted to 25 mL of methanol and analyzed by HPLC. The catalyst was washed three times with 20 mL of NaOH in methanol mixture and dried at 60 °C for 6 h and re-used for the next cycle. The recycle results are given in Fig. 3.14 that clearly show that the performance of the catalyst remains almost same even after being re-used for four times. These results demonstrate excellent stability of the catalyst.

3.4.2.8. Effect of diluent gas

Table 3.4 Product distribution on oxidation of PX.[a]

Entry	Reaction parameter	Conv. of PX (mol%)	Selectivity of PTA (%)	Yield (mol%)				Solvent burn (Area %)
				P-TALD	TA	4-CBA	PTA	
1	100%O_2	93.5	52.5	0.3	37.2	2.2	49.1	2.8
2[b]	50%O_2+ 50%N_2	92.1	48.8	0.9	41.8	1.8	45.0	1.9
3[c]	25%O_2 + 75%N_2	62.0	26.4	4.5	39.7	0.4	16.4	1.1
4[d]	O_2/TEMPO	<1	0	<1	0	0	0	0

[a] Reaction conditions: PX (10 mmol); catalyst (CNNT@350@60, 100 mg); solvent (acetone,18.5 mL); temperature (170 °C); oxygen pressure (20 bar); reaction time (18 h). [b] N_2 (10 bar), O_2 (10 bar). [c] N_2 (15 bar), O_2 (5 bar). [d] TEMPO (10 mmol); reaction time (12 h). P-TALD = p-Tolualdehyde. TA = p-Toluic acid. 4-CBA = 4-Carboxybenzoic acid. PTA = Terephthalic acid.

To investigate the effect of partial pressure of oxygen on the catalytic activity, N_2 was used as diluent while keeping the total pressure constant. When N_2 was used along with O_2, the PX conversion decreased to 92.1 and 62.0 mol%, respectively for 50 and 75% N_2 containing mixtures respectively from 93.5 mol% obtained in pure O_2. The formation of PTA has also decreased with reduction in the partial pressure of O_2 as the formation of PTA from TA is directly proportional to O_2 partial pressure (Table 3.4).[23] However, dilution of O_2 with N_2 has considerable influence on solvent loss due to burn up (Table 3.4). Solvent loss (based on area %) for 100% O_2, 50% O_2+N_2, and 25% O_2+N_2 were 2.8, 1.9 and 1.1%, respectively.

3.4.2.9. Effect of xylene isomer

The catalytic activity of CNNT catalysts was further investigated using different isomers of xylenes. The reaction was conducted for a period of 12 h (Table 3.5). The conversion has decreased in the order p-xylene > o-xylene > m-xylene. This may be attributed to the less resonance stabilization of the radical intermediate formed at the meta position when compared to

para and ortho positions.[33] Formation of di-acid follows the order of terephthalic acid, isophthalic acid and phthalic acid. While the formation of intermediate toluic acid follows the order of para > ortho > meta substitution, the so formed o-toluic acid tend to form phthalide (18.2 mole %) and phthalic anhydride (14.9 mole %) under the reaction conditions that decreases the formation of phthalic acid.[32] The presence of intermediate alcohols like m-tolylmethanol, o-tolylmethanol and 2-(hydroxymethyl) benzoic acid were noticed for both meta and ortho-xylenes, while they were absent in case of para-isomer. Since the presence of carboxylic group decreases the rate of reaction, in the order of para > meta > ortho substitution, the activity is decreased in the same order for di-acid formation. This clearly shows that the presence of electron donating and withdrawing groups on the ring play key role during the reaction.

Table 3.5 Product distribution during oxidation of various xylene isomers.[a]

Entry	Substrate	Conv. of xylene (mol%)	Yield (mol%)						
			Tolyl methanol	Tolualde-hyde	Toluic acid	(hydroxy methyl) benzoic acid	Carboxy benzoic acid	di-acid[e]	others
1[b]	PX	94.5	-	0.6	55.2	-	2.6	34.4	-
2[c]	MX	39.2	1.5	5	19.8	-	0	13.4	-
3[d]	OX	91.1	2.4	1	44	8.7	-	-	35.8

[a] Reaction conditions: xylene (10 mmol); catalyst (CNNT@350@60, 100 mg); solvent (acetone,18.5 mL); temperature (170 ° C); oxygen pressure (20 bar); reaction time (12 h).[b] all are 'para' substituted products. [c] All are 'meta' substituted products. [d] All are 'ortho' substituted products. [e] Terephthalic acid, isophthalic acid and phthalic acid.

3.4.2.10. Mechanistic studies

To investigate the reaction mechanism of oxidation of PX to PTA, we have added 2,2,6,6-Tetramethylpiperidine 1-oxyl (TEMPO) to the reaction mixture (Table 3.4, Entry 4). As a result, the free radicals generated during the reaction are trapped by TEMPO, thus hindering further reaction. This evidence shows that the reaction proceeds through radical formation. FTIR of the reaction mixture containing TEMPO shows no difference in the FTIR spectrum before and after the reaction (Fig. 3.15a), while reaction mixture in the absence of TEMPO showed peaks that belongs to products such as carbonyls and acid groups (1735-1745 cm^{-1}) (Fig. 3.15b). The activation of substrate and O_2 are the chain initiation steps required for the reaction to start, followed by its propagation and termination.

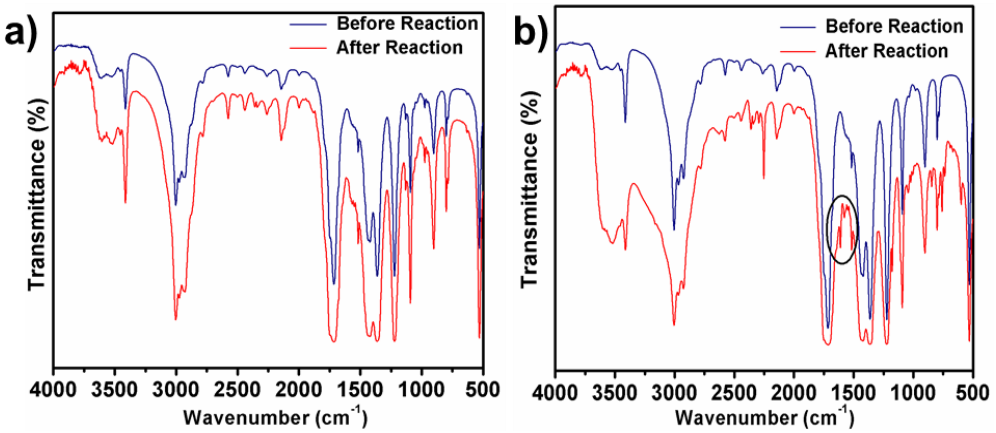

Fig. 3.15 FTIR spectrum of reaction mixture a) with TEMPO and b) without TEMPO.

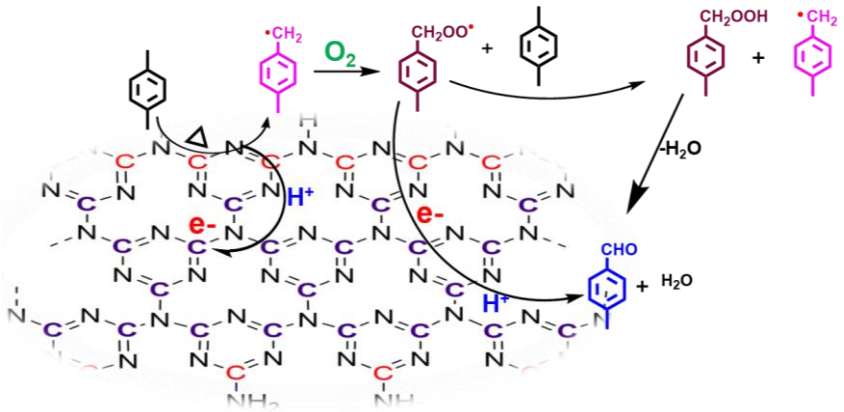

Scheme 3.2. Schematic illustration of oxidation of p-Xylene over CNNT via radical intermediates to give terephthalic acid.

As depicted in scheme-3.2, substrate molecule is initially adsorbed on the catalyst surface, through abstraction of an electron from the substrate by catalyst. In the process, one hydrogen atom is removed to form an alkyl radical (1st step). Then, the generated alkyl radical reacts with O_2 to form peroxy radical (ROO·) (2nd step), which subsequently transforms into alkyl hydroperoxide (3rd step). Water is released from this peroxy radical to give aldehyde (4th step). This propagation is a cyclic process and involves regeneration of the catalyst to its original state. Electron-donor groups such as $–CH_3$ groups on the ring decrease the reactivity of the peroxy radical, by lowering the electron withdrawing power of the peroxy group (the electron density over oxygen atoms increases). Thus, the peroxy radical ($CH_3–C_6H_4–CH_2OO·$) formed in the first step is less reactive for undergoing further oxidation to give $COOH–C_6H_4–CH_2OO·$.[10] A detailed reaction pathway in PX oxidation to PTA is depicted below in Scheme 3.3.

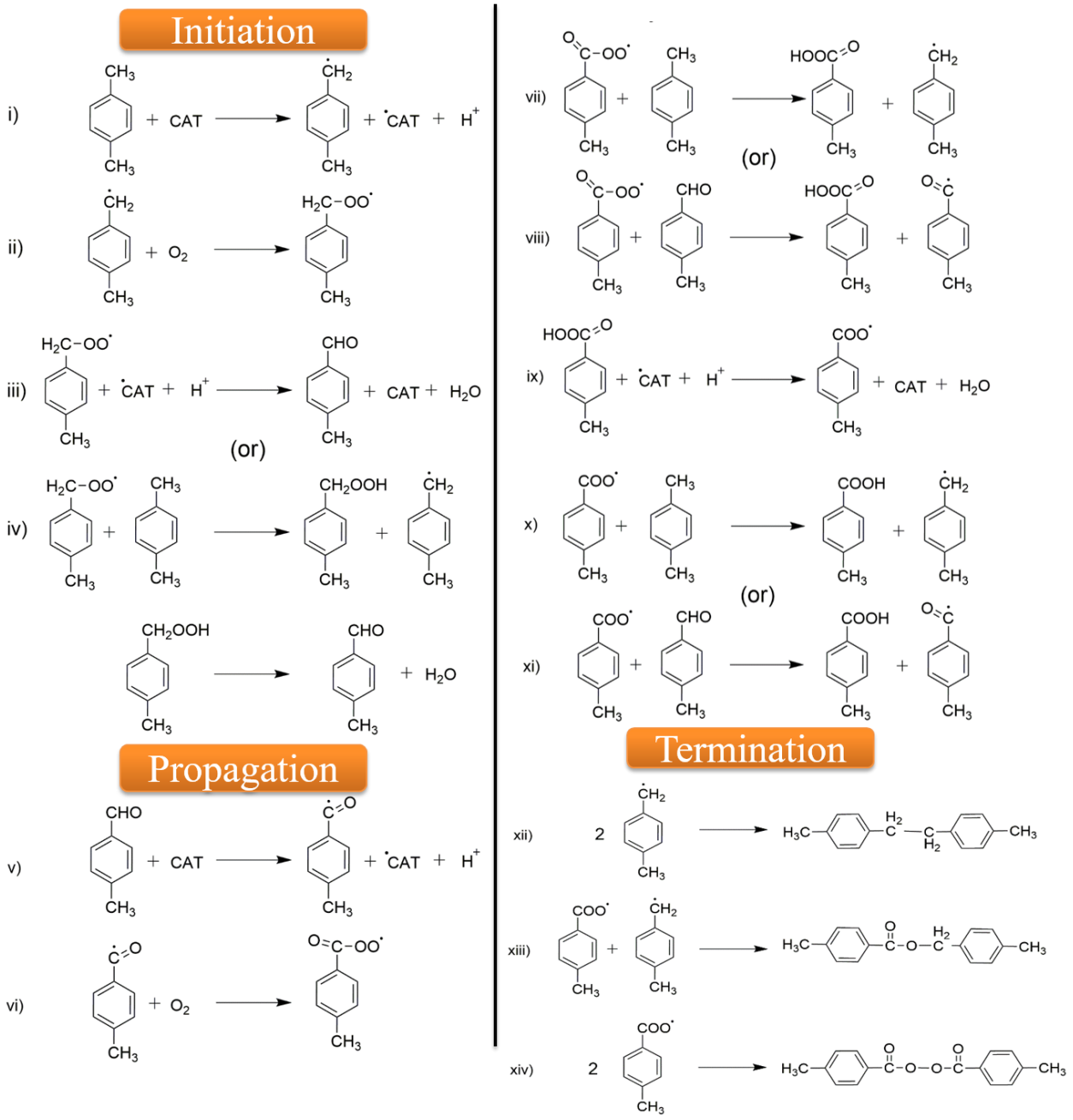

Scheme 3.3. The possible steps involved in the oxidation of PX to PTA via a free radical pathway.

The electron transfer is favored from the substrate to the "C" atoms present on the catalyst (in ring) and vice versa as illustrated in Scheme-3.2. These carbon atoms are electron deficient (electrophilic carbons) due to adjacent nitrogen in the catalyst and these nitrogen's are high in CNNT@350@60 as per MASNMR. The electron deficiency generates +ve charge on the carbon, where it can accommodate electrons in its molecular orbitals (LUMOs) for compensating

charge balance. The number of electrophilic carbons decreased when the catalyst is sintered at higher temperatures (Fig. 3.7). In the case of s-triazine based catalyst (CNNT@350@60) the density of electrophilic carbons atoms are higher than in tri-s-triazine based catalyst (CNNT@425@60). These electrophilic carbons may act as charge/electron carrier due to slight charge (δ^+) on carbon atoms. Superior activity of s-triazine based catalyst (CNNT@350@60) compared to tri-s-triazine based catalyst can be attributed to these differences. Therefore, it can be concluded that electrophilic carbons in the catalyst are the active centers and the catalytic activity is enhanced with their increased numbers.[58] Hence, generation of these electrophilic carbons through substitution of nitrogen is important for getting good hydrocarbon oxidation activity.

3.5 Oxidation of PX by CNNT in presence of an initiator

Though CNNT catalysts are active for PX oxidation, the time required for the reaction to be completed is very high and higher reaction temperatures have to be used for complete conversion of PX to PTA. Hence, we used various initiators to circumvent these issues.

3.5.1. Influence of type of initiator

To find out the appropriate initiator, we have employed *N*-Hydroxyphthalimide (NHPI) and *N*-hydroxysuccinimide (NHSI) as initiators (Table 3.6).

Table 3.6 Influence of the type of initiator.[a]

Entry	Initiator	Conv. of PX (mol%)	PTA selectivity (%)	Yield (mol%)			
				P-TALD	TA	4-CBA	PTA
1	1%NHPI+CNNT	47.7	4.8	6.3	37.4	0	2.3
2	1%NHSI+CNNT	50.0	5.5	5.5	39.1	1.7	2.8
3	CNNT	40.7	3.4	5.1	33.5	0.5	1.4

[a] Reaction conditions: P-xylene (10 mmol); catalyst (50 mg); solvent (acetone, 18.5 mL); temperature (170 °C); oxygen pressure (10 bar); initiator (1 mol %); reaction time (6 h); stirring speed (8000 rpm). P-TALD = P- Tolualdehyde. TA = P-Toluic acid. 4-CBA = 4-Carboxy benzoic acid. PTA = Pure terephthalic acid.

It was observed that the formation of PTA has increased along with the PX conversion with the addition of just 1 mol% of the initiator. NHSI gave higher PX conversion than NHPI, while no 4-CBA was found in the product when NHPI was used as the initiator (Table 3.6).

4-CBA is an intermediate product during the formation of PTA from PX, which has physical properties similar to that of PTA. Presence of 4-CBA will result in the termination of chain propagation step during polymerization of PTA. Hence, 4-CBA has to be removed through hydrogenation to ppm levels, which is a costly step in the PX to PTA process. Hence, it is better if it is not part of the product stream.

3.5.2. Effect of amount of initiator

The PTA yield was very low when the initiator used is only 1mol %. In order to achieve higher PX conversion, better PTA yields and to reduce the intermediates in the product mixture, initiator (NHPI) concentration was varied. The increase in the amount of NHPI from 1 to 10 mol% resulted in increased PX conversion from 47.7 to 92.3 mol% with enhanced (2.3 to 73.9 mol%) yield of PTA (Table 3.7). With the increase in the amount of NHPI, no 4-CBA formation was observed in the product and the amount of P-TALD also decreased from 6.3 to 0 mol%. We observed that presence of initiator (NHPI) increases the rate of reaction as well as decreases the formation of reaction impurities/intermediates similar to P-TALD and 4-CBA by rising PTA selectivity. Prolonging the reaction time further from 6 to 12 h, resulted in increasing PX conversion to 96.5 mol% accompanied by much better (89.1 mol%) yield of PTA.

Table 3.7 Product distribution in PX oxidation using variable amounts of initiator.[a]

Entry	Initiator (mol %)	Conv. of PX (mol%)	Selectivity of PTA (%)	Yield (mol%)			
				P-TALD	TA	4-CBA	PTA
1	1	47.7	4.8	6.3	37.4	0	2.3
2	5	92.4	54.9	0.8	39.7	0	51.4
3	10	92.3	79.9	0.0	17.5	0	73.9
4[b]	10	96.5	92.3	0.0	7.2	0	89.1

[a] Reaction conditions: P-xylene (10 mmol); Initiator (NHPI); catalyst (50 mg); solvent (acetone,18.5 mL); temperature (170 ^{o}C); oxygen pressure (10 bar); reaction time (6 h); stirring speed (1000 rpm). [b] reaction time (12 h). P-TALD = P-Tolualdehyde. TA = P-Toluic acid. 4-CBA = 4-Carboxy benzoic acid. PTA = Pure terephthalic acid.

3.6. Conclusions

A metal-free CNNT catalyst was synthesized at various sintering temperatures and used for the selective oxidation of PX to PTA by using molecular oxygen. In addition, a non-corrosive

solvent acetone was used for the batch reaction. Initially, the catalytic activity was investigated in the absence of an initiator. Catalyst (CNNT@350@60) synthesized at an optimum sintering temperature (350 ^{o}C) exhibited very good activity compared to other catalysts sintered at lower or higher side of this temperature. The presence of s-triazine ring as building block with a tubular morphology in the catalyst appears to be crucial in achieving superior catalytic activity. The experimental results clearly show that reaction proceeds through the free radical mechanism. Based on the results of investigations, a possible reaction pathway is proposed for the oxidation of PX to PTA. Under the optimized reaction conditions, without using any initiator, 49.1 mol% PTA yield at 93.5 mol% PX conversion was obtained after 18 h. The catalyst could be recycled more than four times.

The presence of an initiator enhanced the rate of reaction, with simultaneous reduction in the formation of unwanted byproducts (P-TALD and 4-CBA) accompanied by increased PTA selectivity. The concentration of initiator concentration was optimized for getting high PX conversion and high PTA yield. A maximum of 96.5 mole% PX conversion and 89.1 mol% PTA selectivity's were achieved by using 10% NHPI initiator in the reaction mixture. These results clearly show that it is possible to prepare PTA from PX using a metal free catalyst.

3.7. References

1. Akkihebbal Krishnamurthy Suresh; Man Mohan Sharma; Tamarapu Sridhar. *Ind. Eng. Chem. Res.* **2000,** 39, 3958-3997.
2. Richard J. Sheehan, Terephthalic Acid, Dimethyl Terephthalate and Isophthalic Acid. In *Ullmann's Encyclopedia of Industrial Chemistry*, Wiley-VCH Verlag GmbH & Co. KGaA, Weinheim: United States, 2011; Vol. 36, pp 17-28.
3. Sumanta Kumar Meher; Justin P.; Ranga Rao G. *Nanoscale* **2011,** 3, 683–692.
4. Meng Li; Fenghui Niu; Daryle H. Busch; Bala Subramaniam. *Ind. Eng. Chem. Res.* **2014,** 53, 9017-9026.
5. Alfred Satfer; Bayside N. Y.; Barker, R. S. Preparation of aromatic polycarboxylic acids. May 6, 1958.
6. Rogerio A. F. Tomas; Joao C. M. Bordado; Joao F. P. Gomes. *Chem. Rev.* **2013,** 113, 7421−7469.
7. Falcon H.; Campos-Martin J. M.; Al-Zahrani S.M.; Fierro J.L.G. *Catal. Commun.* **2010,** 12, 5-8.
8. Yasushi Yoshino; Yoshiaki Hayashi; Takahiro Iwahama; Satoshi Sakaguchi; Yasutaka Ishii. *J. Org. Chem.* **1997,** 62, 6810-6813.
9. Basudeb Saha; Nobuyoshi Koshino; James H. Espenson. *J. Phys. Chem. A* **2004,** 108, 425-431.
10. A. L. Plekhov; O. V. Kushch; I. O. Opeida; M. A. Kompanets. *Russ. J. Appl. Chem* **2014,** 87, 982-985.
11. Yasutaka Tashiro; Takahiro Iwahama; Satoshi Sakaguchi; Yasutaka Ishii. *Adv. Synth. Catal.* **2011,** 343, 220-225.
12. Issa Yavari; Elham Karimi. *Synth. Commun.* **2009,** 39, 3420-3427.
13. Youwei Cheng; Xi Li; Qinbo Wang; Lijun Wang. *Ind. Eng. Chem. Res.* **2005,** 44, 7756-7760.
14. Wei Zeng; Jianzhang Li; Shengying Qin. *Supramol. Chem.* **2004,** 16, 569-572.
15. Quan Jiang; Yang Xiao; Ze Tan; Qing-Hong Li; Can-Cheng Guo. *J. Mol. Catal. A: Chem.* **2008,** 285, 162-168.
16. Milan Hronec; Zdenek Hrabe. *Ind. Eng. Chem. Prod. Res. Dev.* **1986,** 25, 257-261.
17. David Raju Burri; Ki-Won Jun; Young-Ho Kim; Ji Man Kim; Sang-Eon Park; Jin S. Yoo. *Chemistry Letters* **2002**, 212-213.

18. Ian C. Chisem; John Rafelt; M. Tantoh Shieh; Janet Chisem (née Bovey); James H. Clark; Roshan Jachuck; Duncan Macquarrie; Ramshawb, C.; Keith Scottb. *Chem. Commun.* **1998**, 1949-1950.

19. Paul Ratnasamy; Darbha, S. *Catal. Today* **2009,** 141, 3-11.

20. Ghiaci M.; Mostajeran M.; Gil A. *Ind. Eng. Chem. Res.* **2012,** 51, 15821-15831.

21. Kalyanjyoti Deori; Dinesh Gupta; Basudeb Saha; Sasanka Deka. *ACS Catal.* **2014,** 4, (3169-3179).

22. Aguadero A.; Falcon H.; Campos-Martin J. M.; Al-Zahrani S. M.; Fierro J. L. G.; Alonso J. A. *Angew. Chem. Int. Ed.* **2011,** 50, 6557-6561.

23. Pavagada Raghavendrachar; Subramania Ramachandran. *Ind. Eng. Chem. Res.* **1992,** 31, 453-462.

24. Giacomo cao; Massima Pisux; Massimo Morbidelli. *Chem. Eng. Sci.* **1994,** 49, 5775-5778.

25. Alberto Cincotti; Roberto Orru Á; Giacomo Cao. *Catal. Today* **1999,** 52, 331-347.

26. Qinbo Wang; Xi Li; Lijun Wang; Youwei Cheng; Gang Xie. *Ind. Eng. Chem. Res.* **2005,** 44, 4518-4522.

27. Kuo-Tseng Li; Shih-Wei Li. *Appl. Catal. A: Gen.* **2008,** 340, 271-277.

28. Walt Partenheimer. *Appl. Catal. A: Gen.* **2014,** 481, 183-189.

29. Eduardo Garcia-Verdugo; Joan Fraga-Dubreuil; Paul A. Hamley; W. Barry Thomas; Keith Whistonb; Martyn Poliakoff. *Green Chem.* **2005,** 7, 294-300.

30. Joan Fraga-Dubreuil; Eduardo Garcia-Verdugo; Paul A. Hamley; Eva M. Vaquero; Lucinda M. Dudd; Ian Pearson; Duncan Housley; Walt Partenheimer; W. Barry Thomas; Keith Whistonb; Martyn Poliakoff. *Green Chem.* **2007,** 9, 1238–1245.

31. Eduardo Perez; Joan Fraga-Dubreuil; Eduardo Garc´ıa-Verdugo; Paul A. Hamley; Morgan L. Thomas; Chong Yan; W. Barry Thomas; Duncan Housley; Walt Partenheimerc; Martyn Poliakoff. *Green Chem.* **2011,** 13, 2397-2407.

32. Eduardo Perez; Joan Fraga-Dubreuil; Eduardo Garc´ıa-Verdugo; Paul A. Hamley; W. Barry Thomas; Duncan Housley; Walt Partenheimer; Martyn Poliakoff. *Green Chem.* **2011,** 13, 2389-2396.

33. Eduardo Garcia-Verdugo; Eleni Venardou; W. Barry Thomas; Keith Whiston; Walter Partenheimer; Paul A. Hamley; Martyn Poliakoff. *Adv. Synth. Catal.* **2004,** 346, (307-316).

34. Jennifer B. Dunn; Douglas I. Urquhart; Phillip E. Savage. *Adv. Synth. Catal.* **2002,** 344, 385-392.

35. Dae Sung kim; Young Ho Shin; Youn-Woo Lee. *Chem. Eng. Commun.* **2014,** 202, 78-84.

36. Xiaobin Zuo; Fenghui Niu; Kirk Snavely; Bala Subramaniam; Daryle H. Busch. *Green Chem.* **2010,** 12, 260-267.

37. Meng Li; Thomas Ruddy; Darryl Fahey; Daryle H. Busch; Bala Subramaniam. *ACS Sustainable Chem. Eng.* **2014,** 2, (823-835).

38. Kelly K. Miller; Peng Zhang; Yukari Nishizawa-Brennen; John W. Frost. *ACS Sustainable Chem. Eng.* **2014,** 2, 2053-2056.

39. Vishnu Malpani; Pralhad A. Ganeshpure; Pradip Munshi. *Ind. Eng. Chem. Res.* **2011,** 50, 2467-2472.

40. Qinbo Wang; Youwei Cheng; Lijun Wang; Haibo Xu; Xi Li. *Ind. Eng. Chem. Res.* **2008,** 47, 5861-5870.

41. S. C. Yan; Z. S. Li; Zou, Z. G. *Langmuir* **2009,** 25(17), 10397–10401.

42. Jun Gao; Yong Zhou; Zhaosheng Li; Shicheng Yan; Nanyan Wang; Zhigang Zou. *Nanoscale* **2012,** 4, 3687-3692.

43. Qixun Guo; Qing Yang; Lei Zhu; Chengqi Yi; Shuyuan Zhang; Yi Xie. *Solid State Commun.* **2004,** 132, (369-374).

44. Qixun Guo; Qing Yang; Chengqi Yi; Lei Zhu; Yi Xie. *Carbon* **2005,** 43, 1386–1391.

45. Arne Thomas; Anna Fischer; Frederic Goettmann; Markus Antonietti; Jens-Oliver Muller; Robert Schloglb; Johan M. Carlsson. *J. Mater. Chem.* **2008,** 18, 4893–4908.

46. David M. Teter; Russell J. Hemeley. *Science* **1996,** 271, 53-55.

47. May H., Pyrolysis of melamine. *J. appl. Chem.* **1959,** 9, 340-344.

48. Valery N. Khabashesku; John L. Zimmerman; John L. Margrave. *Chem. Mater.* **2000,** 12, 3264-3270.

49. Qixun Guo; Yi Xie; Xinjun Wang; Shuyuan Zhang; Tao Hou; Shichang Lv. *Chem. Commun.* **2004**, 26–27.

50. John L. Zimmerman; Robert Williams; Valery N. Khabashesku; John L. Margrave. *Nano Lett.*, **2001,** Vol. 1, No. 12, 731-734.

51. Qixun Guo; Yi Xie; Xinjun Wang; Shichang Lv; Tao Hou; Xianming Liu. *Chem. Phys. Lett.* **2003,** 380, 84–87.

52. Zhengxin Ding; Xiufang Chen; Markus Antonietti; Xinchen Wang. *ChemSusChem.* **2011,** 4, 274-281.

53. Jan Sehnert; Kilian Baerwinkel; Juergen Senker. *J. Phys. Chem. B* **2007,** 111, 10671-10680.

54. Andreas Sattler. Investigations into s-Heptazine-Based Carbon Nitride Precursors. The Ludwig Maximilian University of Munich, Munich, 2010.

55. Barbara Jurgens; Elisabeth Irran; Jurgen Senker; Peter Kroll; Helen Muller; Wolfgang Schnick. *J. Am. Chem. Soc.* **2003,** 125, 10288-10300.

56. Takashi Sato; Yuzo Hamada; Masaru Sumikawa; Sadao Araki; Hideki Yamamoto. *Ind. Eng. Chem. Res.* **2014,** 53, 19331−19337.

57. Golovanov I. B.; Zhenodarova S. M. *Russ. J. Gen. Chem.* **2005,** 75, 1795-1797.

58. Dang Sheng Su; Jian Zhang; Benjamin Frank; Arne Thomas; Xinchen Wang; Jens Paraknowitsch; Schlçgl, R. *ChemSusChem.* **2013,** 3, 169-180.

Chapter 4

Vapor-Phase Oxidation of Benzyl alcohol over Manganese based Oxides, in presence of molecular O_2

4.1. Introduction

Selective oxidation of organic molecules is an important area of research, as many industrially important chemicals and chemical intermediates are obtained through this route. Among selective oxidations, conversion of alcohols to aldehydes is important in the perfume industry.[1] Benzaldehyde is the second most important aromatic molecule with wide commercial applications,[2] it is used as an intermediate in the production of fine chemicals, in flavoring industries, pharmaceutical, foods and cosmetics manufacture.[1] Hence, production of benzaldehyde (BzH) through partial oxidation of benzyl alcohol (BzOH) is highly significant in this connection. Currently, BzH is produced commercially through the liquid phase hydrolysis of benzal chloride and oxidation of toluene. The other methods developed are the partial oxidation or dehydrogenation of BzOH, carbonylation of benzene and the ruthenium-catalyzed oxidation of styrene with periodate or hypochlorite etc.[1]

4.2. Literature background on the oxidation of benzyl alcohol

Benzyl alcohol undergoes variety of reactions depending on the nature of the catalyst and reaction conditions employed. Some of the transformations are (a) partial oxidation to form BzH, benzoic acid and benzyl benzoate,[3] (b) disproportionation to form BzH, toluene and water,[4] (c) dehydration to form dibenzyl ether and (d) self-condensation (benzylation) to form anthracene and stilbene.[5, 6] There are extensive reports on the partial oxidation of alcohols to aldehydes in batch reactors using different catalysts.[7-27] While liquid phase batch reactions require a long time to reach steady state, some of the researchers focused on green approaches such as solvent-free processes;[8, 11, 14, 22, 28] using green oxidants like air/O_2;[7, 10, 12, 14, 18-20, 23] and by means of photocatalysis.[29] Hutchings *et al*, demonstrated solvent-free oxidation of BzOH using supported Au-Pd/TiO_2 nanoparticulate catalysts, in which toluene is formed as a by-product due to disproportionation. The addition of Pd to Au increases the rate of disproportionation, while Au sites do not catalyze the formation of disproportionation products. Further studies by change in the support from TiO_2 to MgO and ZnO suppressed the disproportionation even using Au-Pd as active catalyst.[9]

Choudhary *et al* achieved 100% conversion of BzOH at 94 °C by using TBHP as oxidant and Au/MgO as catalyst with 72.5% BzH yield.[8] Palladium supported on different organosilane-functionalized carbon nanotubes were studied for solvent-free aerobic oxidation of BzOH by

Yibo Yan *et al*.[14] Gold nanoparticles encapsulated in metal-organic frameworks used under solvent-free conditions with O_2 as oxidant at atmospheric pressure to get 53.8% conversion of BzOH and 53.7% BzH yield.[16] CoMgAl hydrotalcites containing different Mg^{2+} contents was investigated with TBHP as the oxidant.[20] Mg^{2+} ions promoted the oxidation process of Co^{2+} to Co^{3+} leading to improved catalytic activity.[17] Effects of Ce and Fe addition to nanostructured MnOx was explored, along with reaction mechanism, kinetics and deactivation pattern of this catalyst in BzOH oxidation.[21] DRIFT studies were used to analyze the fresh and used catalysts, the formation of benzoic acid hindered the oxidation through strong adsorption on active sites leading to deactivation of the catalyst.[18, 19] Benzyl alcohol conversion of 83.6% with 98.0% of BzH selectivity was achieved with 2wt% Pd/carbon nanotubes (CNTs) with toluene and water as solvents in presence of K_2CO_3.[20] Recently carbon quantum dots were reported as catalysts for partial oxidation of benzyl alcohol by Xiao Zhang *et al*, they achieved 99.9% BzH selectivity at BzOH conversion of 75% using NaClO as the oxidant.[24] All these reactions conducted in liquid phase involve costly separation of catalysts, hence have less commercial feasibility.

Recently, there were some reports on partial oxidation of BzOH in the vapor-phase, using air/molecular oxygen as oxidant. These oxidants are favored as they generate only H_2O as a by-product, thus leading to atom economy and a green chemical process. Some of the reported results are shown in Table 4.1.

Table 4.1. Summary of selected BzOH vapor-phase oxidation processes.

Entry	Catalyst	Conv. (%)	Yield (%)	Selectivity (%)	T (°C)	Ref.
1	Cu−Na−ZSM-5	84.4	71.1	84.2	400	[30]
2	5wt% Ag/SiO_2	84.4	84	99.5	350	[31]
3	$Ca-Ag/SiO_2$	66.9	66.7	99.6	240	[32]
4	Co/NaY	-	45	-	350	[33]
5	1% $Au-Cu/SiO_2$	98	98	99	313	[34]
6	$K-Cu-20TiO_2$	72	70.5	98	203	[35]
7	Ag/Ni−fiber	84	78.9	94	380	[36]
8	Nanoporous gold (NPG)	58.1	55.3	95.1	240	[37]
9	2.81 wt% Ag−HMS	100	96	96	310	[38]
10	Au/TiO_2	79	79	100	320	[39]
11	H−OMS−2	92	91.1	99	210	[40]

Results in Table 4.1 show a broad range of reaction temperatures. All catalysts show 95-100% selectivity for BzH (except Entry 1), with a range of conversions between 58-100%. In terms of atom economy and green chemistry point of view selectivity is a primary parameter for any catalytic process compared to BzOH conversion. Ag and Au on various supports are active for the BzOH partial oxidation. From the above Table, it is evident that they are active in the range of 240-350 °C. Though some reactions are transition metal catalyzed like Co/NaY[33] and Cu−Na-ZSM-5,[30] they need higher reaction temperatures of 350 and 400 °C when compared to slightly lower temperatures for noble metal catalyzed BzOH oxidation. Fan J. *et al* have reported BzOH oxidation just above the boiling point of BzOH with 72% conversion and 98% selectivity to BzH using K-Cu-20TiO_2 as catalyst.[35] Naftali N. Opembe *et al* reported OMS-2 as catalyst for the vapor phase oxidation, they achieved 92% conversion of BzOH with 99% BzH selectivity at a low reaction temperature of 210 °C.[40] These studies, with catalyst comprising Cu^{2+} and $Mn^{3/4+}$, show very good activity for partial oxidation of benzyl alcohol.

Here, in our study we have used transition metal oxides as a catalysts with different oxidation states of manganese such as MnO (+2), Mn_2O_3 (+3), MnO_2 (+4) and a mixed oxidation state of Mn in the form of Mn_3O_4 (+2, +3), which is a spinel (AB_2O_4) to find their activity in the absence of any noble metal. Manganese oxides with different oxidation states such as MnO, Mn_2O_3, Mn_3O_4, MnO_2 and K-OMS-1 were studied in the batch by Fanny Schurz *et al* and showed that MnO_2 is more active among them.[41] The activity and the stability of the catalysts was correlated to the ionic state of the manganese, with Co and Cu as the dopant metals; being active for the selective oxidation of BzOH.[10, 30, 33-35] The effect of dopant in the spinel, the substitution of dopant in A or B site were studied by XPS.

4.2.1. Vapor phase oxidation of BzOH over copper incorporated Mn_3O_4

Attempts were made to develop a vapor phase partial oxidation process for BzOH using transition metal oxides (Mn, Cu and Co mixed oxides) in the absence of any noble metal. This reaction was studied to find best experimental conditions for the selective vapor-phase oxidation,

by studying the BzOH flow rate, reaction temperature, oxidant to substrate ratio, amount of catalyst and its composition. 10% of O_2 was used as an oxidant (O_2 + N_2) under optimized reaction conditions. The role of dopant was investigated by using different physico-chemical techniques and how it influences the steady state activity and stability during time on stream (TOS) of the reaction.

4.3. Experimental procedures

4.3.1. Materials and characterization

Benzyl alcohol, Benzaldehyde, benzoic acid, MnO_2, $Mn(OAc)_2{\cdot}4H_2O$, $Cu(OAc)_2{\cdot}H_2O$, $Co(OAc)_2{\cdot}4H_2O$ and KOH were purchased from Merck, India, while MnO was obtained from Alfa-Asser. All the chemicals were used as received without any further purification. The catalysts were characterized using powder XRD, BET surface area, TGA, TPD of CO2 and ammonia, TPR and XPS.

4.3.2. Evaluation of catalysts

Catalysts were evaluated in down flow, fixed bed stainless steel reactor tube placed in a two-zone split furnace (13mm id and mm length, Geomechanique, France). The reaction data were collected at atmospheric pressure in the temperature zone of 260-320 °C, using 0.5 g of the catalyst particles in the range of 180-300 microns. The catalyst bed temperature was continuously monitored by a Cr–Al thermocouple. Before the reaction, catalysts were activated in presence of air (30 ml/min) at 450 °C for 6 h, followed by cooling to the reaction temperature in presence oxidant (50 ml/min). The reactant was fed to the reactor using a high-precision syringe pump (ISCO Model 500D) at required flow rate. The reactant was vaporized in the upper zone of the reactor (pre-heating zone) before it entered the catalyst bed. The product mixture was cooled using a chilled water condenser and collected in a gas-liquid separator. Analysis of the product mixture was done at regular intervals using a GC (Agilent 7890A) equipped with a flame

ionization detector (FID) and HP-5 capillary column (50 m length, 0.32 mm diameter). All the products were identified using pure authentic standards and by using GC-MS (Agilent MS-5975C single Quadruple in EI mode). Conversion of BzOH was calculated based on the fraction of BzOH reacted, while the BzH selectivity was calculated based on its percentage among the total products.

4.4. Results and discussion

4.4.1. Catalyst characterization

4.4.1.1. X-ray diffraction (XRD)

XRD of MnO, MnO_2 and Mn_2O_3 show that the MnO_2 is in tetragonal form while MnO and Mn_2O_3 are with cubic lattice (JCPDS Nos. 81-2261, 77-2363 and 71-0636 respectively). XRD patterns of fresh and spent Cu and Co doped Mn_3O_4 catalysts are shown in Fig. 4.1. The sample without cobalt/copper show Mn_3O_4 with hausmannite structure (JCPDS file No. 24-734, tetragonal) after calcination at 500 °C. A small amount of Mn_5O_8 (JCPDS file No. 39-1218) was also found in freshly calcined Mn_3O_4 sample. The diffraction lines at 2θ values of 39.27, 47.76 and 66.16 are assigned to Mn_5O_8. In addition to Mn_5O_8, a small concentration of Mn_2O_7 (peak at 21.49°, JCPDS file No. 27-0083) was also found in the Mn_3O_4 catalyst. The hausmannite structure did not undergo any change after incorporation of cobalt and copper in small amounts.

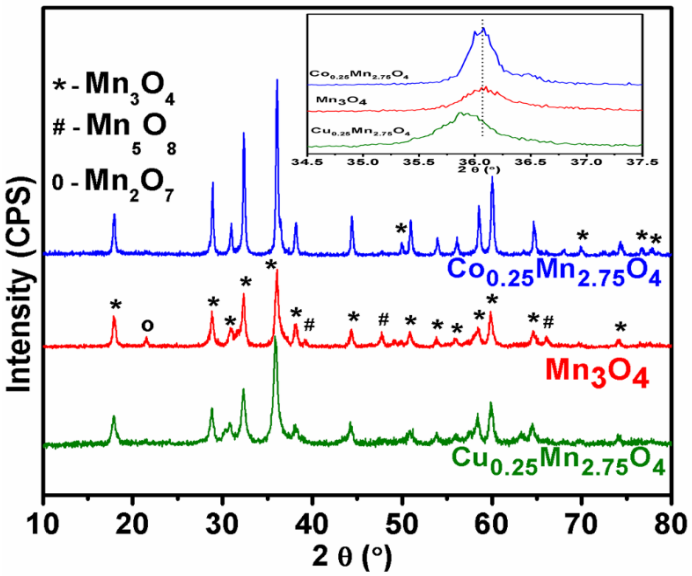

Fig. 4.1. XRD of fresh Mn_3O_4, copper and cobalt doped catalyst.

The absence of individual cobalt and copper oxides in respective samples indicate the substitution of cobalt and copper into the manganese oxide (Mn_3O_4) lattice.[44, 45] A clear shift in 2θ values was observed for all the peaks, this was shown for the peak at 2θ ~36 as an inset (Fig. 4.1). The peaks have shifted to lower 2θ for copper containing samples[46] and slightly to higher side for cobalt[44] containing catalysts. Cell parameters show a gradual transformation of tetragonal spinel to cubic (i.e., a decrease in "c" value and an increase in "a" value) with gradual increase in copper content. The respective values are a = 5.7540 and c = 9.4072 Å for Mn_3O_4, a = 5.7560 and c = 9.3912 Å for $Cu_{0.125}Mn_{2.875}O_4$, a = 5.7616 and c = 9.3658 Å for $Cu_{0.25}Mn_{2.75}O_4$ and a = 5.7640 and c = 9.2456 Å for $Cu_{0.5}Mn_{2.5}O_4$, respectively (Table 4.2).

XRD of spent catalysts after 8 h of BzOH partial oxidation at 300 °C, are shown in Fig. 4.2. No changes observed in case of Mn_3O_4, $Cu_{0.125}Mn_{2.875}O_4$, $Cu_{0.25}Mn_{2.75}O_4$, $Co_{0.25}Mn_{2.75}O_4$ and MnO catalysts after the reaction and hence no phase change was observed for these catalysts. No individual oxides of cobalt/copper were observed in spent catalysts (Fig. 4.2a, b, c, e and h). In spent $Cu_{0.5}Mn_{2.5}O_4$ there is formation of MnO phase at 2θ - 40.4 (Fig. 4.2d). In Mn_2O_3 spent catalyst there is formation of Mn_3O_4 phases at 2θ -17.92, 23.16, 29.26 and 36.40 (Fig. 4.2f). On the other hand MnO_2 catalyst has changed completely to Mn_3O_4 oxide (JCPDS no. 80-0382) after the reaction (Fig. 4.2g).

4.4.1.2. N_2-Physisorption

BET surface areas of all the catalysts are given in Table 4.2. It was observed that the surface area of the copper doped catalyst increased compared to the parent spinal (Mn_3O_4),[46] while the surface area of the cobalt doped catalysts decreased. The increase in the surface area of the copper catalyst might be due to decrease in the crystallite size, which was clearly observed from XRD investigations. The presence of cobalt increases the crystallite size and decreases the surface area. The results shows change in the cell parameter of tetragonal form of Mn_3O_4 as a result of dopant metal. Calculated and actual wt.% of metals present in the samples is also given in Table 4.2.

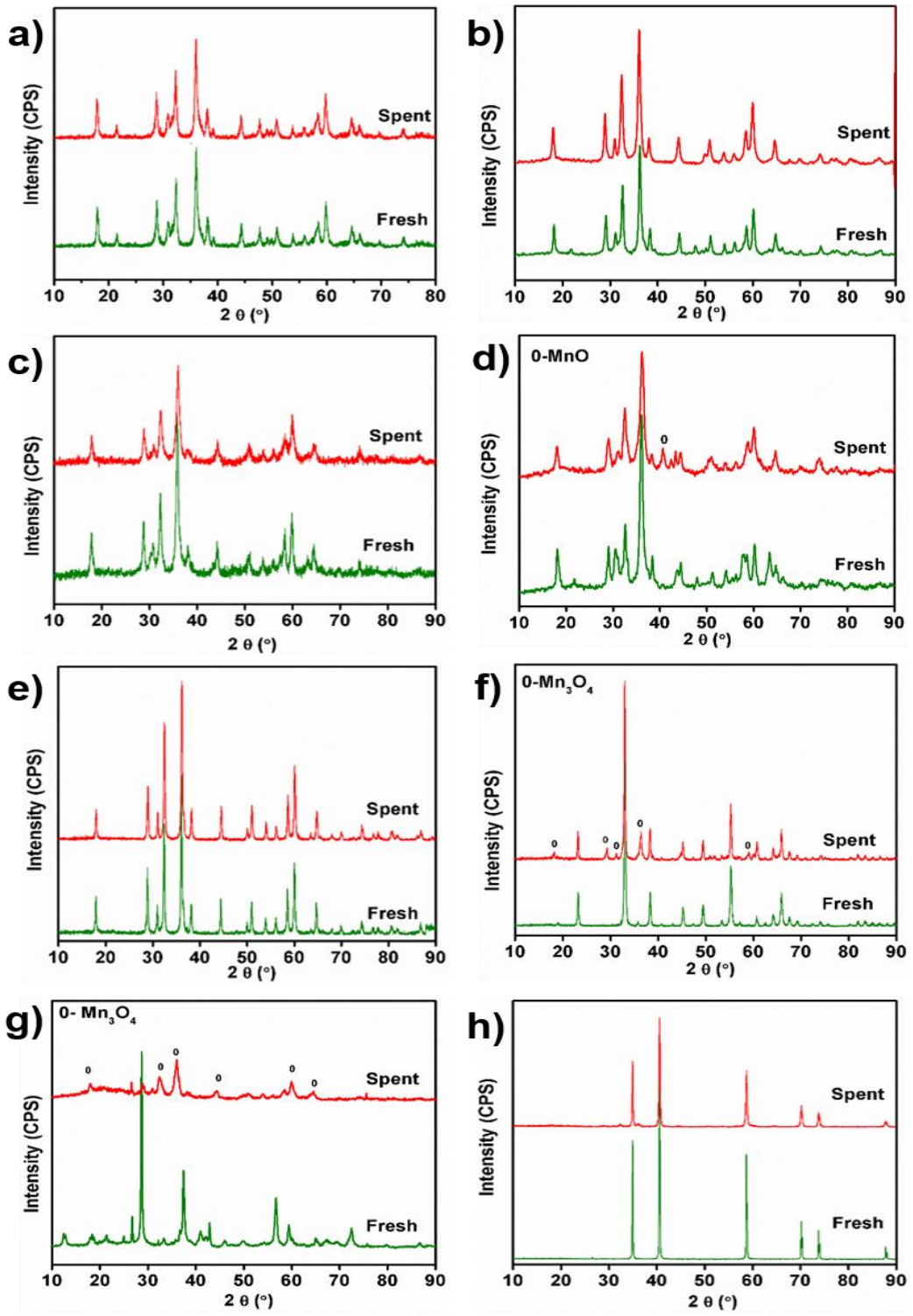

Fig. 4.2. XRD of fresh and spent catalyst of (a) Mn_3O_4, (b) $Cu_{0.125}Mn_{2.875}O_4$, (c) $Cu_{0.25}Mn_{2.75}O_4$, (d) $Cu_{0.5}Mn_{2.5}O_4$, (e) $Co_{0.25}Mn_{2.275}O_4$, (f) Mn_2O_3, (g) MnO_2 and (h) MnO.

Table 4.2 Catalyst composition, crystallites size and BET surface area values of copper/cobalt-manganese oxide ($M_xMn_{3-x}O_4$) catalysts.

S. No	Catalyst	Metal concentration (wt%)[a]		Cell parameter (Å)		Crystallite size (nm)	S_{BET} (m^2/g)
		Mn	Cu/Co	a	b		
1	MnO	76.8(77.4)[b]	-	4.4425	-	70.7(42.9)[c]	10.2
2	Mn_2O_3	67.6(69.5)	-	4.6880	-	34.1(41.2)	18.2
3	MnO_2	63.8(63.1)	-	4.4003	2.8682	38.4(35.0)	18.0
4	Mn_3O_4	71.6(72.0)	-	5.7540	9.4072	21.6(18.3)	21.5
5	$Co_{0.25}Mn_{2.75}O_4$	66.9(70.5)	6.6(6.8) [b]	5.7532	9.5346	41.6(39.5)	16.1
6	$Cu_{0.125}Mn_{2.875}O_4$	67.5(68.7)	2.9(3.4)	5.7560	9.3912	21.5(16.0)	34.5
7	$Cu_{0.25}Mn_{2.75}O_4$	64.3(65.3)	6.2(6.8)	5.7616	9.3658	17.8(12.3)	37.1
8	$Cu_{0.5}Mn_{2.5}O_4$	53.6(58.9)	14.1(13.7)	5.7640	9.2456	13.2(11.4)	41.3

(a) Chemical analysis values are obtained from ICP-OES. (b) Numbers in brackets are expected values based on input metal. (c) Values of used catalysts.

4.4.1.3. Thermo gravimetric analysis (TGA)

Thermogravimetric analysis of fresh and spent catalyst of Mn oxides with different oxidation states +4, +3, +2, combination of +3 & +2 of MnO_2, Mn_2O_3, MnO, Mn_3O_4, and copper/cobalt doped Mn_3O_4 respectively are shown in Fig. 4.3. For fresh samples, no weight loss was observed for Mn_2O_3, while there is a slight weight loss for Mn_3O_4 above 600 °C (Fig. 4.3a), it was found that at high temperatures (>600 °C) Mn_3O_4 tend to form more stable oxides like Mn_2O_3 (determined by heating the Mn_3O_4 at 600 °C for 6 h, 5 °C/min.). Two weight losses observed for MnO_2 at >300 °C and at >600 °C (Fig. 4.3a), both weight loss are due to rearrangement of MnO_2 into more stable Mn_3O_4 (>300 °C) and Mn_2O_3 (>600 °C) (determined by heating the MnO_2 at 500 and 600 °C for 6 h @ 5 °C/min.). In case of MnO, the gain in weight around 350 °C is due to oxidation of Mn^{2+} (in MnO) to higher oxides in the presence of air (Fig. 4.3a). Similar observations were made with spent MnO catalyst. In case of spent MnO_2 and Mn_3O_4, they show little weight loss at around 350 °C attributed to any adsorbed carbonaceous species. Whereas, Mn_2O_3 shows high weight loss at around 350 °C (~30%) due to removal of adsorbed carbonaceous (product) species (Fig. 4.3b). This study reveals that the presence of only Mn^{+3} doesn't help rapid desorption of product formed during the reaction. On the otherhand, Mn_3O_4 catalyst shows only 4% of weight loss at around 350 °C.

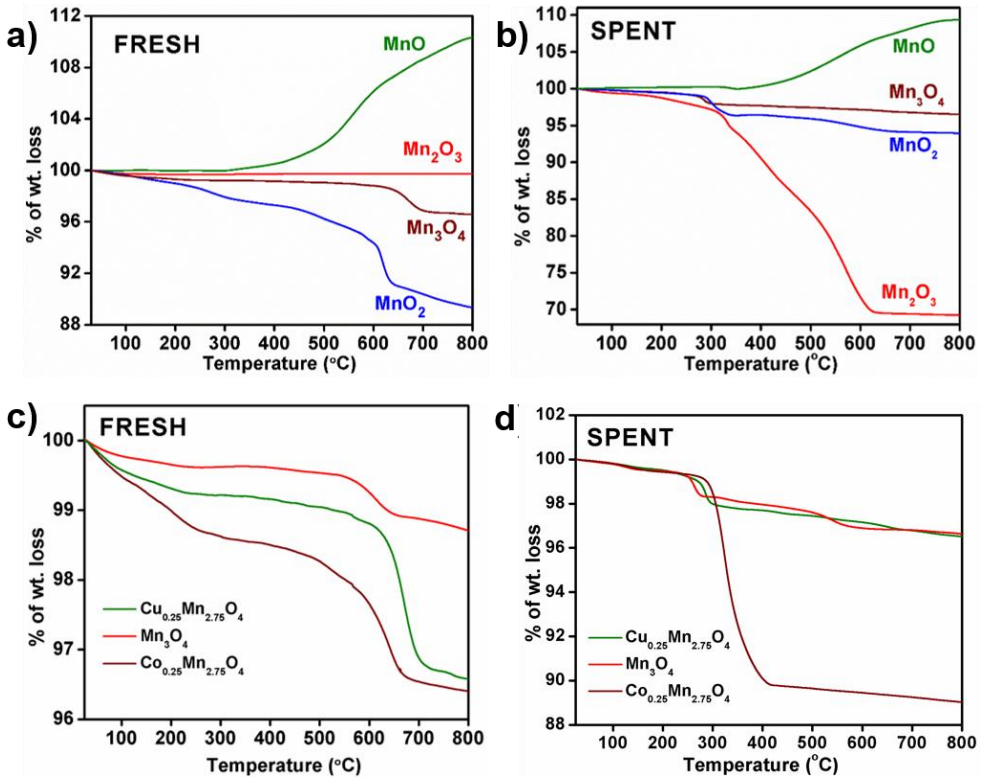

Fig. 4.3. TGA of fresh and spent catalysts of MnO, Mn_2O_3, MnO_2, Mn_3O_4, $Cu_{0.25}Mn_{2.75}O_4$ and $Co_{0.25}Mn_{2.75}O_4$ in air.

TGA of fresh cobalt or copper containing catalysts do not show substantial weight loss till 600 °C, the weight loss around >100 °C is due to the removal of water (Fig. 4.3c). The weight loss (~3.5%) above 600 °C is attributed to lattice rearrangement of the catalyst to form more stable oxide i.e., Mn_2O_3. In TGA of spent catalyst, a weight loss around 300-350 °C was observed for all the catalysts. This weight loss is attributed to the desorption of carbonaceous (product) species from the surface of the catalyst which was deposited during the reaction (Fig. 4.3d). The order of weight loss follows the order $Cu_{0.25}Mn_{2.75}O_4$ ~ Mn_3O_4 < $Co_{0.25}Mn_{2.75}O_4$, which implies that high amount of adsorbed species was present on Co doped catalyst compared to Cu doped Mn_3O_4. This indicates that the presence of Co does not help faster desorption of product species from the catalyst surface.

4.4.1.4 Temperature programmed reduction

Temperature programmed reduction (TPR) of samples with Mn in different oxidation states (+4, +3, +2) corresponding to MnO_2, Mn_2O_3, MnO and Mn_3O_4 oxides shows different reduction temperature maxima (Fig. 4.4). MnO_2 shows a single broad peak centered at around

310 °C with a shoulder, which may be attributed to step wise reduction of $Mn^{4+} \rightarrow Mn^{3+} \rightarrow Mn^{2+}$, while Mn_2O_3 show two sharp peaks centered at 286 and 398 °C assigned to the reduction of surface and bulk Mn^{3+}. Whereas, MnO shows only one reduction maximum centered around 368 °C. TPR profiles of freshly calcined Mn_3O_4 show two reduction peaks centered at 405 and 260 °C. These peaks may be assigned to the reduction of surface and bulk of Mn^{3+} (Fig. 4.4a).[46] Results Cu doped spinel demonstrate that the presence of Cu promotes Mn reduction, due to which a decrease in reduction temperature was observed on its incorporation, giving a broad low-temperature reduction peak at about 210 °C (Fig. 4.4b).[46] Co doped spinel shows three reduction peaks at 230 and 405 °C, assigned to reduction of Mn^{3+} at surface and bulk, and a high temperature reduction peak at >600 °C attributed to bulk Co^{3+} reduction (Fig. 4.4b).[47, 48] Results observed in our study are in agreement with those reported in literature for Cu doped spenels.[46]

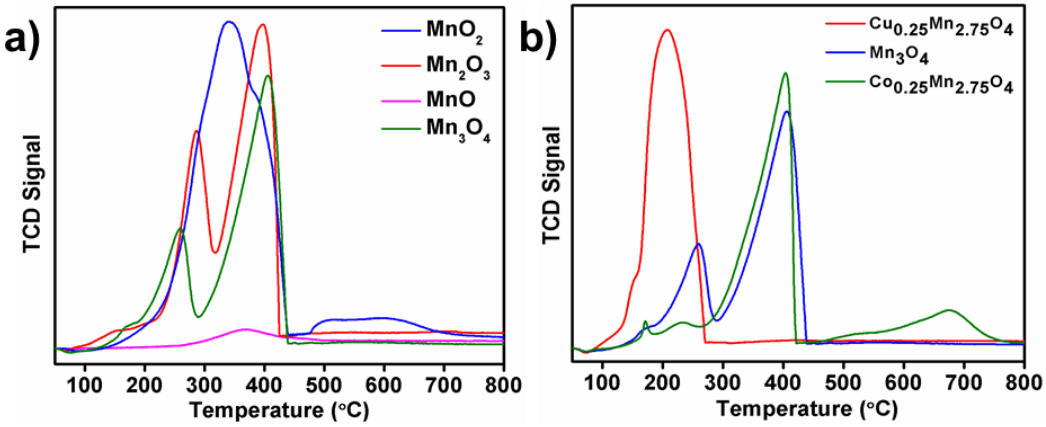

Fig. 4.4. TPR of (a) Mn with different oxidation states and (b) Mn_3O_4, $Cu_{0.25}Mn_{2.75}O_4$ and $Co_{0.25}Mn_{2.75}O_4$.

4.4.1.5. CO_2 and NH_3 -Temperature program desorption

The results of TPD of CO_2 and NH_3 of fresh catalysts are shown in Fig. 4.5. TPD of CO_2 shows that desorption occurs below 300 °C, with peaks centered around 177 °C for Mn_3O_4, at 155 and 240 °C for $Cu_{0.25}Mn_{2.75}O_4$; 162 and 289 °C for $Co_{0.25}Mn_{2.75}O_4$ catalysts (Fig. 4.5a). From the desorption curves, it is clear that catalyst have two kinds of sites for CO_2 binding on the surface of these catalysts, which may be attributed to weak and moderately strong basic sites. For copper containing catalyst, a shift in desorption peak towards lower temperature was observed for weak basic sites and increase in the strength of moderately strong basic sites was observed. The above results show that the overall basicity in $Cu_{0.25}Mn_{2.75}O_4$ is higher than that of Mn_3O_4 and $Co_{0.25}Mn_{2.75}O_4$ respectively.[46]

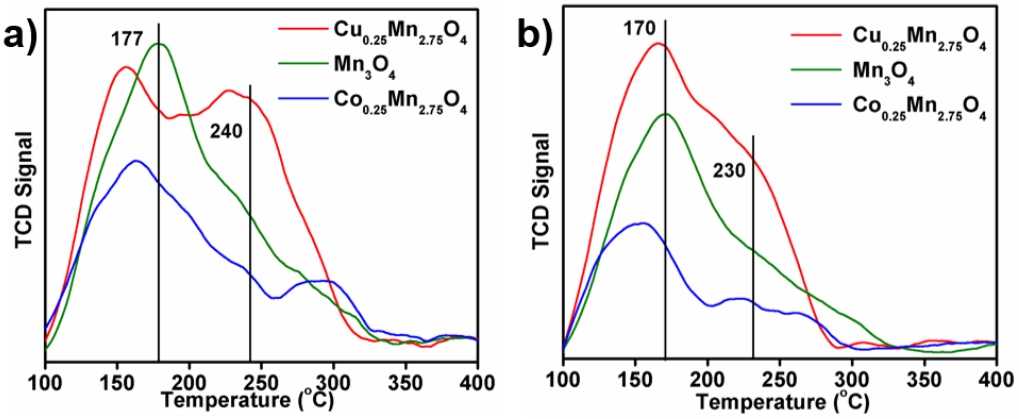

Fig. 4.5. TPD of Mn_3O_4, $Cu_{0.25}Mn_{2.75}O_4$ and $Co_{0.25}Mn_{2.75}O_4$; (a) CO_2-TPD and (b) NH_3-TPD.

Table 4.3. Surface acidity and basicity of copper/cobalt-manganese oxide ($M_xMn_{3-x}O_4$) catalysts by TPD.

S. No	Catalyst	CO_2 desorption T_{max} (°C)	CO_2 desorbed (μmol)	NH_3 desorption T_{max} (°C)	NH_3 desorbed (μmol)
1	Mn_3O_4	178	22.0	170	70.2
2	$Cu_{0.125}Mn_{2.875}O_4$	152	42.4	171	160.3
3	$Cu_{0.25}Mn_{2.75}O_4$	159	39.2	170	184.6
4	$Cu_{0.5}Mn_{2.5}O_4$	167	41.7	171	237.2
5	$Co_{0.25}Mn_{2.75}O_4$	167	16.5	155	55.0
6	Mn_2O_3	150	22.2	132	65.2
7	MnO_2	129	20.0	150	92.9
8	MnO	105	9.7	103	03.5

TPD of NH_3 of the above samples shows that desorption occurred below 300 °C, with peaks centered for Mn_3O_4 at 170 °C, $Cu_{0.25}Mn_{2.75}O_4$ at 166 and 230 °C and in the case of $Co_{0.25}Mn_{2.75}O_4$ the desorption peaks were at 152 and 225 °C (Fig. 4.5b). From the desorption curves, it is clear that catalysts have two kinds of binding sites for NH_3 on the surface of these catalysts, which may be attributed to acid sites of weak and moderate strength. In case of cobalt catalyst, a shift in desorption peak towards lower temperatures was observed for weak acidic sites. An increase in the strength of moderately strong acidic sites of the Cu doped catalyst was observed relative to Mn_3O_4 (Fig. 4.5b). The above results clearly show that the overall acidity and basicity in $Cu_{0.25}Mn_{2.75}O_4$ is relatively higher compared to Mn_3O_4 and $Co_{0.25}Mn_{2.75}O_4$. Doping of copper in Mn_3O_4 results in increased - acidity as well as basicity which is in agreement with our earlier report.[46] Further increase or decrease in the copper doping varies the

acid strength, but basic strength remains more or less same. Total acidity obtained from desorbed CO_2 and NH_3 are given in Table 4.3.

4.4.1.6. Temperature program desorption of O_2

Figure. 4.6 shows the O_2-TPD profiles of catalysts. The desorption peak around 100 °C is assigned to weekly adsorbed molecular O_2.[49] The desorption peak in the range of 350-375 °C is attributed to the desorption of adsorbed atomic oxygen and some lattice oxygen as O_2^-.[49, 50] The atomic oxygen species adsorb strongly compared to molecular oxygen species. In general the rate of dissociative adsorption of oxygen to atomic oxygen species is lower than that of molecular species adsorption.[49] The amount of adsorbed oxygen species such as O_2 and O_2^- on $Cu_{0.25}Mn_{2.75}O_4$ is higher than that on Mn_3O_4 or $Co_{0.25}Mn_{2.75}O_4$ (Fig. 4.6). This clearly demonstrates that the presence of copper increases the oxygen uptake capacity when compared to the cobalt substituted spinel ($Co_{0.25}Mn_{2.75}O_4$) and Mn_3O_4 at 300 °C.

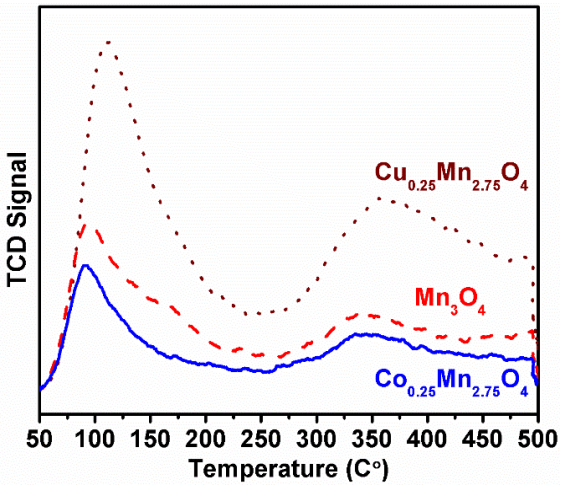

Fig. 4.6. O_2-TPD of Mn_3O_4, $Cu_{0.25}Mn_{2.75}O_4$, and $Co_{0.25}Mn_{2.75}O_4$.

4.4.1.7. XPS analysis

Surface characterization of Mn oxides (MnO, Mn_2O_3, MnO_2 and Mn_3O_4), copper/cobalt (x = 0.25) doped fresh catalysts and spent copper doped catalyst ($Cu_{0.25}Mn_{2.75}O_4$) was carried out by using XPS.

Mn 2p core level and Mn 3s level

Hausmannite (Mn_3O_4) has a spinel structure containing both Mn^{2+} and Mn^{3+} ions. Distinguishing between the oxidation states of Mn in Mn_3O_4 using XPS is tough[51] as the reported

values for the $2p_{3/2}$ peak of the manganese cations in MnO, Mn_3O_4, Mn_2O and MnO_2 are close at 640.9, 641.7, 641.8 and 642.4 eV, respectively.[52] In our study similar values were observed for $2p_{3/2}$ Mn cations in MnO, Mn_3O_4, Mn_2O_3 and MnO_2 at 641.6, 642.0, 641.4 and 642.3 eV, respectively (Fig. 4.7a). Though the BE values of $2p_{3/2}$ are very close for these Mn cations, the presence of Mn^{2+} can be seen through a satellite peak split of 6.0 eV in MnO while this is not clearly identified in Mn_3O_4 (Fig. 4.7a).[53] The presence of Mn^{2+} can be inferred from Mn 3s peaks which have two multiplet split components as a result of the coupling of non-ionized 3s electron with 3d valence-band electrons. The magnitude of peak splitting is characteristic of oxidation state with expected ΔE for MnO (Mn^{2+}) 5.64 eV; Mn_2O_3 (Mn^{3+}) 5.28 eV and MnO_2 (Mn^{4+}) 4.60 eV (Fig. 4.7b).[51] The ΔE =5.36 eV observed for Mn_3O_4 is in between Mn_2O_3 (Mn^{3+}) and MnO (Mn^{2+}), which clearly indicate that a part of Mn is present as Mn^{2+} in Mn_3O_4.

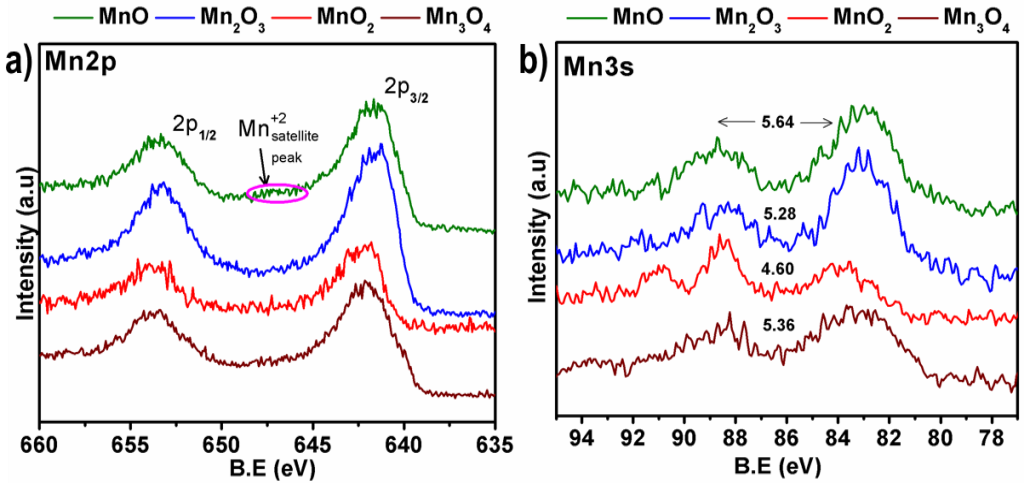

Fig. 4.7. XPS of MnO, Mn_2O_3, MnO_2 and Mn_3O_4 of (a) Mn2p and (b) Mn3s.

Mn 2p and Mn 3s XPS spectra of fresh Mn_3O_4, $Cu_{0.25}Mn_{2.75}O_4$, $Co_{0.25}Mn_{2.75}O_4$, and spent $Cu_{0.25}Mn_{2.75}O_4$ catalysts are shown in Fig. 4.8. The binding energy (BE) values of 641.4 ±0.1 eV for $2p_{3/2}$ and 653.15 ±0.1 eV for $2p_{1/2}$ were observed for all of the catalysts which strongly suggests that Mn is in +3 and +2 oxidation states (Fig. 4.8a). The BE observed for Mn $2p_{3/2}$ and $2p_{1/2}$ for copper and Mn_3O_4 are in good agreement with those reported in literature.[46] The ΔE of Mn3S for the fresh ($Cu_{0.25}Mn_{2.75}O_4$, $Co_{0.25}Mn_{2.75}O_4$) and spent ($Cu_{0.25}Mn_{2.75}O_4$) catalysts was in the same range of 5.64 - 5.28 eV (observed for Mn +2 and +3), for $Cu_{0.25}Mn_{2.75}O_4$ (5.28 eV); $Co_{0.25}Mn_{2.75}O_4$ (5.49 eV) and spent $Cu_{0.25}Mn_{2.75}O_4$ catalyst (5.38 eV) respectively (Fig. 4.8b).

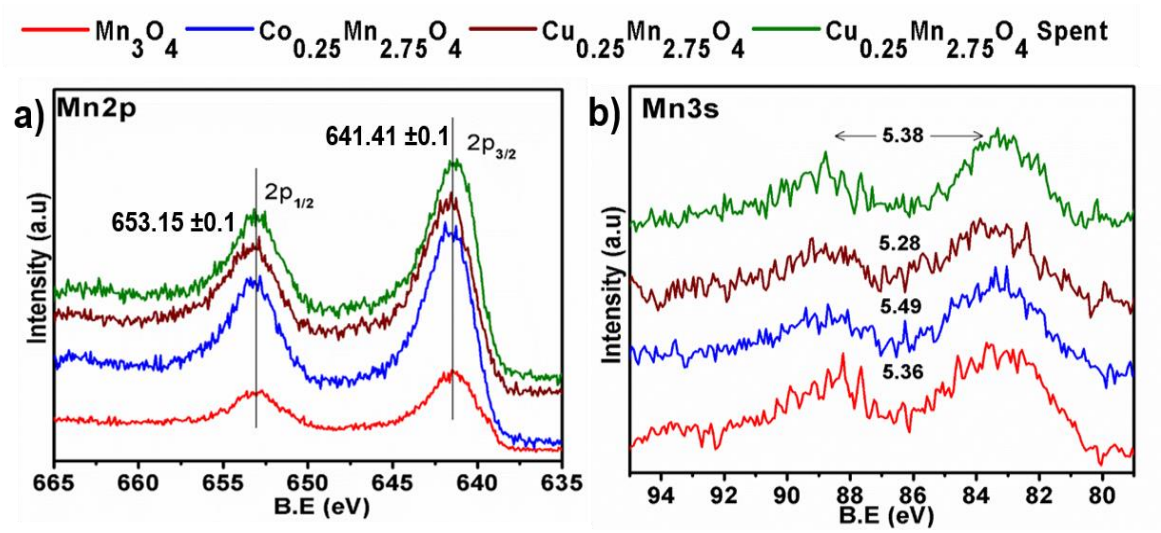

Fig. 4.8. XPS of fresh Mn_3O_4, $Cu_{0.25}$, $Co_{0.25}$, and spent $Cu_{0.25}$ catalysts; (a) Mn2p and (b) Mn3s.

Cu 2p core-level

XPS spectra of Cu $2p_{3/2}$ core level for fresh and spent $Cu_{0.25}Mn_{2.75}O_4$ catalysts are shown in Fig. 4.9a. The main peak at 933.3 eV for $2p_{3/2}$ with a satellite peak at around 943.6 eV was observed for both the catalysts. The BE values of our samples are in good agreement with those reported previously.[54] These results show that the copper is present in +2 oxidation state.

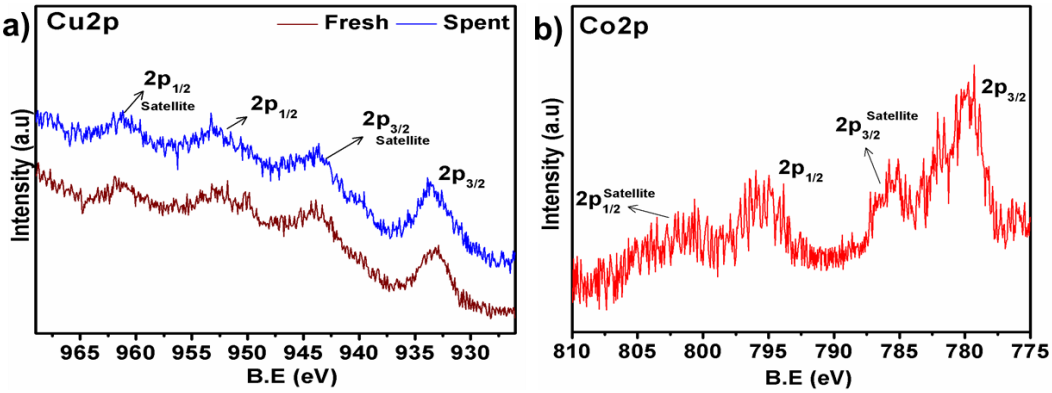

Fig. 4.9. XPS of fresh $Cu_{0.25}$, $Co_{0.25}$ and spent $Cu_{0.25}$ catalysts; (a) Cu2p and (b) Co2p.

Co 2p core level

XPS spectra of Co $2p_{3/2}$ core level of fresh $Co_{0.25}Mn_{2.75}O_4$ catalysts is shown in Fig. 4.9b. Peak at 779.9 eV for $2p_{3/2}$ with a satellite peak at around 786.2 eV and a peak at 795.9 eV for $2p_{1/2}$ with a satellite peak at around 801.4 eV were observed for this Co doped catalyst. The satellite splittings of Co $2p_{3/2}$ and Co $2p_{1/2}$ for the octahedrally coordinated cobaltous ions is

expected to be 6.2 eV.[55] Whereas, satellite splittings of Co $2p_{3/2}$ and Co $2p_{1/2}$ for the tetrahedral coordinated cobaltous ions are reported to be 5.3 eV and 6.2 respectively.[55] We observed the satellite splittings of 5.4 eV and 6.3 eV for Co $2p_{3/2}$ and Co $2p_{1/2}$ respectively. This clearly shows that Co^{2+} is in tetrahedral coordination. The spin−orbit splitting of Co $2p_{3/2}$−$2p_{1/2}$ is of 15.9 eV which shows the existence of Co^{2+}. Due to paramagnetic nature of Co^{2+} (d^7, e_g^4, t_{2g}^3) and Cu^{2+} (d^9,e_g^4, t_{2g}^5), the charge transfer (Δ) from the oxygen ligand to metal ion occurs, as a result the satellite peaks appear at higher energy.[54]

4.5. Catalytic activity of BzOH in oxidation

All the above described Mn containing oxide catalysts were evaluated for partial oxidation of benzyl alcohol to yield benzaldehyde.

4.5.1. Effect of catalyst composition: Mn with different oxidation states

Benzyl alcohol conversion and benzaldehyde (BzH) selectivity were studied systematically using various manganese oxide catalysts in which Mn is present in different oxidation states (+4, +3, +2) (Table 4.4). The catalyst screening was carried out under identical conditions (at 300 ºC) using O_2 to BzOH mole ratio of 0.5 at a weight hourly space velocity (WHSV) of 5 h^{-1}. Benzyl alcohol was converted to BzH with high (93-99%) selectivity; with other products (1-7%) being benzoic acid (a over oxidation product), benzyl benzoate and benzyl ether (condensed products). Some benzene and toluene were also present, being decarboxylation and disproportionation products. The BzOH conversion and BzH selectivity varied drastically based on the Mn oxidations states and catalyst composition. Among the catalysts studied, MnO (Mn^{2+}) shows least activity (<6% of BzOH conversion), MnO_2 (Mn^{4+}) shows improved activity with ~40% of BzOH conversion, while Mn_2O_3 (Mn^{3+}) show relatively much higher activity. However, the BzH selectivity decreased at higher conversions due to over oxidation of BzOH to benzoic acid. Spinel Mn_3O_4 ($Mn^{2+,\ 3+}$) shows the best activity among the manganese oxide catalysts studied accompanied by high (98.8%) BzH selectivity. The catalytic activity of this catalyst was also relatively stable with time on stream.

Reaction results show that Mn with +3 oxidation state shows the highest activity compared to Mn-oxides that are present in other oxidation states (+2 and +4). The catalyst that contains Mn^{4+} shows moderate activity. The worst among these oxides is the MnO (Mn^{2+}) that

shows the least activity as reported in literature.[40] The selectivity to BzH has increased with the introduction of Mn^{2+} and Mn^{3+}cations in the form of spinel (Mn_3O_4). We have also observed that the presence of +3 cation leads to the over oxidation of BzOH to benzoic acid. Though +2 cation of Mn does not show appreciable activity in partial oxidation of BzOH, it plays a crucial role in the selective formation of BzH by suppressing the formation of side products.

Table 4.4 Product distribution over different manganese oxides.[a]

Entry	Catalyst	Conversion of BzOH (%)	Selectivity (%)	
			BzH	Others
1	MnO_2	39.5	97.9	2.0
2	Mn_2O_3	82.7	92.6	7.3
3	Mn_3O_4	81.3	98.8	1.2
4	MnO	5.6	97.6	2.4

[a]Reaction conditions: 0.5 g of catalyst, 300 °C, 50 $mL.min^{-1}$ (10% O_2 in N_2; volume to volume), oxygen to substrate ratio (0.5), WHSV- 5 h^{-1} and time (8 h).

4.5.2. Effect of doping cobalt and copper into Mn_3O_4 spinel

While the steady state activity of the Mn_3O_4 in partial oxidation of BzOH is not noteworthy, stable activity could be achieved on doping Mn_3O_4 spinel with Cu. Moreover, slight increase in BzOH conversion was seen with copper-containing catalysts ($Cu_{0.25}Mn_{2.75}O_4$) while the activity was lower with cobalt doped catalyst ($Co_{0.25}Mn_{2.75}O_4$) (Fig. 4.10a). The deactivation of the catalyst was also rapid with cobalt doped catalyst. On all catalysts, there is an initial increase in the catalytic activity upto 2 h on stream, which starts dropping thereafter, particularly in the case of catalysts that do not have copper in their framework. The activity was found to be reasonably stable with copper-containing spinel catalyst with time stream (TOS) as compared to other spinel catalysts ($Co_{0.25}Mn_{2.75}O_4$ and Mn_3O_4). The catalyst with *Cu* = 0.25 showed good activity and as well as high BzH selectivity (98.0%), with hardly any deactivation even after

longer hours on stream (section 4.5.7). Selectivity of the other products with TOS is shown in the Fig. 4.10b.

Doping with small amounts of copper helped in reducing over oxidation and also helped in fast desorption of products formed. On the other hand the Co doped spinel did not show stable activity. As discussed earlier, acidity and basicity on copper catalyst ($Cu_{0.25}Mn_{2.75}O_4$) is higher when compared to $Co_{0.25}Mn_{2.75}O_4$ or Mn_3O_4 catalysts (Table 4.2). The decrease in the activity or the deactivation of $Co_{0.25}Mn_{2.75}O_4$ and Mn_3O_4 catalysts with time may be due to blockage of active sites by the strongly adsorbed reaction species as can be seen from the TGA of spent catalyst (Fig. 4.2d). It is presumed that the catalytically active sites are blocked by the acid product formed, as it is not desorbed faster from the surface of catalyst under the reaction conditions.[21, 22] It shows that the presence of copper is somehow helping the reaction of benzoic acid and benzyl alcohol to form benzyl ester, which is easily desorbed from the catalyst surface. Thus, Cu is promoting ester formation and helping in the retention of catalytic activity for longer durations. Since the benzoic acid formed during the reaction is desorbed in the form of benzyl ester, catalyst sites are regenerated. The presence of Cu result in the formation of benzyl ester, while cobalt promotes the formation of benzyl ether which is not desorbed quickly, resulting in the blockage of active sites (Fig. 4.10b). The deactivation was observed on all other catalyst studied here, which is attributed to the blockage of active sites by the products formed.

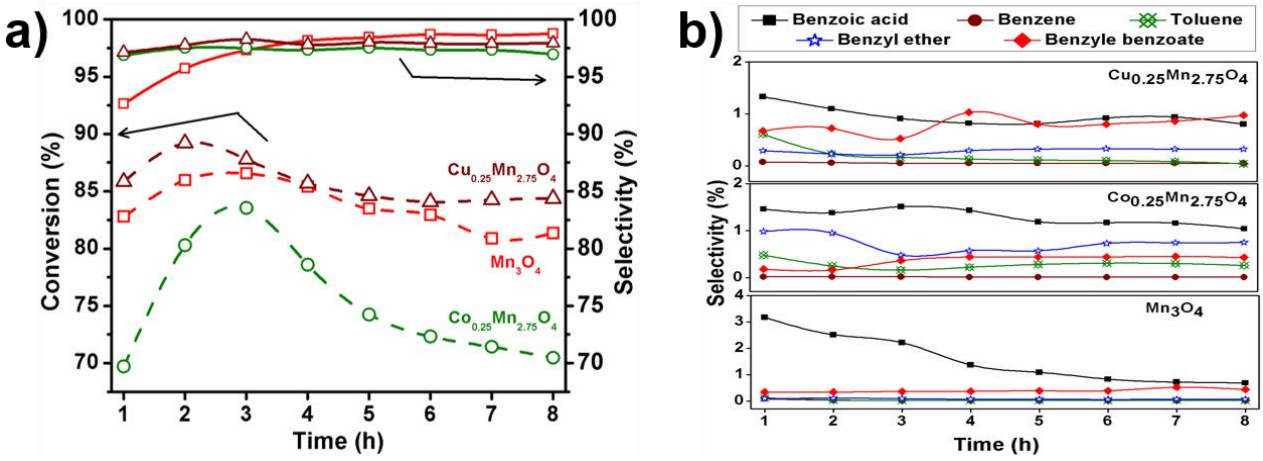

Fig. 4.10. Effect of cobalt and copper doping in Mn_3O_4 catalysts: (a) Conversion (dash line) and selectivity (solid line), (Mn_3O_4 (□), $Cu_{0.25}Mn_{2.75}O_4$ (Δ), $Co_{0.25}Mn_{2.75}O_4$ (○) and (b) Selectivity of other products except BzH.

Reaction conditions: 0.5 g of catalyst, 300 °C, 50 mL.min^{-1} (10% O_2 in N_2; volume to volume), oxygen to substrate ratio 0.5 and WHSV- 5 h^{-1}.

4.5.3. Effect of temperature on catalytic activity

Fig. 4.11a shows the variation of BzOH conversion and BzH selectivity as a function of temperature (260-320 °C) on $Cu_{0.25}Mn_{2.75}O_4$ catalyst. The conversion of BzOH increased with temperature and reached maximum of 84.5% at 300 °C compared to a value of 50.7% at 260 °C. The conversion remains nearly flat with further increase in reaction temperature to 320 °C. Similarly, the selectivity of BzH reached a maximum of 98% at 300 °C and reduced somewhat on further increasing the temperature. It was found that at lower temperatures, the deactivation of the catalyst is predominant as a function of time. However, the selectivity of BzH was always between 97-98% at all the temperatures studied. Selectivity of the other products is shown in Fig. 4.11b.

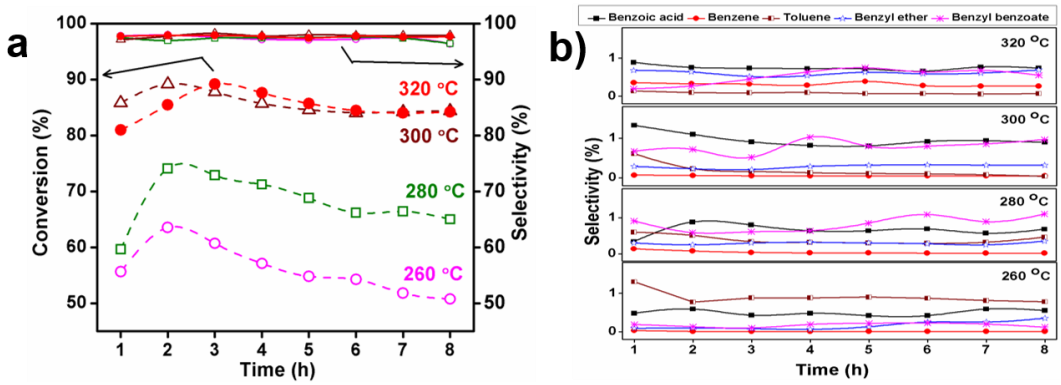

Fig. 4.11. Influence of reaction temperature on benzyl alcohol conversion and product selectivity over $Cu_{0.25}Mn_{2.75}O_4$ catalyst: (a) Conversion (dash line) and selectivity (solid line) as a function of time, 320 °C (●), 300°C (Δ), 280 °C (□), 260 °C (○) and (b) Selectivity of other products.

Reaction conditions: 0.5 g of catalyst ($Cu_{0.25}Mn_{2.75}O_4$), 50 mL/min (10% O_2 in N_2; volume to volume), oxygen to substrate ratio 0.5 and WHSV- 5 h^{-1}.

Temperature study reveals that a reaction temperature of 300 °C is optimum for all the catalysts. Below 300 °C, the catalysts deactivated rapidly due to non-desorption of products formed. Moreover, boiling of point of benzoic acid is 249.2 °C, hence it does not readily desorb from the catalyst at lower temperatures. The formation of benzoic acid and benzyl ether blocks the active sites of the catalysts that in turn lower the activity with TOS.[21, 22] Smooth desorption of benzoic acid from catalyst is observed at high temperatures. Along with that, the formation of benzyl ester increased by increasing the temperature, which further helps in desorption of

benzoic acid formed in the form of ester (Fig. 4.11b). The conversion remains same with further rise in reaction temperature to 320 from 300 °C, with steady state selectivity of BzH (98.0% at 300 °C) with the $Cu_{0.25}Mn_{2.75}O_4$ catalyst.

4.5.4. Effect of oxidant

Oxidation of BzOH was also carried by changing the oxidant partial pressure, using various ratios of oxidant to alcohol over $Cu_{0.25}Mn_{2.75}O_4$ catalyst at 300 °C. These results are depicted in Fig. 4.12, with respect to benzaldehyde selectivity. As expected, alcohol conversion increased linearly with increasing oxidant concentration in the feed, reaching maximum of 84.5 and 86.2% of conversion for O_2 to substrate mole ratios of 0.5 and 1. Even though the conversion increased at higher O_2 to substrate mole ratio, the BzH selectivity decreased from 98 to 96.6%.

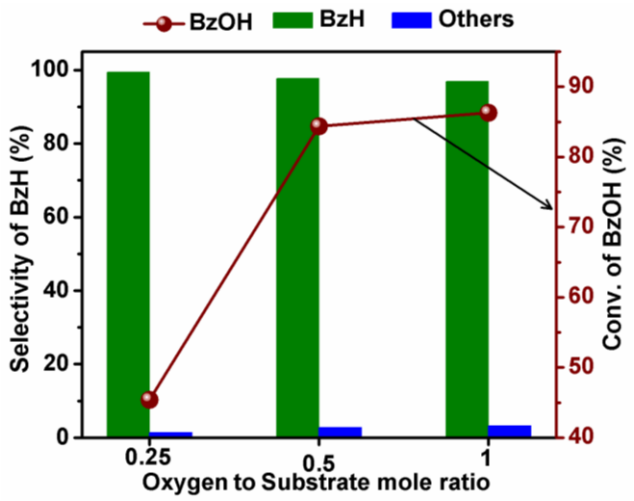

Fig. 4.12. Effect of oxidant (O_2) to benzyl alcohol mole ratio on BzOH conversion and BzH selectivity. Reaction conditions: 0.5 g of catalyst ($Cu_{0.25}Mn_{2.75}O_4$), 300 °C, 50 mL/min (O_2 in N_2), WHSV- 5 h^{-1} and TOS-8 h.

This shows that oxygen to substrate ratios has a profound role in the selectivity and conversion. A controlled amount of oxidant in the feed with the mole ratio of oxygen to substrate being 0.25, steady state conversion (45.3%) with BzH selectivity of 99.4% was achieved. When the mole ratio of oxygen to substrate increased to 1, the availability of oxygen in the feed is high leading to the formation of over oxidation products thus resulting in the fall of BzH selectivity. In case of industrial application, selectivity gets more importance compared to the conversion, as the reactant can in principle be re-circulated in a continuous reaction.

4.5.5. Effect of WHSV

Fig. 4.13 shows effect of WHSV on BzOH conversion and BzH selectivity as a function of time over $Cu_{0.25}Mn_{2.75}O_4$ catalyst, using oxidant to BzOH mole ratio of 0.5. The BzOH conversion decreased at high WHSV, though there is marginal increase in aldehyde (BzH) selectivity. The conversion of BzOH was 84.3, 70.4 and 58.6% for WHSV at 5, 10 and 15 h^{-1} respectively after 8 h of reaction. Since the contact time of substrate with the catalyst decreased with increasing WHSV, it led to the decrease in BzOH conversion. Hence, WHSV of 5 h^{-1} with O_2 to substrate mole of 0.5 was found to be optimum for steady and stable activity.

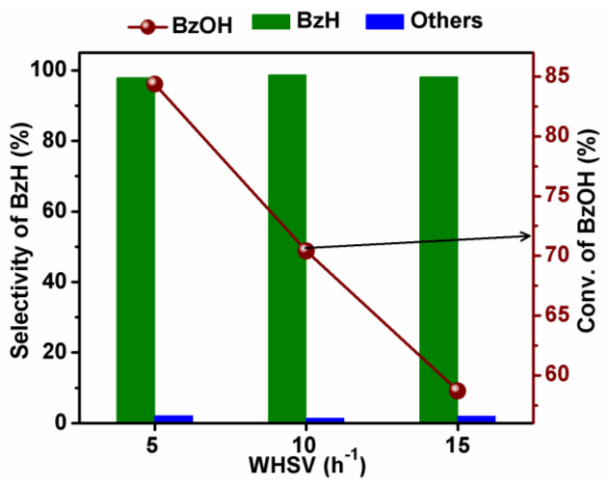

Fig. 4.13. Effect of WHSV on benzyl alcohol conversion on $Cu_{0.25}Mn_{2.75}O_4$ catalyst.

Reaction conditions: 0.5 g of catalyst ($Cu_{0.25}Mn_{2.75}O_4$), 300 °C, 50 mL/min (10% O_2 in N_2), oxygen to substrate mole 0.5 and TOS-8 h.

4.5.6. Effect of copper content on activity

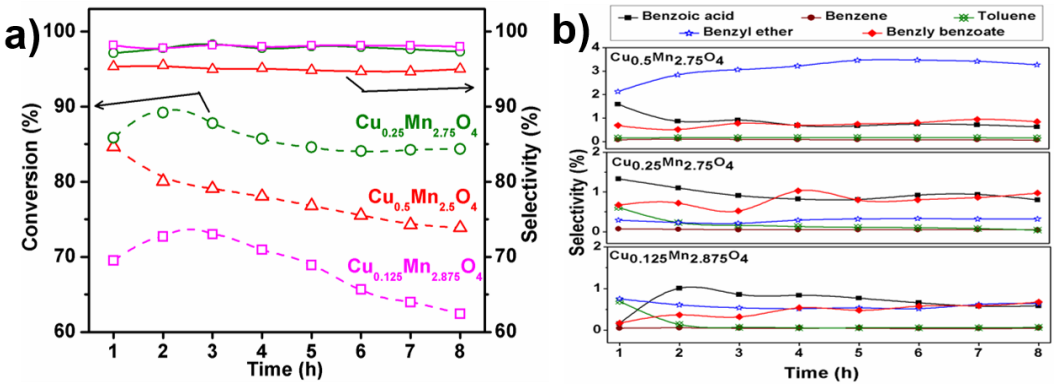

Fig. 4.14. Influence of Cu content on partial oxidation of benzyl alcohol:

(a) Conversion (dash line) and selectivity (solid line) as functions of time for ($Cu_{0.125}Mn_{2.875}O_4$ (□), $Cu_{0.25}Mn_{2.75}O_4$ (Δ) and $Cu_{0.5}Mn_{2.5}O_4$ (○)) and (b) Selectivity of products other than BzH.

Reaction conditions: 0.5 g of catalyst, 50 mL/min (10% O_2 in N_2; volume to volume), oxygen to substrate mole 0.5 and WHSV- 5 h^{-1}.

Figure 4.14 shows Influence of doped copper content on BzOH conversion and BzH selectivity as a function of time. The increase in copper ($Cu_{0.5}Mn_{2.5}O_4$) content decreased both the activity and selectivity of BzH. Lower selectivity is due to the presence of high copper which helps in the formation of benzyl ethers. At low copper content ($Cu_{0.125}Mn_{2.875}O_4$), there is a decrease in the activity as a function of time. This fall in the activity is due to the deactivation of the catalyst as a result of blockage of active sites by the product molecules formed (Fig. 4.14a). The BzH selectivity and BzOH conversion were stable for catalyst with copper doped to the tune of $x = 0.25$. Selectivity of the other products are also shown in the Fig. 4.14b.

4.5.7. Long-term on-stream stability of $Cu_{0.25}Mn_{2.75}O_4$

Long-term stability of $Cu_{0.25}Mn_{2.75}O_4$ catalyst was studied and compared with Mn_3O_4 at oxygen to substrate mole 0.5 and WHSV 10 h^{-1}. It was found that the activity of the Mn_3O_4 catalyst decreased rapidly with TOS, while the activity of the $Cu_{0.25}Mn_{2.75}O_4$ catalyst remained steady even after 24 h (Fig. 4.15). From these experiments, it is clear that the $Cu_{0.25}Mn_{2.75}O_4$ catalyst shows better activity with TOS even after long duration. This catalyst system appears to be superior to those reported so far in the literature, in terms of better conversion, BzH selectivity and on stream stability

.

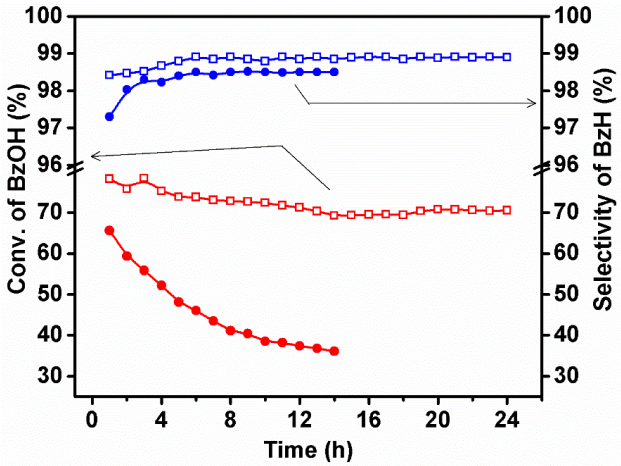

Fig. 4.15. Steady state activity of Mn_3O_4 and $Cu_{0.25}Mn_{2.75}O_4$ catalysts: Conversion of BzOH (red), selectivity of BzH (blue), catalyst Mn_3O_4 (●) and $Cu_{0.25}Mn_{2.75}O_4$ (□).

Reaction conditions: 0.5 g of catalyst, 300 °C, 50 mL/min (20% O_2 in N_2) and WHSV- 10 h^{-1}.

Hausmannite (Mn_3O_4) doped with different copper contents were studied and the better activity of the catalyst mainly depends on the acid-basic properties and oxygen uptake of the materials. Here we observed the same with different amounts of copper, where the copper is in +2 oxidation state if the mole fraction is <1 as reported.[46] The stability of the catalytic activity depends on desorption of products formed as product molecules bound to the catalytic sites lead to reduction in activity. Hence, there is a need for optimum copper content in the catalyst. Hence, very low copper ($Cu_{0.125}Mn_{2.875}O_4$) contents are not helpful (Fig. 4.14). Similarly, high Cu in the framework may drive the formation of benzyl ethers, thus decreasing the formation of BzH. From O_2-TPD experiments, it was clear that the oxygen uptake capacity is high for $Cu_{0.25}Mn_{2.75}O_4$ catalyst compared to other two catalysts (Mn_3O_4 and $Co_{0.25}Mn_{2.75}O_4$). This could be another reason behind better activity of $Cu_{0.25}Mn_{2.75}O_4$ catalyst. The acid-basic properties and the amount of oxygen uptake/mobility play vital role in sustaining high activity. The stable activity of the catalyst mainly depends on the byproduct desorption, which in turn depends on the amount of Cu present in the catalyst. Thus presence of copper in the catalyst plays a key role in the stable activity of the catalyst.

4.6. Conclusions

A series of manganese oxides and copper and cobalt doped manganese spinel ($Cu_xMn_{3-x}O_4$, $Co_xMn_{3-x}O_4$) catalysts were prepared and studied using various physico-chemical characterization techniques. They were tested for partial oxidation of benzaldehyde. Mn_3O_4 spinel type oxide was found to be more active among Mn oxides, but was not stable for long hours on stream. On the otherhand, on Cu doping the $Cu_{0.25}Mn_{2.75}O_4$ catalyst was found to be more active and stable. Among the spinel oxides that contain different Cu contents, catalyst doped with x=0.25 in $Mn_{3-x}O_4$ ($Cu_{0.25}Mn_{2.875}O_4$) was relatively better compared to other two compositions ($Cu_{0.125}Mn_{2.875}O_4$, $Cu_{0.5}Mn_{2.875}O_4$). Whereas Mn_3O_4 doped with Co was less active and less stable. Formation of by-products like benzoic acid due to over oxidation and their subsequent reaction with benzyl alcohol to give benzyl ether appears to be responsible for rapid deactivation of the catalyst. The presence of copper in optimum concentration ($Cu_{0.25}Mn_{2.75}O_4$), helps in the desorption of the ester by-products formed during the reaction. The oxygen

uptake/mobility and well balanced acidity-basicity associated with the catalysts must be responsible for the selective formation of BzH and on-stream stability.

4.7. References

1. Friedrich Brühne; Elaine Wright. "Benzaldehyde" in Ullmann's Encyclopedia of Industrial Chemistry. In Wiley-VCH Verlag GmbH & Co. KGaA, Weinheim: 2005.
2. Cristina Della Pina; Ermelinda Falletta; Michele Rossi. *J. Catal.* **2008,** 260, 384–386.
3. Dimitratos N.; Lopez-Sanchez J. A.; Morgan D.; Carley A. F.; Tiruvalam R.; Kiely C. J.; Bethell D.; Hutchings G. J. *Phys. Chem. Chem. Phys.* **2009,** 11, 5142–5153.
4. Meenakshisundaram S.; Nowicka E.; Miedziak P. J.; Brett G. L.; Jenkins R. L.; Dimitratos N.; Taylor S. H.; Knight D. W.; Bethell D.; Hutchings G. J. *Faraday Discuss.* **2010,** 145, 341–356.
5. Jayamani M.; Pillai C. N. *J. Catal.* **1983,** 82, 485–488.
6. Valarivan R.; Pillai C. N.; Swamy C. S. *React. Kinet. Catal. Lett.* **1996,** 59, 343–350.
7. Ragupathi C.; Judith Vijaya J.; Thinesh Kumar R.; John Kennedy L. *J. Mol. Struct.* **2015,** 1079, 182–188.
8. Anas Benyounes; Stéphane Louisia; Rosa Axet; Ziyad Mahfoud; Mohamed Kacimi; Philippe Serp. *Catal. Today* **2015,** 249, 137–144.
9. Hengwei Wang; Chunlei Wang; Huan Yan; Hong Yi; Junling Lu. *J. Catal.* **2015,** 324, 59–68.
10. Yibo Yan; Xinli Jia; Yanhui Yang. *Catal. Today* **2016,** 259, 292–302.
11. Chunmei Zhou; Zhen Guo; Yihu Dai; Xinli Jia; Hao Yu; Yanhui Yang. *Appl. Catal. B: Env.* **2016,** 181, 118–126.
12. Xiao Zhang; Xiaobo Fu1; Yuanming Zhang; Yi Zhu; Jun Yang. *Catal Lett.* **2016,** 146, 945–950.
13. Sumathi R.; Johnson K.; Viswanathan B.; Varadarajan T. K. *Appl. Catal. A: Gen.* **1998,** 172, 15-22.
14. Vasant R. Choudhary; Pankaj A. Chaudhari; Vijay S. Narkhede. *Catal. Commun.* **2003,** 4, 171–175.
15. Vasant R. Choudhary; Deepa K. Dumbre. *Catal. Commun.* **2009,** 10, 1738–1742.
16. Meenakshisundaram Sankar; Ewa Nowicka; Ramchandra Tiruvalam; Qian He; Stuart H. Taylor; Christopher J. Kiely; Donald Bethell; David W. Knight; Graham J. Hutchings. *Chem. Eur. J.* **2011,** 17, 6524–6532.

17. Dong Qiao; Chunli Xu; Jin Xu. *Catal. Commun.* **2014,** 45, 44–48.

18. Qian He; Peter J. Miedziak; Lokesh Kesavan; Nikolaos Dimitratos; Meenakshisundaram Sankar; Jose Antonio Lopez-Sanchez; Michael M. Forde; Jennifer K. Edwards; David W. Knight; Stuart H. Taylor; Christopher J. Kiely; Graham J. Hutchings. *Faraday Discuss.* **2013,** 162, 365–378.

19. Saad Alabbad; Adil S.F.; Assal M. E.; Mujeeb Khan; Abdulrahman Alwarthan; Rafiq H. Siddiqui M. *Arabian Journal of Chemistry* **2014,** 7, 1192-1198.

20. Mosaed Alhumaimess; Zhongjie Lin; Qian He; Li Lu; Nickolaos Dimitratos; Nicholas F. Dummer; Marco Conte; Stuart H. Taylor; Jonathan K. Bartley; Christopher J. Kiely; Graham J. Hutchings. *Chem. Eur. J.* **2014,** 20, 1701 – 1710.

21. Yibo Yan; Yuanting Chen; Xinli Jia; Yanhui Yang. *Appl. Catal. B: Env.* **2014,** 156–157 385–397.

22. Yejiang Hong; Xiaoqing Yan; Xiaofeng Liao; Renhong Li; Shaodan Xu; Liping Xiao; Jie Fan. *Chem. Commun.* **2014,** 50, 9679--9682.

23. Jie Zhu; Peng Cheng Wang; Ming Lu. *Appl. Catal. A: Gen.* **2014,** 477, 125–131.

24. Narayanan S.; Judith Vijaya J.; Sivasanker S.; Mahboob Alam; Tamizhdurai P.; John Kennedy L. *Polyhedron* **2015,** 89, 289–296.

25. Weiyou Zhou; Jie Liu; Jiugao Pan; Fu'an Sun; Mingyang He; Qun Chen. *Catal. Commun.* **2015,** 69, 1-4.

26. Francesco Arena; Bianca Gumina; Agata F. Lombardo; Claudia Espro; Antonio Patti; Lorenzo Spadaro; Leone Spiccia. *Appl. Catal. B: Env.* **2015,** 162, 260–267.

27. Francesco Arena; Bianca Gumina; Catia Cannilla; Lorenzo Spadaro; Antonio Patti; Leone Spiccia. *Appl. Catal. B: Env.* **2015,** 170-171, 233–240.

28. Lu-Cun Wang; Lin He; Qian Liu; Yong-Mei Liu; Miao Chen; Yong Cao; He-Yong He; Kang-Nian Fan. *Appl. Catal. A: Gen.* **2008,** 344, 150–157.

29. Tongtong Jiang; Chuancheng Jia; Lanchun Zhang; Shuren He; Yuanhua Sang; Haidong Li; Yanqing Li; Xiaohong Xu; Hong Liu. *Nanoscale* **2015,** 7, 209–217.

30. Hayashibara; Nishiyama S.; Tsuruya S.; Masai M. *J. Catal.* **1995,** 254, 153.

31. Yamamoto R.; Sawayama Y.-S.; Shibahara H.; Ichihashi Y.; Nishiyama S.; Tsuruya S. *J. Catal.* **2005,** 234, 308.

32. Sawayama Y.-S.; Shibahara H.; Ichihashi Y.; Nishiyama S.; Tsuruya S. *Ind. Eng. Chem. Res.* **2006,** 45, 8837.

33. Nakashima D.; Ichihashi Y.; Nishiyama S.; Tsuruya S. *J. Mol. Catal. A: Chem.* **2006,** 259, 108.

34. Pina C. D.; Falletta E.; Rossi M. *J. Catal.* **2008,** 260, 384.

35. Fan J.; Dai Y.; Li Y.; Zheng N.; Guo J.; Yan X.; Stucky G. D. *J. Am. Chem. Soc.* **2009,** 131, 15568.

36. Mao J.; Deng M.; Xue Q.; Chen L.; Lu Y. *Catal. Commun.* **2009,** 10, 1376.

37. Han D.; Xu T.; Su J.; Xu J.; Ding Y. *ChemCatChem* **2010,** 2, 383.

38. Jia L.; Zhang S.; Gu F.; Ping Y.; Guo X.; Zhong Z.; Su F. *Microporous Mesoporous Mater* **2012,** 149, 158.

39. Kumar A.; Kumar V. P.; Kumar B. P.; Vishwanathan V.; Chary K. V. R. *Catal. Lett.* **2014**, 144.

40. Naftali N. Opembe; Curtis Guild; Cecil King'ondu; Nicholas C. Nelson; Igor I. Slowing; Steven L. Suib. *Ind. Eng. Chem. Res.* **2014,** 53, (49), 19044-19051.

41. Fanny Schurz; Jorg M. Bauchert; Thorsten Merker; Thomas Schleid; Hans Hasse; Glaser R. *Appl. Catal. A: Gen.* **2009,** 355, 42–49.

42. Thattarathody Rajesh; Devi, R. N. *J. Mol. Catal. A: Chem.* **2014,** 395, 534–542.

43. Thattarathody Rajesh; Devi, R. N. *J. Phys. Chem. C* **2014,** 118, 20867−20874.

44. Mandal S.; Rojas R. M.; Amarilla J. M.; Calle P.; Kosova N. V.; Anufrienko V. F.; Rojo J. M. *Chem. Mater.* **2002,** 14, 1598-1605.

45. Ruiting Dong; Qinglan Ye; Lili Kuang; Xu Lu; Ying Zhang; Xue Zhang; Guojin Tan; Yanxuan Wen; Wang, F. *ACS Appl. Mater. Interfaces* **2013,** 5, 9508−9516.

46. Satyanarayana Reddy A.; Chinnakonda S. Gopinath; Satyanarayana Chilukuri. *J. Catal.* **2006,** 243, 278-291.

47. Lu Qiu; Yun Wang; Dandan Pang; Feng Ouyang; Changliang Zhang; Gang Cao. *Catalysts* **2016,** 6, 2-12.

48. Sania Maria de Lima; José Mansur Assaf. *Materials Research* **2002,** 5, 329-335.

49. Kung, H. H. Elsevier B.V.: 1989; Vol. 45, p 100-120.

50. Zhao-Yang Fei; Bo Sun; Liang Zhao; Wei-Jie Ji; Au, C.-T. *Chem. Eur. J.* **2013,** 19, 6480 – 6487.

51. Masaoki Oku; Kichinosuke Hirokawa. *J. Electron Spectrosc. Relat. Phenom.* **1975,** 7, 465-473.

52. Allen G.C.; Harris S.J.; Jutson L. A. *Appl. Surf. Sci.* **1989,** 37, 111-134.

53. Di Castrro V.; Polzonetti G. *J Electron Spectros. Relat. Phenom.* **1989,** 48, 117-123.

54. Kanak Roy; Vinod C. P.; Gopinath C. S. *J. Phys. Chem. C* **2013,** 117, 4717−4726.

55. Masaoki Oku; Kichinosuke Hirokawa. *J. Electron Spectrosc. Relat. Phenom.* **1976,** 8, 475-481.

Chapter 5

Selective oxidation of biomass-derived compounds over supported metal catalysts using molecular O_2

5.1. Introduction

Oxidation products of some of the biomass derived compounds have important applications. Two such important products are gluconic acid (GA) and glucaric acid (GCA), which are obtained on partial oxidation of glucose. The weak acidic property of GA can dissolve oxides, hydroxides and carbonates of polyvalent cations without attacking metallic or nonmetallic surfaces. As a result, gluconic acid is used for the removal of calcareous and rusty deposits of metals, including by beer and milk scale on galvanized iron, magnesium alloys etc. The GA is also used in the textile industry along with magnesium salts as a stabilizer for peroxide bleach baths, food, beverage and the pharmaceutical industries.[1] Gluconic acid and its salts are currently produced by the enzymatic oxidation of glucose by *Aspergillus niger* and *Gluconobacter suboxydans*,[1] the bulk of production (85 %) being in the form of sodium gluconate and other alkali gluconate salts.

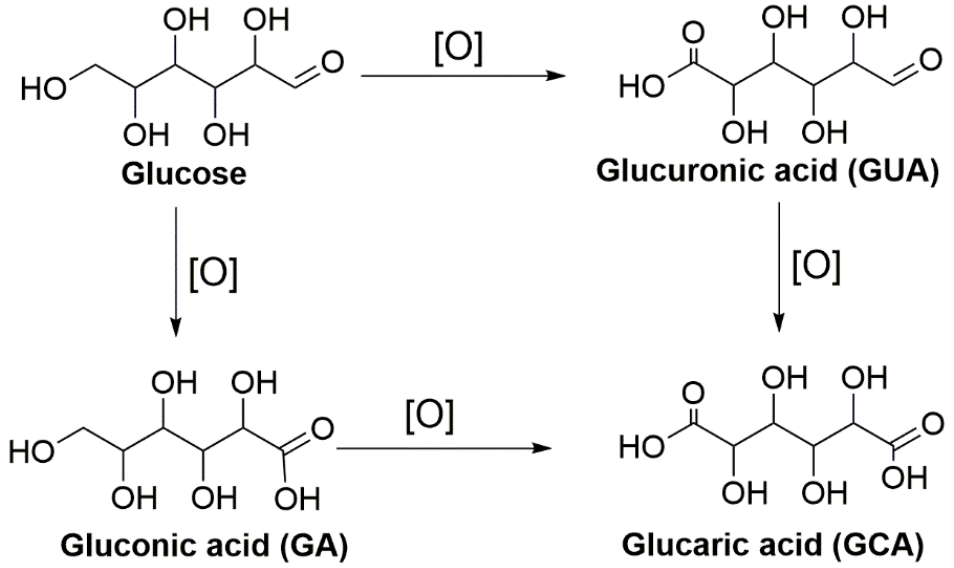

Scheme 5.1 Catalytic oxidation pathway of glucose. [2, 3, 4]

The other important oxidation product of glucose is glucaric acid (GCA), which is classified as one of the top 12 platform chemicals obtained from biomass.[5] Glucaric acid is an important precursor for a variety of important and useful products, such as nylons, plastics and food additives.[5] Glucaric acid upon selective hydrogenation gives adipic acid (AA), a key intermediate for nylon 6-6 and other products in the plastics and textile industries.[5, 6] Thus, GCA from glucose offers a renewable alternative route for AA synthesis. Adipic acid is currently produced on a large scale (>2.3 million tons per year) from petroleum-based KA oil, a mixture of

cyclohexanol and cyclohexanone.[7, 8] Therefore, the current focus is on the development of sustainable manufacturing processes for AA, preferably utilizing abundant non-food biomass in an environmentally friendly way.[9]

5.2. Literature on the synthesis of gluconic acid from biomass-derived glucose

Selective oxidation of glucose with different catalyst systems is of great interest, as it is complicated by the fact that the glucose has more than one functional group. To overcome these problems, it is necessary to choose a highly suitable and selective catalytic system. The chemoselective oxidation of glucose to GA was studied over various supported metal catalysts.

5.2.1. Use of external base

For the efficient production of GA from glucose, nobel metals like Pt,[10-13] Pd,[10, 11] Ru[14] and Au[11] have shown good activity. Some electrochemical processes were also reported for GCA from glucose.[15] Gold based catalysts show superior activity and desired product selectivity in the oxidation of glucose, among other precious metal catalysts. Haruta *et al* and Ulf Prüße *et al* extensively studied selective oxidation of glucose to get GA using gold catalysts. Gold nanoparticles with different sizes on a variety of supports were prepared and interaction of the support with gold particles and its effect on activity were explored.[16, 17, 18] Ulf Prüße and coworkers have prepared gold colloids using polymers as stabilizing agents in aqueous solution and used them to prepare catalysts like Au/TiO_2,[19] Au/Al_2O_3,[20, 21, 22] Pt/Al_2O_3[21] and Pd/Al_2O_3.[21] Bimetallic catalyst systems have been studied with different combination of nobel metals like Au-Pd,[23, 24] Au-Pt,[24] Pd-Bi[11] and Pd-Te[25]. Trimetallic systems such as Pt-Pd-Bi[11] on different supports like carbon, Al_2O_3, etc were also studied. In order to achieve good GA selectivity, all the above catalytic systems require addition of external base. This is an important drawback for the process intensification of glucose to GA reaction.

5.2.2. Glucose to GA in the absence of external base

Base free oxidation of glucose to GA was reported by Hutchings and coworkers for the first time by using 0.5% Au–Pd/MgO bimetallic catalyst. Their studies demonstrated that the monometallic catalysts were less active than bimetallic catalysts for this reaction. Bimetallic catalysts supported on different supports such as graphite, TiO_2 and $Mg(OH)_2$ were also

studied.[26] When different methods of preparation of Au on TiO_2 were investigated, the results showed that the particle size is an important factor for the catalytic activity of Au in the partial oxidation of glucose.[27] About 92% conversion of glucose with 87% selectivity to GA was obtained with Au supported on ordered mesoporous carbon (CMK-3) catalysts.[28] Wang *et al* developed a 1.1wt% Au/μCeO_2 catalyst, prepared by the deposition–precipitation method that showed stable activity. The activity was found to be particle-size dependent, for the selective glucose oxidation, in the absence of an external base.[29] Solid basic supports were used to prepare catalysts such as 3.5wt% Pt/hydrotalcite,[30] 1.7Au%/CeO_2[4] for partial oxidation of glucose. Rautiainen *et al* studied microwave-assisted base-free oxidation of glucose to GA with Au/Al_2O_3[31] catalysts. High reaction temperatures were reportedly required when non-basic supports were used to achieve high glucose conversion.[27, 31, 32] The above literature shows that the oxidation of glucose is favored at lower temperature when basic supports were used. The controlled selective oxidation of glucose to GA without over oxidation is also of great challenge.

5.3. Synthesis of glucaric acid using supported metal catalysts

Partial oxidation of glucose to glucaric acid (GCA) is not a single step reaction. It involves two steps with glucose as substrate, in the first step glucose is partially oxidized to GA and in a consecutive step, GA is oxidized to GCA. The second step, i.e., oxidation of 1° alcohol to acid is a slower step and hence need highly active and selective catalysts. To achieve this, it is essential to choose a suitable metal and an appropriate support. The selective oxidation of glucose and GA to GCA was studied over various supported metal catalysts.

5.3.1. Processes based on homogenous catalysts

Catalytic oxidation of glucose with mineral acids such as HNO_3, nitroxides and $NaNO_2$ have been reported. These were active in the reaction temperatures range of 25 to 80 °C to yield nearly 50% GCA.[33-36] However, use of corrosive and hazardous mineral acids is not advisable and the process is no longer green. In addition, it leads to problems like separation of products and recyclability. High concentrations of these oxidants in the reaction medium and generation of significant amounts of toxic by-products and inorganic salts pose major challenges in commercial practice, though these processes are currently in practice.

5.3.2. Electrochemical catalysis routes

Electrochemical oxidation of glucose to GCA with nitroxide, NaBr, NaOCl, mineral acids and bleaches has been reported.[33, 37, 38] These reactions generate significant amounts of by-products that have disposable problems, thus qualifying them to be less sustainable and not so environmental friendly.[38-40]

5.3.3. Heterogeneous catalyst systems that use external base

Jin *et al* reported catalytic oxidation of glucose and GA to GCA using heterogeneous catalysts. A series of Pt- and Cu-based mono- and bimetallic catalysts over TiO_2 support were studied in presence of high concentration of NaOH. Yield of ~25% GCA at 45 °C with 100% conversion of glucose was observed when Pt–Cu/TiO_2 catalyst system was used.[6] Further studies on the structure-dependent oxidation activity of bimetallic PtPd nanoparticles on TiO_2 were investigated. Studies showed that PtPd catalysts are synergistically active compared to the monometallic Pt or Pd, both for primary and secondary oxidation of glucose at 45 °C and at 0.1 MPa of O_2 to give 44% yield of GCA at 100% glucose conversion.[41]

5.3.4. Heterogeneous catalyst systems without an external base

Boussie *et al* studied the partial glucose oxidation to produce 57% GCA in a 5 h reaction at 80 °C under 5 bar O_2 with 5 wt% Pt/C catalyst.[42] Supported mono- and bimetallic Pt and Au catalysts on TiO_2, ZrO_2 and SiO_2 were investigated in the temperature range of 90-112 °C under high pressure (27 bar) of O_2 to obtain yield of 70% GCA after 5 h of reaction.[43] However, these reactions were conducted on a micro-liter scale reactor system which were neither reproduced nor conducted on a reasonable laboratory scale. Jechan Lee *et al* in his studies achieved 74% of GCA yield under base-free conditions using 5 wt% Pt/C at 80 °C and 13.8 bar O_2. The activity of catalyst remained nearly same even after five cycles, with glucose/Pt molar ratio of 54, showing that Pt/C catalyst is robust and stable.[44]

Since, we are interested in exploring and developing catalyst systems to get glucaric acid in two steps involving glucose partial oxidation to gluconic acid (GA) followed by its further oxidation to glucaric acid, this chapter is divided into two parts, part-A and part-B that describe our efforts for development of catalysts for gluconic and glucaric acids respectively.

Part -5A

5.4 Oxidation of glucose to GA over Au/Mg-OMS-1 catalysts

Gold catalysts supported on Mg-OMS-1, K-OMS-2 and other basic and non-basic supported Au catalysts were tested for the partial oxidation of glucose to GA. Various reaction parameters were optimized with an objective to improve glucose conversion and GA selectivity.

5.4.1. Experimental procedures

5.4.1.1. Materials

D-Glucose, D-Saccharic acid potassium salt and tartronic acid were procured from Sigma-Aldrich, USA. D-Gluconic acid, D-glucuronic acid and $HAuCl_4 \cdot 3H_2O$ were sourced from Alfa Aesar Johnson Matthey, Europe. $Mg(OAc)_2 \cdot 4H_2O$ was purchased from Loba Chemie Pvt. Ltd. Oxalic acid, $Mn(OAc)_2 \cdot 4H_2O$, MnO_2, γ-Al_2O_3 and MgO were purchased from Merck, India. $KMnO_4$ and $MgCl_2 \cdot 6H_2O$ were obtained from sd Fine-chem Ltd, India. All the chemicals were used as received without any further purification.

5.4.1.2. Synthesis of 2wt% Au deposited Mg-OMS-1

Mg-OMS-1 was synthesized as per the detailed procedure given in the section 2.2.3. 2wt% of Au metal was loaded onto Mg-OMS-1 by simple deposition-precipitation method. In a typical synthesis, the desired amount of metal solution ($HAuCl_4$, Au content 7.5 mg/mL) was taken in 20 mL of distilled water, to which required amount of support was added and allowed to be stirred for 30 min. To this slurry, 0.2 M $NaHCO_3$ solution was added drop wise to reach a pH of 8.5 and subsequently it was stirred for 60 min at room temperature, filtered, washed and dried at 60 °C for 6 h. The resulting catalyst has been named as 2wt% Au/Mg-OMS-1. The detailed procedure is given in section 2.2.3.1.

5.4.1.3. Evaluation of catalysts

The oxidation reaction was carried out in 50 mL Parr (4848) autoclave. In a typical reaction experiment, required quantity of glucose was taken in 25 mL of Millipore water and to it freshly activated catalyst was added. The reaction was conducted at the desired temperature under continuous stirring (1000 rpm). When the reaction mixture reached desired temperature, O_2 was slowly released into the autoclave. About 0.5 mL of the reaction product was removed at

desired intervals and analyzed after filtration through a nylon 0.22 µm filter. At the end of the reaction, the reaction mixture was filtered using Whatman filter paper and analyzed using HPLC, equipped with RI detector and H^+ Aminex column (305 mm × 7.8 mm) fitted with a guard column in series. Mobile phase used was 1 mmol of succinic acid at a flow rate of 0.3 $mL.min^{-1}$ while maintain the column temperature at 25 °C. All the peaks were confirmed using authentic standards and quantification was done by preparing standard curves obtained by the injection of solutions at different concentrations.

5.4.1.4. Recycling of catalysts

To reuse the catalyst, reaction was performed under standard conditions then the catalyst was collected by centrifuging the reaction mixture at 12000 RPM. Reactants and products were removed by using milliQ water and by repeatedly (at least thrice) centrifuging to wash the catalyst free of products/reactant. Thus recovered catalyst was dried (60 °C, 6 h) and re-used.

5.5. Results and discussion- Partial oxidation of glucose to gluconic acid

5.5.1. Catalyst characterization

5.5.1.1. X-ray diffraction

Figure 5.1 shows the XRD patterns of catalyst materials used at different stages of preparation of Mg-OMS-1.

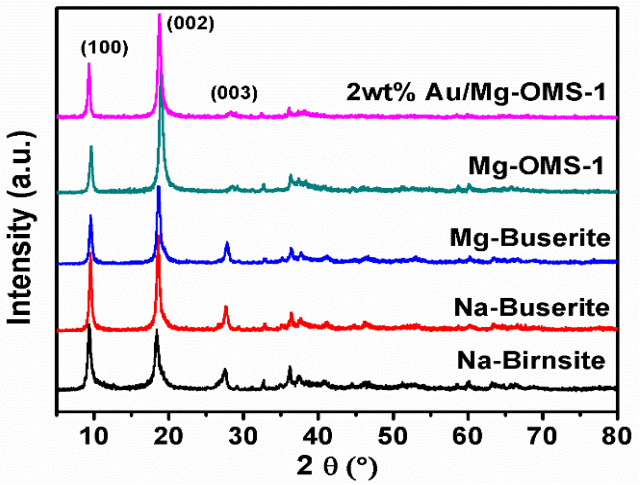

Fig. 5.1 XRD pattrens of Mg-OMS-1 as synthesized.

The major peaks at d-spacings of 9.8, 4.9 and 3.3 Å, that correspond to (1 0 0), (0 0 2), (0 0 3) reflections respectively match with the reported data of todorokite (Mg-OMS-1) (JCPDS 13-

164). The changes in the relative intensities of XRD reflections at 4.9 and 9.8 Å suggest a gradual transformation of buserite to todorokite (Mg-OMS-1). It is clearly observed that there is a clear translation of disordered to ordered structure i.e. from Na-birnasite to Mg-OMS-1 (Fig. 5.1). Gold loading on Mg-OMS-1 did not lead to any noticeable changes in powder XRD pattern, suggesting that no structural changes occurred on Au loading.

5.5.1.2. Physisorption of Nitrogen

The Mg-OMS-1 materials before and after Au loading were studied for their N_2 sorption properties. As shown in Fig. 5.2, Mg-OMS-1 and 2wt% Au/Mg-OMS-1 samples give type IV adsorption isotherm with an N_2 hysteresis loop during desorption, which is typical of mesoporous materials.

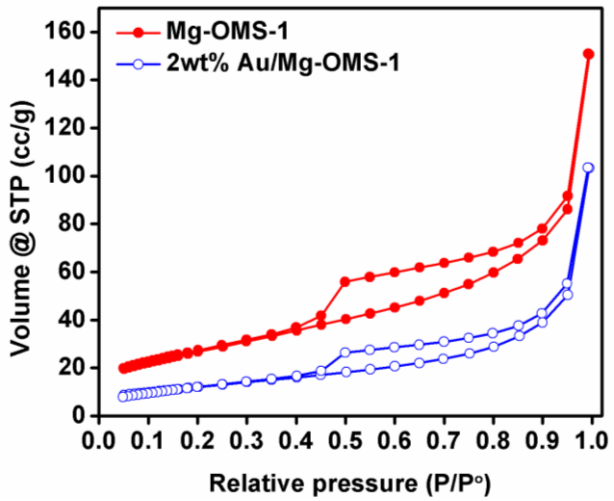

Fig. 5.2 N_2 adsorption-desorption isotherm of Mg-OMS-1 and 2wt% Au/Mg-OMS-1 catalyst.

The BET specific surface area values of Mg-OMS-1 and 2wt% Au/Mg-OMS-1 are included in Table 5.1. Mg-OMS-1 has surface area of 84.0 m^2g^{-1} which has increased to 97.3 m^2g^{-1} on Au loading. This Au containing sample has higher external surface area compared to the support, as determined by t-method (Table 5.1). The increase in surface area of the Au containing catalyst is attributed to the additional surface area accrued from the metal present on the support. However, the internal surface area, total pore volume, pore diameter of Au loaded material has declined due to the replacement of Mg by larger Au leading to the partial blockage of pores. The catalysts loaded with different metals such as Ru, Pd and Pt on Mg-OMS-1 has similar kind of observation of Au loaded on Mg-OMS-1. The catalyst system of Au on K-OMS-2 and H-OMS-2

have seen an increase in the surface area after metal loading, the surface are of K-OMS-2 is 99.7 m^2/g, which decreased to 85.0 m^2/g after exchanging with H^+ (Table 5.1).

Table 5.1 N_2 adsorption and CO_2-TPD results of the catalysts.

Entry	Catalyst	BET surface area (m^2/g)	Pore volume (cc/g)	Average pore diameter (Å)	T-method surface area		Basicity (mmol/g)[a]
					Ext.	Int.	
1	Mg-OMS-1	84.0	0.13	5.7	70.3	13.7	1.09
2	2wt% Au/Mg-OMS-1	97.3	0.11	4.6	97.3	0	0.89
3	2wt% Pd/Mg-OMS-1	117.0	0.12	4.1	117.0	0	0.79
4	2wt% Ru/Mg-OMS-1	122.1	0.11	3.6	122.1	0	0.95
5	2wt% Pt/Mg-OMS-1	72.3	0.11	4.3	72.3	0	0.40
6	K-OMS-2	99.7	0.13	5.5	76.3	23.3	0.67
7	2wt% Au/K-OMS-2	109.0	0.12	5.2	89.0	20.0	0.38
8	H-OMS-2	85.0	0.11	5.6	67.0	18.0	0.42
9	2wt% Au/H-OMS-2	101.9	0.13	5.4	86.0	15.8	0.41

[a] Determined by CO_2-TPD.

5.5.1.3. Chemical analysis of the prepared materials

Chemical analyses of various catalysts used in this study were carried using ICP-OES Table 5.2). It was observed that on Au exchange, Mg content decreased somewhat, compared to parent Mg-OMS-1. This clearly shows that the Mg is exchanged with precious metals.

Table 5.2 ICP-OES analysis of the catalysts for chemical composition.

Entry	Catalyst	Metal wt.%			
		Mn	Mg	K	X*
1	Mg-OMS-1	45.0	4.5	-	-
2	2wt% Au/Mg-OMS-1	44.4	4.1	-	1.95
3	2wt% Pd/Mg-OMS-1	45.2	3.7	-	2.02
4	2wt% Ru/Mg-OMS-1	43.8	3.9	-	2.10
5	2wt% Pt/Mg-OMS-1	44.7	2.9	-	1.91
6	K-OMS-2	51.3	-	3.1	-
7	2wt% Au/K-OMS-2	51.2	-	2.8	1.88
8	H-OMS-2	50.6	-	2.3	-
9	2wt% Au/H-OMS-2	50.8	-	2.1	1.90

* Noble metal

5.5.1.4. Temperature programmed desorption of CO_2

The basicity of Mg-OMS-1 was investigated by using CO_2-TPD (Fig. 5.3). Three CO_2 desorption peaks were seen centered around 140, 320 and >450 °C.[45] These peaks are assigned to weak (low temperature), moderate (medium temperature) and strong basicity (high temperature) of the sample, corresponding to CO_2 desorbed from different sites of Mg^{2+} located at different positions. The Mg^{2+} ions are expected to be present on the surface, inside the tunnel and framework.

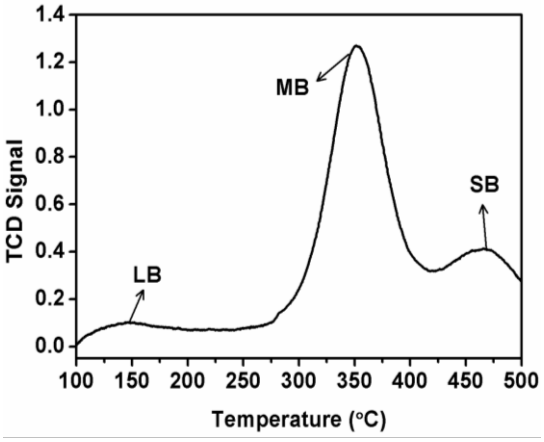

Fig. 5.3 CO_2 TPD of Mg-OMS-1.

Since, the ionic radii of Mn^{2+} (0.81 Å) and Mg^{2+} (0.86 Å) are close,[46] hydroxide sphere of $Mn(OH)_6^{4-}$ and $Mg(OH)_6^{4-}$ also must be in similar size.[47] The basicity of all precious metal loaded catalysts was lower than the corresponding bare Mg-OMS-1 support (Table 5.1, Entry 1-5). The decrease in the basicity was high for Pt loaded on Mg-OMS-1. There must be exchange of Mg^{2+} ions present in the tunnels of the support with Pt^{4+}, as a result of similarity in their ionic radii (ionic radii of Pt^{4+} is 0.76 Å and 0.86 Å for Mg^{2+}).[48] Results of ICP-OES show that the amount of Mg^{2+} decreased in metal loaded catalysts. The basicity of K-OMS-2 is lower than Mg-OMS-1, which again decreased for H-OMS-2 after exchanging with H^+ (Table 5.2).

5.5.1.5. Thermogravimetric analysis (TGA)

Thermogravimetric analysis of various catalyst materials was carried out in air flow in the temperature range of 25-800 °C, while heating the sample @ 5 °C/min. The TGA curves of Mg-OMS-1 and 2wt% Au/Mg-OMS-1 show weight loss in three temperature zones, i.e., 50-250 °C, 250-400 °C and 400-650 °C (Fig. 5.4a and b). Weight loss up to 250 °C is due to the loss of physically adsorbed water. The second weight loss is attributed to the water bound to the tunnels.

The third high temperature weight loss is attributed to the collapse of tunnel structure, which results in the formation of $MgMn_2O_4$.[49] As the temperature increased, Mn gets reduced releasing oxygen which led to the breakdown of octahedral framework. TGA curve shows that the Mg-OMS-1 can be thermally stable up to 300 °C. DTG analysis of the materials shows a major weight loss around 300 °C and 650 °C which correspond to loss of water in tunnel and loss of lattice oxygen respectively (Fig. 5.4b).

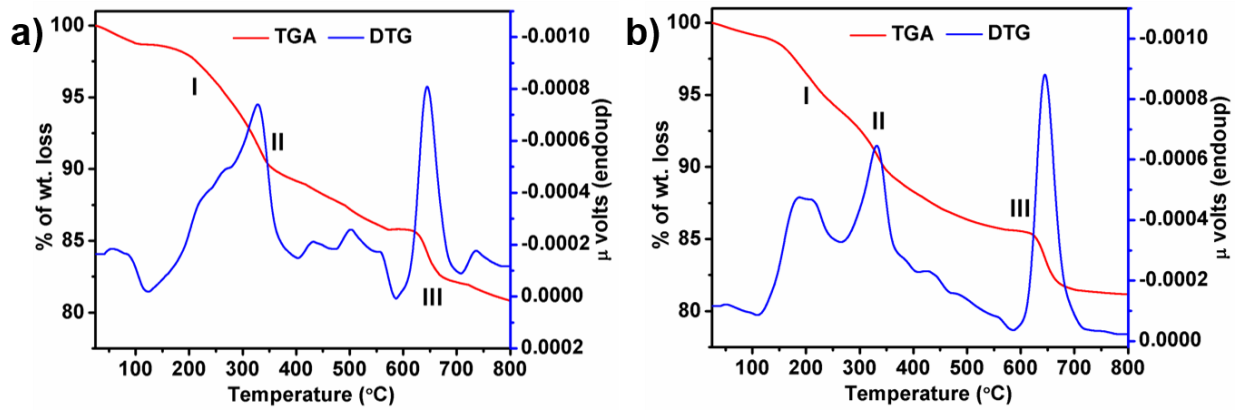

Fig. 5.4 TGA and DTG of (a) Mg-OMS-1, (b) 2wt% Au/Mg-OMS-1.

5.5.1.6. Scanning electron microscopy

The scanning electron micrographs of Mg-OMS-1 and 2wt% Au/Mg-OMS-1 show fibrous needle and platelet like morphology (Fig. 5.5). The morphology of 2wt% Au/Mg-OMS-1 is similar to that of parent Mg-OMS-1. The results show that the Au loading has no effect on the morphology of the support.

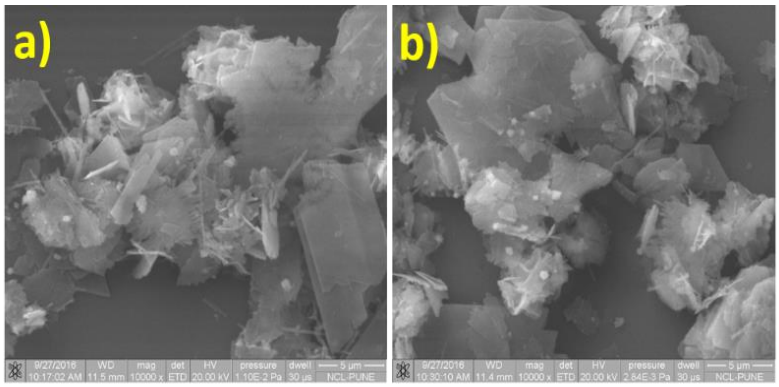

Fig. 5.5 SEM image of the (a) Mg-OMS-1 and (b) 2wt% Au/Mg-OMS-1.

5.5.1.7. Transmission electron microscopy

The needle like structure of Mg-OMS-1 was confirmed by TEM (Fig. 5.6a). The mean particle size and the distribution of particles were analyzed by TEM for 2wt% Au/Mg-OMS-1. It can be seen that the Au nanoparticles with an average size of 3.0 nm were homogeneously distributed throughout the Mg-OMS-1 support (Fig. 5.6b, 3c).

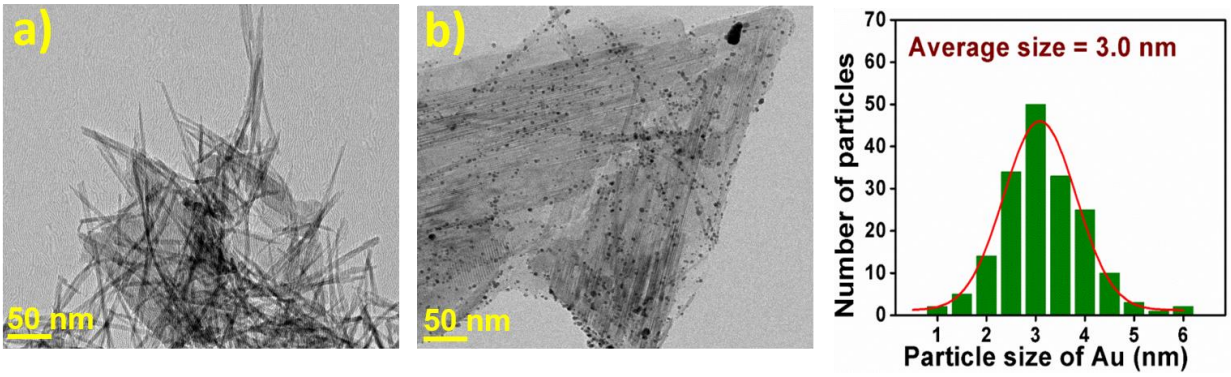

Fig. 5.6 TEM images of (a) Mg-OMS-1, (b) 2wt% Au/Mg-OMS-1 and (c) particle size distribution of 2wt% Au/Mg-OMS-1.

5.5.1.8. XPS of various Mg-OMS-1 materials

In order to understand the chemical states of the elements, XPS of various Mg-OMS-1 catalysts were studied. After background subtraction, the curves were deconvoluted to their components using a mix of Gaussian–Lorentzian (G–L) functions.

The O1s spectrum of 2wt% Au/Mg-OMS-1 (Fig. 5.7a) clearly shows the presence of three different oxygens. These oxygen species were identified and deconvoluted. The low binding energy peak (530.0 eV, O^{I}) is associated with lattice oxygen (O^{2-}) in Mn octahedral, while the medium BE peak (531.6 eV, O^{II}) is attributed to surface oxygen (O^{2-}or O^{-}), OH^{-} groups and oxygen vacancies, the high BE peak (533.0 eV, O^{III}) is assigned to the molecular water present in the tunnels of Mg-OMS-1. The major component corresponds to the lattice oxygen, the nature of the O^{II} species in these materials may be related to the presence of oxygen vacancies that creates defects. The interaction of these point defects with molecular oxygen and/or water generates peroxides, super oxides and hydroxyl species.[50, 51]

Figure 5.7b shows the XPS spectra of Mn 2p in Mg-OMS-1 catalyst. The prominent peaks at 641.4 and 652.6 eV correspond to Mn $2p_{3/2}$ and Mn $2p_{1/2}$ respectively for +4 oxidation

state. The peaks at 643.3 and 654.9 eV corresponds to Mn $2p_{3/2}$ and Mn $2p_{1/2}$ respectively for +3 oxidation state.

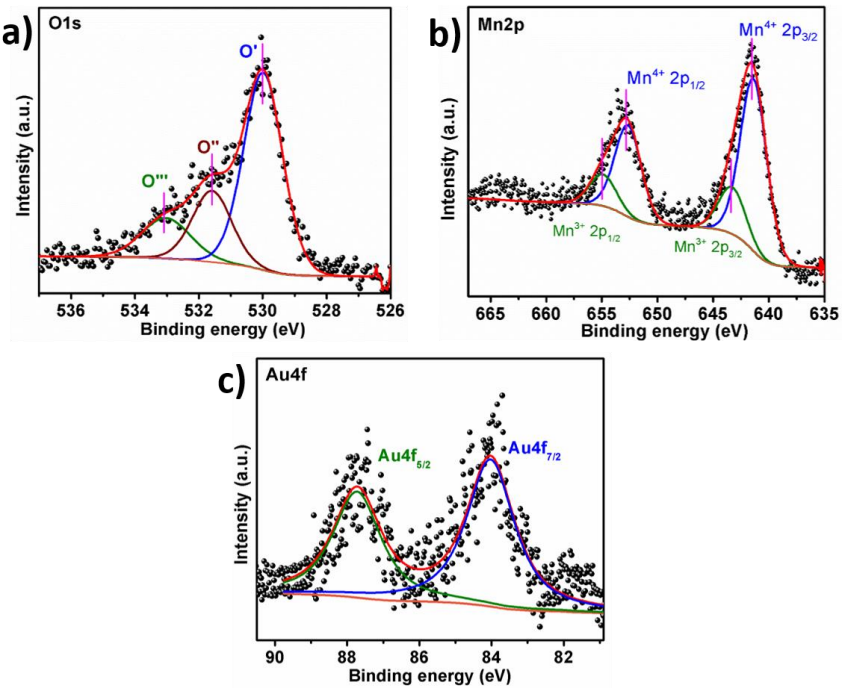

Fig. 5.7 XPS spectrum of Au/Mg-OMS-1, (a) O1s, (b) Mn2p and (c) Au4f.

Fig. 5.7c shows the high-resolution XPS spectrum of the Au 4f core level region. Two distinct lines separated by 3.7 eV were observed, namely the Au $4f_{5/2}$ and $4f_{7/2}$, which occur because of the spin–orbit splitting of the Au 4f level.[52] The BE corresponds to $4f_{7/2}$ and $4f_{5/2}$ are 84.0 and 87.7 eV, respectively shows that the gold is present in its metallic state (Au^0).

5.5.2. Catalytic activity in partial oxidation of glucose to GA

Partial oxidation of glucose to GA was studied in the absence of an added base. Various process parameters such as reaction temperature, O_2 pressure, reaction time, type of precious metal and different OMS structure were investigated.

5.5.2.1. Oxidation of glucose over different supported precious metal catalysts

Glucose oxidation was initially compared on different precious metals as catalysts, supported on Mg-OMS-1. The reaction was carried at glucose/metal mole ratio of 100 and at 70 ^oC. The results are given in Table 5.3. High conversion of glucose along with high yield of GA was obtained when Au is the active metal, with the activity following the order Au>Pt>Pd>Ru. It

is reported in the literature that Au shows superior activity among the precious metals.[24, 53] When support Mg-OMS-1 alone was used as catalyst, no glucose oxidation activity was observed. Further investigations were carried out to optimize reaction conditions in order to get high glucose oxidation activity and good GA yields.

Table 5.3 Product distribution during glucose oxidation over precious metal loaded Mg-OMS-1.[a]

Entry	Catalyst	Conv. of glucose (mol %)	Yield of GA (mol %)	Selectivity (%)				
				GA	GUA	GCA	TA	OA
1	No catalyst	0	0	0	0	0	0	0
2	Mg-OMS-1	0	0	0	0	0	0	0
3	2wt% Au/Mg-OMS-1	100.0	94.1	94.1	1.8	3.7	2.3	4.5
4	2wt% Pd/Mg-OMS-1	4.6	4.6	100.0	0	0	0	0
5	2wt% Ru/Mg-OMS-1	0	0	0	0	0	0	0
6	2wt% Pt/Mg-OMS-1	20.7	17.7	85.4	2.5	4	1.4	3.7

[a] Reaction conditions: Glucose = 0.04 M (1 mmol), H_2O = 25 mL, Catalyst (glucose/metal = 100), Temperature = 70 ^oC, Time = 10 h, Pressure = 5 bar O_2. GA = gluconic acid. GUA = glucuronic acid. GCA = glucaric acid. TA = tartronic acid and OA = oxalic acid.

5.5.2.2. Effect of O_2 pressure

The effect of oxygen pressure on the reaction was investigated and the results are given in Table 5.4. The results show that at all O_2 pressures, 100 mol% conversion of glucose was observed. However, the time for reaching 100 mol% glucose conversion increased with decreasing O_2 pressure. The optimum yield of GA was 94.1 mol% at 5 bar O_2 pressure after 10 h of reaction (Table 5.4, Entry 2). The rate of reaction is directly proportional to the O_2 pressure is clearly evident from the results. When 5 bar air was used instead of 5 bar pure O_2, the reaction rate decreased and only 93.4 mol% conversion of glucose with 86.2 mol% yield was observed after 12 h of reaction (Table 5.4, Entry 4). But, when the reaction temperature was increased at 5 bar air pressure, the reaction rate increased to reach 100 mol% glucose conversion in 6 h, leading to GA yield of 90.8 (Table 5.4, Entry 5). While the GA yield and selectivity depends on other reaction parameters, long duration of the reaction at high O_2 pressures led to lowering of GA selectivity. This decrease in GA selectivity is due to further oxidation of GA to GCA and cleavage of C-C results in the formation of lower carbon acids (tartronic and oxalic acids) and even carbon oxides.[6, 41, 44]

Table 5.4 Product distribution during glucose partial oxidation.[a]

Entry	Time (h)	Oxygen pressure (bar)	Conv. of glucose (mol %)	Selectivity GA (%)	Yields (mol %)				
					GA	GUA	GCA	TA	OA
1	12	2	100	90.9	90.9	1.7	3.0	1.8	3.3
2	10	5	100	94.1	94.1	1.8	3.7	2.3	4.5
3	8	8	100	91.8	91.8	1.2	4.4	2.1	2.3
4[b]	12	5	93.4	92.3	86.2	1.8	3.8	2.1	3.1
5[c]	6	5	100.0	90.8	90.8	2.5	5.4	1.3	4.0

[a] Reaction conditions: Glucose = 0.04M (1 mmol), H_2O = 25 mL, Catalyst = 2wt% Au/Mg-OMS-1, (glucose/metal = 100), Temperature = 70 °C, stirring speed (1000 rpm). [b] Air. [c] Air, Temperature = 90 °C. GA = gluconic acid. GUA = glucuronic acid. GCA = glucaric acid. TA = tartronic acid and OA = oxalic acid

5.5.2.3. Effect of reaction temperature

The influence of reaction temperature on glucose oxidation was examined; a clear influence of temperature on glucose conversion and product selectivity was observed (Fig. 5.8).

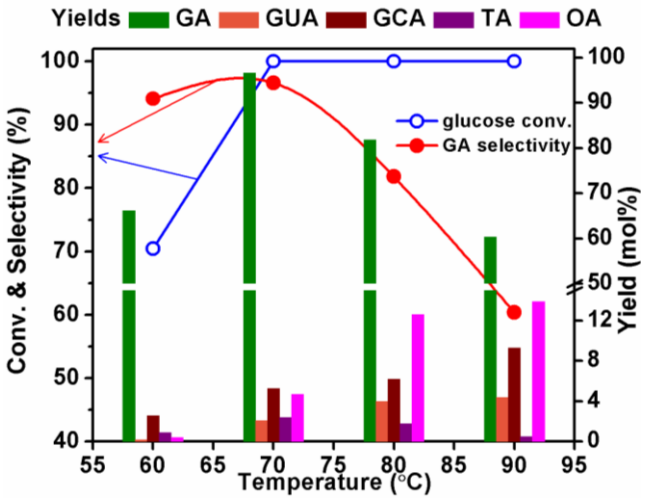

Fig. 5.8 Effect of temperature on oxidation of glucose.

Reaction conditions: Glucose = 0.04 M (1 mmol), H_2O = 25 mL, Catalyst = 2wt% Au/Mg-OMS-1, (glucose/metal = 100), stirring speed (1000 rpm), Time = 10 h, Pressure = 5 bar O_2. GA = gluconic acid. GUA = glucuronic acid. GCA = glucaric acid. TA = tartronic acid and OA = oxalic acid.

Glucose conversion increased progressively from 70.4 to 100 mol%, when temperature is raised from 60 to 70 °C and remained same beyond 80 °C (Fig. 5.8). Though 100 mol% glucose conversion could be achieved at 80 and 90 °C within shorter durations (6 and 4 h respectively), better GA selectivity could be obtained at 70 °C, as higher temperatures led to a fall in GCA

selectivity even in a shorter time. This could be attributed to the C-C cleavage of products formed leading to the formation of tartronic and oxalic acids at these high temperatures.[3, 6, 44] The decrease in selectivity is also partly attributed to the consecutive oxidation of GA to GCA.

5.5.2.4. Time on stream performance of 2wt% Au/Mg-OMS-1

By taking into consideration the effects of various parameters, reaction was monitored with time on stream with 2wt% Au/Mg-OMS-1 catalyst. As can be seen in Fig. 5.9, continuous increase in the glucose conversion was observed upto 9 h (30.7 to 100 mol%). The GA yield also increased from 29.2 to 92.8 mol% during this period, which further went up to 94.1 mol% after 10 h. Beyond this reaction time, GA yield fell due consecutive oxidation of products. The decrease in the yield of GA is mainly due to C-C cleavage, as C6 and C3 polyols undergo C-C cleavage under oxidation conditions in presence of base or basic support. The results also show that the rate of GCA formation from GA is much slower compared to glucose conversion to GA. The formation of GCA needs much longer time as the activation of GA is dificult compared to acivation of glucose. Moreover, at the initial stages of the reaction glucose is the only substrate that competes for the active catalytic sites, whereas with increasing time the products formed including GA competes for the same catalytic sites. This results in the decreased rate of reaction for GA to GCA, till the completer conversion of glucose. The activation of 1° alcohol group in GA is more difficult than activation of aldehyde group in glucose.

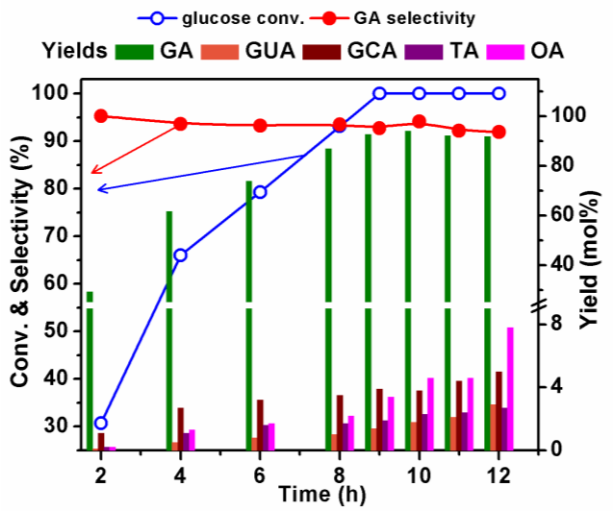

Fig. 5.9 Time on stream study of glucose oxidation.

Reaction conditions: Glucose = 0.04 M (1 mmol), H_2O = 25 mL, Catalyst = 2wt% Au/Mg-OMS-1, (glucose/metal = 100), stirring speed (1000 rpm), Pressure = 5 bar O_2. GA = gluconic acid. GUA = glucuronic acid. GCA = glucaric acid. TA = tartronic acid and OA = oxalic acid.

5.5.2.5. Effect of OMS structure on GA yield

The effect OMS structure (OMS-1 or OMS-2), their pore size and the basic metal constituting them was investigated for glucose to GA reaction. The results are given in the Table 5.5. Mg-OMS-1 has pore size of about 6.9 Å, which is larger than the K-OMS-2 (pore size of 4.6 Å). In order to find the role of pore size, reaction was conducted over 2wt% Au/Mg-OMS-1 and 2wt% Au/K-OMS-2 catalysts. Highest glucose conversion and GA selectivity were obtained with Mg-OMS-1 as the support (Table 5.5, Entry 1 & 2), but with K-OMS-2, glucose conversion was only 65.1%, which decreased further to 54.2% when H^+ is exchanged for K^+ in K-OMS-2 support (Table 5.5, Entry 2 & 3). These results imply that the basicity of the support plays crucial role in the glucose oxidation activity. The decrease in the activity with change in the basic metal is due to decrease in the basicity of the support (Table 5.1) and the adsorption coefficient of glucose to support varies with support. Table 5.5 (Entry 2 & 3) also demonstrates the utility of basic metal (K^+ and H^+) on the yield. The results given in Table 5.5 also show that the yield of GA was high for Mg-OMS-1 support compared to other supports under identical reaction conditions (Entry 4-7). The lower yield of GA may be attributed to the fact that substrate is better activated in the presence of strong basic metal ions.

Table 5.5 Product distribution in glucose oxidation over Au supported on different supports.[a]

S. No	Catalyst	Conv. (mol %)	Selectivity GA (%)	Yield (mol %)				
				GA	GUA	GCA	TA	OA
1	2wt% Au/Mg-OMS-1	100.0	94.1	94.1	1.8	3.7	2.3	4.5
2	2wt% Au/K-OMS-2	65.1	78.2	51.0	0.0	3.5	5.2	5.4
3	2wt% Au/H-OMS-2	54.2	87.5	47.4	0.0	2.7	3.7	6.7
4	2wt% Au/MgO	57.0	79.6	45.4	4.8	2.0	5.0	4.9
5	2wt% Au/MnO_2	7.2	100.0	7.2	0.0	0.0	0.0	0.0
6	2wt% Au/Al_2O_3	17.4	100.0	17.4	0.0	0.0	0.0	0.0
7	2wt% Au/HT(3:1)	28.8	100.0	28.8	0.0	0.0	0.0	0.0

Reaction conditions: Glucose = 0.04 M (1 mmol), H_2O = 25 mL, Catalyst = (glucose/metal = 100), Temperature = 70 °C, Pressure = 5 bar O_2, Time = 10 h. GA = gluconic acid. GUA = glucuronic acid. GCA = glucaric acid. TA = tartronic acid and OA = oxalic acid.

Gold impregnated on different supports were used to investigate the role of support on the activity. Among other supports, MgO was found to be better compared to MnO_2, Al_2O_3 and

hydrotalcite (HT). These studies reveal that the presence of basic metal in the support or a basic oxide as support is necessary in conjunction with Au for better oxidation of glucose.

5.5.2.7. Recyclability study

The recyclability of the 2wt% Au/Mg-OMS-1 catalyst was probed by repeating the glucose selective oxidation reaction at least four times using the same catalyst, after washing it as described in section 5.4.1.4. After each run, the catalyst was separated by centrifugation and washed with 100 mL of milliQ water, dried at 60 °C for 6 h and reused for the next cycle. The results given in Fig. 5.10 show that the catalytic performance remains almost same, with 100% glucose conversion and 94.1% GA yield even after recycling the catalyst for four times. These results show excellent stability of the catalyst. In order to gain more insight into catalytic activity, XRD, SEM and TEM analysis of the used catalysts was performed. XRD results revealed that no change of the catalyst phase occurred even after its repeated use (Fig 5.11). The TEM image of the 2wt% Au/Mg-OMS-1 after 4 recycles exhibited average Au nanoparticle size of 3.4 nm (Fig. 5.12b and 5.12c), which was almost similar to that of the fresh catalyst (Fig. 5.6b and 5.6c).

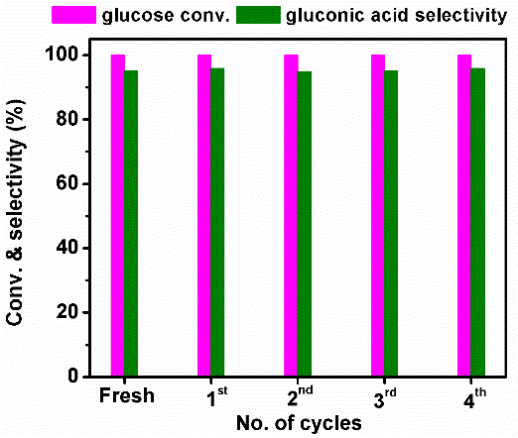

Fig. 5.10 Recyclability study of 2wt% Au/Mg-OMS-1 in glucose oxidation to GA.

Reaction conditions: Glucose to metal mole ratio of 100, 25 mL of 0.04 M glucose in H_2O, 2wt% Au/Mg-OMS-1 catalyst, Reaction time 10 h, Temperature = 70 ^oC, Pressure = 5 bar O_2.

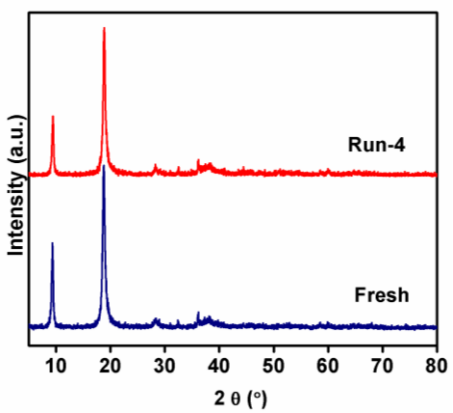

Fig. 5.11. XRD of fresh and used 2wt% Au/Mg-OMS-1 catalyst

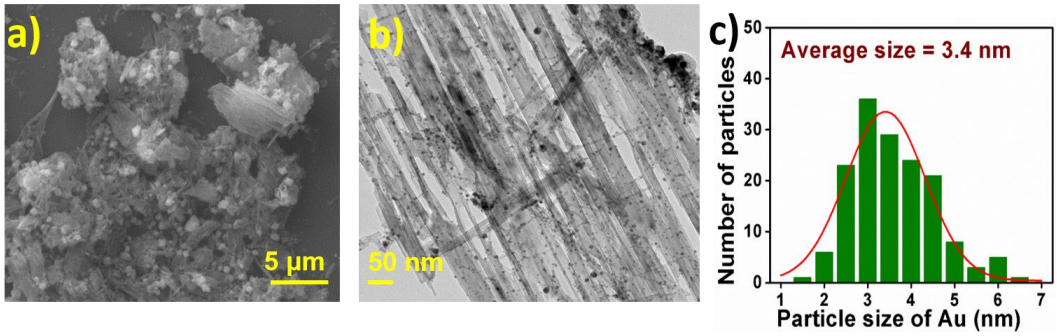

Fig. 5.12. Spent 2wt% Au/Mg-OMS-1; (a) SEM, (b) TEM and (c) particle size distribution.

5.6. Conclusions

The present study of glucose partial oxidation to gluconic acid shows that the chemo selective liquid phase oxidation of glucose can be done under very simple reaction conditions using Au catalysts supported on Mg-OMS-1. Catalyst with 2wt% Au on Mg-OMS-1 support shows good catalytic activity and high GA selectivity (94.1%) at 70 °C under 5 bar O_2 pressure. Choice of basic support is crucial for the reaction thus paving the way to carry out the reaction in the absence of a sacrificial base. Higher the basicity of the base, the more active is the catalyst that should have active metal as nanoparticles. Further, milder reaction conditions are highly beneficial to get better GA selectivity resulting in high yield of GA. The catalyst can be reused 4 times without any loss in activity or selectivity. Reduced catalytic activity was observed when K-OMS-2 and H-OMS-2 were used to supports Au nanoparticles. This decrease in the activity is due to the lower basicity of the support compared to Mg-OMS-1. These studies clearly demonstrate the utility of basic support in the absence of sacrificial external base for the reaction. Milder oxidation reaction conditions are a must to achieve higher GA yield during oxidation of glucose in presence of molecular oxygen.

Part 5B

5.7. Oxidation of GA to GCA over Pt/K-OMS-2 catalysts using molecular O_2

5.7.1. Experimental procedures

5.7.1.1. Materials

Tartaric acid, tartronic acid and potassium salt of D-Saccharic acid were procured from Sigma-Aldrich, USA. D-Gluconic acid, D-glucuronic acid and $HAuCl_4 \cdot 3H_2O$ were procured from Alfa Aesar, Johnson Matthey. Glyceric acid and $Mg(OAc)_2 \cdot 4H_2O$ were sourced from Loba Chemie Pvt. Ltd. Oxalic acid, $KMnO_4$, $MnSO_4 \cdot H_2O$ and HNO_3 were purchased from Merck, India. All the chemicals were used as received without any further purification.

5.7.1.2. Preparation of 2wt% Pt exchanged K-OMS-2

K-OMS-2 was synthesized as per the procedure given in the section 2.2.4. Catalyst Pt/K-OMS-2 containing 2wt%Pt was prepared through wet impregnation method. In a typical synthesis, required quantity of H_2PtCl_6 was taken in 20 mL distilled water and to this support was added under constant stirring for 2 h at 70 °C. This slurry was cooled to the room temperature and the metal was reduced using Aq. $NaBH_4$ (5 eq. to metal) under vigorous stirring. The sample was filtered, washed and dried at 60 °C for 6 h. The resulting catalyst is named as 2wt% Pt/K-OMS-2. The detailed procedure is given in section 2.2.4.1.

5.7.1.3. Evaluation of catalysts for GA oxidation to GCA

The GA oxidation reaction was conducted using a 50 mL Parr (4848) autoclave. In a typical reaction, required quantity of GA was dissolved in 25 mL of water, to it freshly activated catalyst was added. The reactor was closed and flushed with O_2 before heating it to the desired temperature under continuous stirring (1000 rpm). When the reaction mixture reached the temperature, O_2 was fed into the reactor. To monitor progress of the reaction, 0.5 mL of product mixture was removed at regular intervals, filtered through nylon 0.22 µm filter and analyzed by HPLC. At the end of the reaction, the product mixture was filtrated through a filter paper to separate the catalyst and the filtrate was analyzed using HPLC, equipped with RI detector and H^+ Aminex column (305 mm × 7.8 mm) using 1 mmol of succinic acid as the mobile phase. The flow rate of mobile phase was 0.3 $mL.min^{-1}$, while column temperature was maintained at 25 °C. All product components were confirmed by matching with authentic standards.

5.8. Results and discussion on gluconic acid to glucaric acid

5.8.1. Characterization of catalysts

K-OMS-2 support was prepared as described in the experimental section of chapter-2 and used to prepare precious metal supported catalysts through wet impregnation method. These materials were characterized using an array of physic-chemical methods.

5.8.1.1. X-ray diffraction (XRD)

Figure 5.13 shows XRD pattern of as synthesized K-OMS-2 and 2wt% Pt/K-OMS-2. XRD pattern of both match with the reported data of cryptomelane K-OMS-2 (JCPDS 05-0681). Peaks belonging to 2wt% Pt/K-OMS-2 catalysts are sharp and are similar to the K-OMS-2, showing that no changes occurred in K-OMS-2 on Pt loading, confirming that its cryptomelane structure is retained even after metal loading. No additional peaks corresponding to platinum oxides or Pt metal were seen, indicating the absence of any other Pt containing phases, thus confirming the homogeneous distribution of metal in Pt/K-OMS-2.

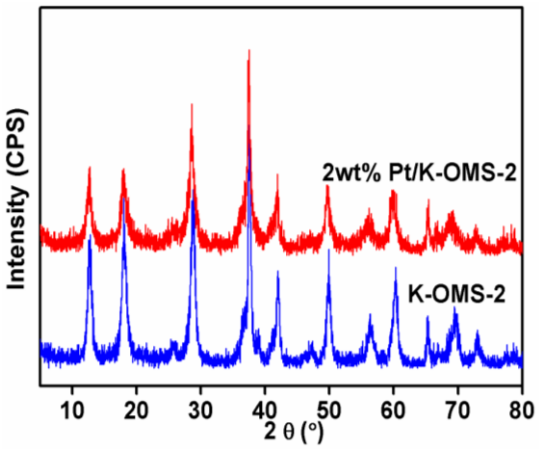

Fig. 5.13 XRD pattern of K-OMS-2 and 2wt% Pt/K-OMS-2.

5.8.1.2. Chemical analysis and N_2 physisorption of the prepared materials

The K-OMS-2 and 2wt% Pt/K-OMS-2 were investigated by N_2 sorption. As may be seen from Fig. 5.13, K-OMS-2 and 2wt% Pt/K-OMS-2 samples showed characteristic Type II sorption and H3-type hysteresis loop for P/P0 > 0.6 that may be attributed to inter crystalline mesopores between particles with non uniform size or shapes. The BET specific surface area values of K-OMS-2 and 2wt% Pt/K-OMS-2 are included in Table 5.6. Sample K-OMS-2 has

surface area of 99.7 m^2g^{-1}, which has increased to 103 m^2g^{-1} after Pt loading. The Pt loaded sample has higher surface area compared to the support, as determined by the t-method (Table 5.6). This increase in surface area of the Pt loaded catalyst is attributed to the additional surface area gained from the metal present in the catalyst. Similar result was observed for 2wt% Au/K-OMS-2 catalyst, as its surface area increased to 109 m^2g^{-1}. Even in the case of Au loaded Mg-OMS-1 (2wt% Au/Mg-OMS-1) its BET surface area was 97.3 m^2g^{-1} compared to 84 m^2g^{-1} of Mg-OMS-1.

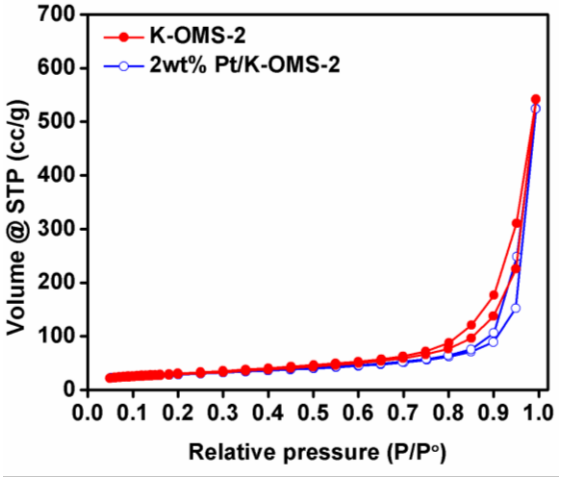

Fig. 5.13 N_2 adsorption-desorption isotherm of K-OMS-2 and 2wt% Pt/K-OMS-2 catalyst.

Table 5.6 ICP-OES analysis and N_2 adsorption results of the catalysts.

Entry	Catalyst	Metal wt.%				BET surface area (m^2/g)	Pore volume (cc/g)	Average pore diameter (Å)
		Mn	Mg	K	X*			
1	K-OMS-2	51.3	-	3.1	-	99.7	0.13	5.5
2	2wt% Au/K-OMS-2	51.2	-	2.8	1.88	109.0	0.12	5.2
3	2wt% Pt/K-OMS-2	51.3	-	2.9	1.92	103.1	0.11	5.2
4	Mg-OMS-1	45.0	4.5	-	-	84.0	0.13	5.7
5	2wt% Au/Mg-OMS-1	44.4	4.1	-	1.95	97.3	0.11	4.6

* Precious (Au, Pt) metal in the sample

Chemical analysis of various catalysts used in this study was carried out by ICP-OES. It was observed that on Pt exchange, K content decreased compared to parent K-OMS-2. This clearly shows that the potassium has been replaced by precious metals through exchange.

5.8.1.3. Thermogravimetric analysis (TGA)

Thermogravimetric analysis of various catalysts was carried out in air flow in the temperature range of 25-800 °C, by heating the sample @ 5 °C/min. The TGA curves of K-OMS-2 and 2wt% Pt/K-OMS-2 show weight loss in three temperature zones, i.e., 200-400, 400-650 and 650-800 °C (Fig. 5.14a and b). Weight loss of up to 400 °C is due to the loss of physically adsorbed water bound to the sample. The second high temperature weight loss (6.7%) is attributed to the collapse of tunnel structure, as a result of loss of lattice oxygen and the Mn cations reduce to lower oxidation state forming manganese oxide such as bixbyite (Mn_2O_3).[54] As the temperature increased, Mn gets reduced releasing the oxygen leading to the breakdown of octahedral framework in the temperature zone of 650-800 °C. This is attributed to further loss of oxygen from bixbyite leading to the formation of more stable manganese oxides.[55]

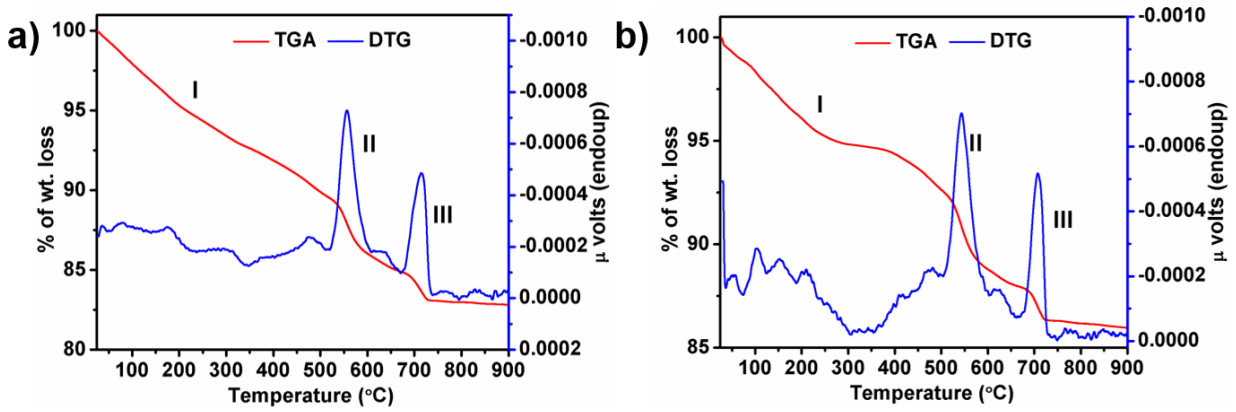

Fig. 5.14 TGA and DTG of (a) K-OMS-2, (b) 2wt% Pt/K-OMS-2.

TGA analysis shows that the K-OMS-2 is thermally stable up to 400 °C. DTG analysis of the materials shows major weight losses around 500 and 700 °C that corresponds to loss of water in tunnels and loss of lattice oxygen respectively (Fig. 5.14).

5.8.1.4. Scanning electron microscopy

The scanning electron micrographs show fibrous needle-like morphology of the particles aggregated together for K-OMS-2 and 2wt% Pt/K-OMS-2 (Fig. 5.15). The morphology of 2wt% Pt/K-OMS-2 is similar to that of K-OMS-2 with 20 to 200 nm size of fiber length. The fibrous morphology of the produced materials is indicative of the anisotropic growth behavior of K-OMS-2. During the crystallization process of the undoped synthetic K-OMS-2 material, the crystal growth in the c-direction leads to the formation of fibrous material with 1×1 and 2×2

tunnels running along the length of the nanofibers. The results show that the Pt loading has no effect on the morphology of the K-OMS-2 support.

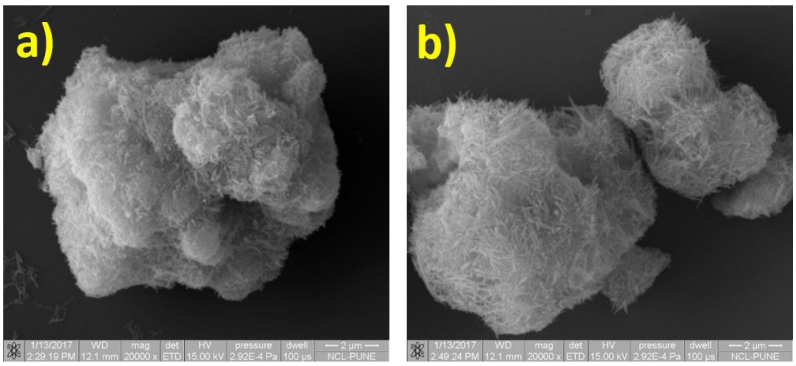

Fig. 5.15 SEM image of the (a) K-OMS-2 and (b) 2wt% Pt/K-OMS-2.

5.8.1.5. Transmission electron microscopy

TEM images of K-OMS-2 and 2wt% Pt/K-OMS-2 can be seen in Fig. 5.16. The nanoscale sized fibers are self-assembled into complex hollow structures. The mean particle size and the distribution of particles is analyzed by TEM for 2wt% Pt/K-OMS-2. It can be seen that the Pt nanoparticles with an average size of 3.2 nm were homogeneously distributed throughout the K-OMS-2 support (Fig. 5.16b and c).

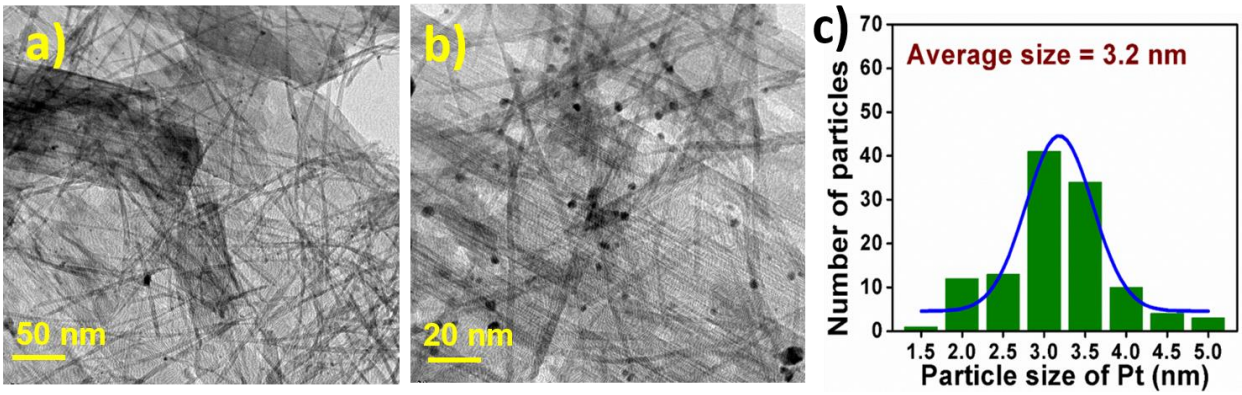

Fig. 5.16 TEM image of the (a) K-OMS-2 and (b) 2wt% Pt/K-OMS-2 and (c) particle size distribution of 2wt% Pt/K-OMS-2.

5.8.2 Catalytic activity in selective oxidation of GA to GCA

Part-A of this chapter had dealt with partial oxidation of glucose to gluconic acid (GA). In Part-B, we discuss on the results of the GA to glucaric acid (GCA), which is a consecutive step in glucose to glucaric acid (glucose → GA → GCA) preparation. Since, 2wt% Au/Mg-

OMS-1catalyst was found to be good for glucose to GA conversion; initially the same catalyst was screened for GA to GCA partial oxidation. But, our investigations showed that this catalyst is not good for partial oxidation of GA, hence we have tried to develop another octahedral molecular sieve based catalyst, i.e., precious metal supported on K-OMS-2, for this study.

5.8.2.1. Oxidation of GA over Mg-OMS-1 and K-OMS-2 supported precious metal catalysts

As mentioned above, initial studies were conducted to explore the activity of 2wt% Au/Mg-OMS-1 in partial oxidation of GA to GCA. The results in Table 5.7 shows GA conversion of 15.0 mol% with GCA yield of 1.5 mol% (Table 5.7, Entry 3), showing poor activity of 2wt% Au/Mg-OMS-1 for GA to GCA step. On the otherhand, this catalyst was very good for glucose to GA oxidation under similar reaction conditions. Hence, we have changed the support to K-OMS-2 and used it for supporting 2wt% Au. On this catalyst, GA conversion was 18.8 mol%, but GCA yield was only 2.2 mol%, only slightly better compared to 2wt% Au/Mg-OMS-1 (Table 5.7, Entry 3, 4). These results show that there is only marginal improvement even after changing the support from Mg-OMS-1 to K-OMS-2. Glucose is in pyranose form and can be activated with Mg-OMS-1 support which has 3x3 tunnels of 6.9 Å, whereas GA is in open chain form and is better activated by K-OMS-2 which has 2x2 tunnels of 4.6 Å.

Table 5.7 Product distribution during oxidation of gluconic acid to glucaric acid.[a]

Entry	Catalyst	Conv. of GA (mol %)	Selectivity of GCA (%)	Yield (mol %)					
				GUA	GCA	TA	GLY	OA	TTA
1	No catalyst	0	0	0	0	0	0	0	0
2	Mg-OMS-1	0	0	0	0	0	0	0	0
3	K-OMS-2	0	0	0	0	0	0	0	0
4	2wt% Au/Mg-OMS-1	15.0	10.1	0.7	1.5	4.2	0	1.0	0
5	2wt% Au/K-OMS-2	18.8	11.7	0	2.2	1.8	3.2	4.8	1.2
6	2wt% Pt/K-OMS-2	20.8	35.6	0	4.2	4.2	3.5	5.0	2.7

[a] Reaction conditions: GA = 0.04 M (1 mmol), H_2O = 25 mL, Catalyst (glucose/metal = 100), Temp. 70 ^oC, Time = 8 h, Pressure = 5 bar O_2. GA = gluconic acid. GUA = glucuronic acid. GCA = glucaric acid. TA = tartronic acid. GLY = glyceric acid. TTA = tartaric acid and OA = oxalic acid.

Though both the supports (Mg-OMS-1 and K-OMS-2) contain same metal (Au) content, the activity differed due to change of support. The activity may depend on factors such as adsorption coefficient of substrate to support, orientation of the adsorbed substrate etc. To

improve the activity of K-OMS-2 based catalyst further, reaction was carried out using Pt supported on K-OMS-2 under similar reactions conditions, using GA to metal ratio of 100 at reaction temperature of 70 °C. This will provide the role of active metal. Very good conversion of GA (20.8 mol%) and improved yield of GCA (4.2 mol%) were observed using the Pt/K-OMS-2 catalyst (Table 5.7, Entry 5). The better activity of Pt catalyst may be due to the selective activation of 1° alcohol in GA by Pt. The activity follows the order of Au/Mg-OMS-1<Au/K-OMS-2<Pt/K-OMS-2. It is reported in the literature that Pt shows superior activity among the noble metals.[6, 12, 41, 44] When K-OMS-2 alone was used as support, no glucose oxidation activity was observed. Further investigations were carried out to optimize the reaction conditions in order to improve oxidation activity and good GCA yields from GA/glucose.

5.8.2.2. Effect of reaction temperature

The influence of reaction temperature on GA oxidation to GCA was examined; clear promotional effect of temperature on GA conversion was observed (Fig. 5.17). The conversion progressively increased from 20.8 to 52.1 mol%, when the temperature was raised from 70 to 100 °C. Though the conversion increased, the GCA formed improved only marginally to ~6 mol%. At high reaction temperatures, the GCA selectivity might be low due to C-C bond cleavage of products formed and could also be attributed to consecutive reactions. The C-C cleavage results in the formation of tartronic acid, tartaric acid, glyceric acid and oxalic acids.

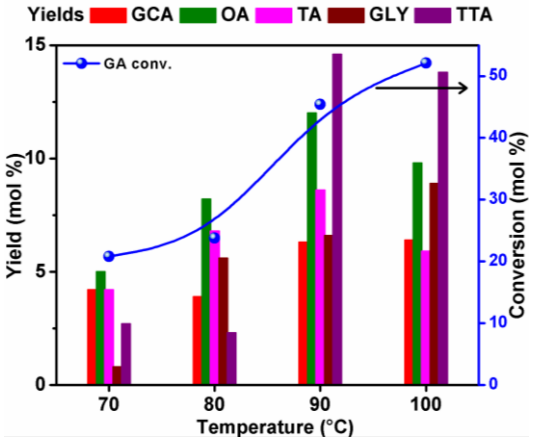

Fig. 5.17 Effect of temperature on oxidation of glucose.

Reaction conditions: GA = 0.04 M (1 mmol), H_2O = 25 mL, Catalyst = 2wt% Pt/K-OMS-2, (GA/metal = 100), stirring speed (1000 rpm), Time = 8 h, Pressure = 5 bar O_2. GA = gluconic acid. GUA = glucuronic acid. GCA = glucaric acid. TA = tartronic acid. GLY = glyceric acid. TTA = tartaric acid and OA = oxalic acid.

5.8.2.3. Effect substrate to metal mole ratio

Table 5.8 Effect of mole ratio of substrate to metal on GA oxidation.[a]

Entry	Substrate to metal mole ratio	GA Conversion (mol %)	Selectivity of GCA (%)	Yield (mol %)					
				GUA	GCA	TA	GLY	OA	TTA
1	100	29.4	22.5	0	6.6	8.5	5.0	13.0	7.6
2	75	20.6	39.0	0	13.6	7.8	3.9	9.0	6.3
3	50	38.5	53.6	0	20.6	8.6	3.3	8.6	9.3

[a] Reaction conditions: GA = 0.04 M (1 mmol), H_2O = 25 mL, Catalyst = 2wt% Pt/K-OMS-2, Temperature = 90 °C, Time = 4 h, Pressure = 5 bar O_2. GA = gluconic acid. GUA = glucuronic acid. GCA = glucaric acid. TA = tartronic acid. GLY = glyceric acid. TTA = tartaric acid and OA = oxalic acid.

Different mole ratios of substrate to active metal were studied at two temperatures, i.e., 90 and 100 °C. The results obtained at 90 °C are shown in Table 5.8. A maximum yield of 20.6 mol% of GCA was obtained with substrate/metal ratio 50, showing that a higher metal/substrate ratio results in better GCA yields. Further, conducting the reaction for longer duration's results in the reduction of GCA yields as a result of its consecutive reactions of GCA.

5.8.2.4. Effect of O_2 pressure

The effect of O_2 pressure on the reaction with time on stream was studied and the results are given in Table 5.9. The results show that the conversion has increased with increasing O_2

Table 5.9 Effect of oxygen pressure on products distribution during GA oxidation.[a]

Entry	Oxygen pressure (bar)	Conv. of GA (mol %)	Selectivity of GCA (%)	Yield (mol %)					
				GUA	GCA	TA	GLY	OA	TTA
1	2	23.5	47.5	0	11.2	8.4	4.7	4.1	8.7
2	5	38.5	53.6	0	20.6	8.6	3.3	8.6	9.3
3	8	57.7	18.8	0	10.9	7.1	5.1	8.1	8.6

[a] Reaction conditions: GA = 0.04 M (1 mmol), H_2O = 25 mL, Catalyst = 2wt% Pt/K-OMS-2 (GA/metal = 50), Temperature = 90 °C, Time = 4 h, Pressure = 5 bar O_2. GA = gluconic acid. GUA = glucuronic acid. GCA = glucaric acid. TA = tartronic acid. GLY = glyceric acid. TTA = tartaric acid and OA = oxalic acid.

pressure, but the selectivity and GCA yield increased only in the O_2 pressure range of 2 to 5 bar and declined on further rise in the O_2 pressure. Optimum GCA yield and selectivity obtained were 20.6 mol% and 53.6% respectively at 5 bar O_2 pressure, 90 °C reaction temperature and

reaction time of 4 h (Table 5.9, Entry 2). The results show the rate of reaction is directly proportional to the O_2 pressure. Longer the duration of the reaction or higher O_2 pressure, the GCA selectivity decreased. The decrease in GCA selectivity in the presence of basic metal results in C-C cleavage thereby giving low carbon products.[6, 44]

5.8.2.5. Time on stream performance

By taking into consideration of the effect of all the above parameters, time on stream study of GA to GCA was conducted using 2wt% Pt/K-OMS-2 catalyst. As shown in Fig. 5.18, there is a steady increase in the GA conversion from 2 to 8 h (14.5 to 93.4 mol%) (Fig. 5.18a).

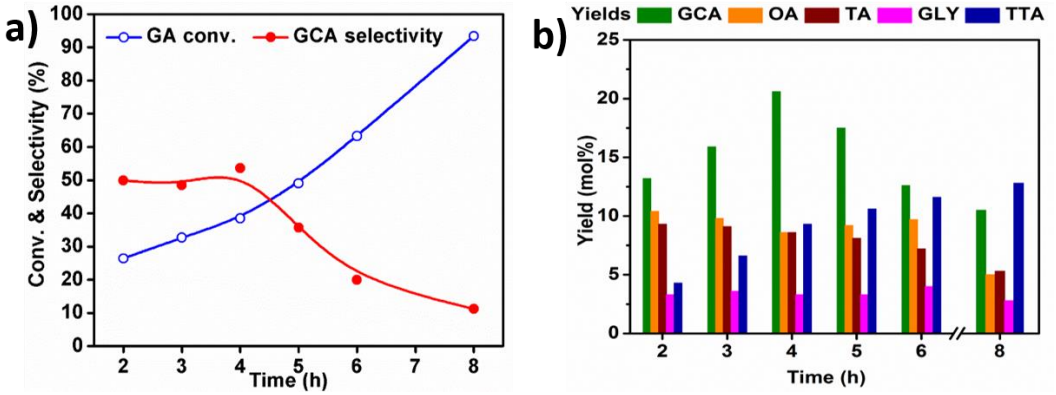

Fig. 5.18 Time on stem study, on glucose oxidation.

Reaction conditions: GA = 0.04 M (1 mmol), H_2O = 25 mL, Catalyst = 2wt% Pt/K-OMS-2 (GA/metal = 50), Temperature = 90 °C, Pressure = 5 bar O_2. GA = gluconic acid. GUA = glucuronic acid. GCA = glucaric acid. TA = tartronic acid. GLY = glyceric acid. TTA = tartaric acid and OA = oxalic acid.

The yield of GCA has increased from 13.2 to 20.6 mol% from 2h to 4 h, but on longer duration beyond 4h, the yield of GCA has reduced with time. The GCA formed reacts further and forms byproducts, leading to decrease in its yield. The decrease in the selectivity and yield of GCA is mainly due to C-C cleavage, C6 polyols undergo C-C cleavage under oxidation condition in presence of base/basic supports.[6,44] Since the rate of reaction for the selective formation of GCA from GA is slower than the C-C cleavage of C6 sugars, the formation of GCA takes longer duration and higher reaction temperatures are required to activate the 1° alcohol group on GA. Within this time, the product formed (GCA) undergoes C-C cleavage and total oxidation resulting in smaller chain carbon containing products.

5.9. Conclusions

Selective oxidation of glucose to glucaric acid (GCA) is a very important towards preparation of a monomeric intermediate with potential to get renewable adipic acid. However, it is difficult to get good yield of glucaric acid in a single step. Hence, we have planned to carry out this reaction in two steps; glucose → gluconic acid followed by gluconic acid → glucaric acid. Attempts were made to develop two active, selective and stable for these partial oxidation reactions. First part of the study reports selective oxidation of glucose to gluconic acid while the second part deals with gluconic to glucaric acid, both using precious metal catalysts supported on OMS materials. It was found that Mg-OMS-1 supported Au catalysts are highly active and selective for gluconic acid preparation. Whereas, this catalyst was not suitable for gluconic acid to glucaric acid conversion. On the other hand, Pt supported on K-OMS-2 catalysts showed reasonable yield of GCA, in liquid phase partial oxidation of GA under base free conditions. This catalyst shows good catalytic activity and high GCA yield (20.6 mol%) under optimized reaction conditions (90 °C, 5 bar O_2). Among the noble metals Au and Pt, the later was found to be more active for the selective oxidation of 1° alcohol group in GA with K-OMS-2 as the support. High yield of GCA was obtained within short reaction time under mild reaction conditions. It was observed that higher reaction temperature and longer duration of reaction led to C-C cleavage of products formed resulting in lower yield of GCA. Support plays key role in obtaining good yield of GCA. This study clearly shows that the presence of a basic metal on the support is necessary for better activity along with active metal.

5.10. Reference

1. Hustede H.; Haberstroh H. -J.; Schinzig E. In *Ullmann's Encyclopedia of Industrial Chemistry*, Wiley-VCH Verlag GmbH & Co: 2000.
2. Valentin Y. Doluda; Irina B. Tsvetkova; Alexey V. Bykov; Valentina G. Matveeva; Alexander I. Sidorov; Mikhail G. Sulman; Pyotr M. Valetsky; Barry D. Stein; Esther M. Sulman; Bronstein L. M. *Green Process Synth.* **2013,** 2, 25–34.
3. Hermans S.; Devillers M. *Appl. Catal. A: Gen.* **2002,** 235, 253–264.
4. Robert Wojcieszak; Iolanda M. Cuccovia; Márcia A. Silva; Liane M. Rossi. *J. Mol. Catal. A: Chem.* **2016,** 422, 35–42.
5. Werpy T.; Petersen G. *Top Value Added Chemicals from Biomass: Vol. 1: Results of Screening for Potential Candidates from Sugars and Synthesis Gas*; National Renewable Energy Laboratory: Golden, CO: 2004.
6. Xin Jin; Meng Zhao; Jian Shen; Wenjuan Yan; Liming He; Prem S. Thapa; Shenqiang Ren; Bala Subramaniam; Raghunath V. Chaudhari. *J. Catal.* **2015,** 330, 323–329.
7. Vyver S. V. d.; Román-Leshkov Y. *Catal. Sci. Technol.* **2013,** 3, 1465–1479.
8. Beerthuis R.; Rothenberg G.; Shiju N. R. *Green Chem.* **2015,** 17, 1341–1361.
9. Boussie T. R.; Dias E. L.; Fresco Z. M.; Murphy V. J.; Shoemaker J.; Archer R.; Jiang H. 2010.
10. Irina V. Delidovich; Oxana P. Taran; Lyudmila G. Matvienko; Alexander N. Simonov; Irina L. Simakova; Alesya N. Bobrovskaya; Valentin N. Parmon. *Catal Lett.* **2010,** 140, 14–21.
11. Serena Biella; Laura Prati; Michele Rossi. *J. Catal.* **2002,** 206, 242–247.
12. Dirkx J. M. H.; Van Der Baan H. S. *J. Catal.* **1981,** 67, 14-20.
13. Abbadi A.; van Bekkum H. *J. Mol. Catal. A: Chem.* **1995,** 97, 111-118.
14. Esther Sulman; Valentine Doluda; Stanislaw Dzwigaj; Eric Marceau; Leonid Kustov; Olga Tkachenko; Alexey Bykov; Valentina Matveeva; Mikhail Sulman; Natalia Lakina. *J. Mol. Catal. A: Chem.* **2007,** 278, 112–119.
15. Larry A. Larew; Dennis C. Johnson. *J. Electroanal. Chem.* **1989,** 262, 167-182.
16. Tamao Ishida; Naoto Kinoshita; Hiroko Okatsu; Tomoki Akita; Takashi Takei; Masatake Haruta. *Angew. Chem. Int. Ed.* **2008,** 47, 9265 –9268.
17. Hiroko Okatsu; Naoto Kinoshita; Tomoki Akita; Tamao Ishida; Masatake Haruta. *Appl. Catal. A* **2009,** 369, 8–14.
18. Tamao Ishida; Hiroto Watanabe; Takao Bebeko; Tomoki Akita; Masatake Haruta. *Appl. Catal. A* **2010,** 377, 42–46.

19. Agnes Mirescu; Heinz Berndt; Andreas Martin; Ulf Pru¨ße. *Appl. Catal. A* **2007,** 317, 204–209.

20. Nadine Thielecke; Mehmet Aytemir; Ulf Pru¨sse. *Catal. Today*. **2007,** 121, 115–120.

21. Agnes Mirescu; Ulf Pru¨ße. *Appl. Catal., B* **2007,** 70, 644-652.

22. Ulf Prüße; Mirko Herrmann; Christine Baatz; Nadine Decker. *Appl. Catal. A: Gen.* **2011,** 406, 89– 93.

23. Sophie Hermans; Aurore Deffernez; Michel Devillers. *Appl. Catal. A: Gen.* **2011,** 395, 19–27.

24. Massimiliano Comotti; Cristina Della Pina; Michele Rossi. *J. Mol. Catal. A: Chem.* **2006,** 251, 89–92.

25. Witon´ ska I.; Frajtak M.; Karski S. *Appl. Catal., A* **2011,** 401, 73– 82.

26. Peter J. Miedziak; Hamed Alshammari; Simon A. Kondrat; Tomos J. Clarke; Thomas E. Davies; Moataz Morad; David J. Morgan; David J. Willock; David W. Knight; Stuart H. Taylor; Graham J. Hutchings. *Green Chem.* **2014,** 16, 3132-3141.

27. Yueling Cao; Xi Liu; Sarwat Iqbal; Peter J. Miedziak; Jennifer K. Edwards; Robert D. Armstrong; David J. Morgan; Junwei Wang; Graham J. Hutchings. *Catal. Sci. Technol.* **2016,** 6, 107–117.

28. Puyu Qi; Shasha Chen; Jin Chen; Jianwei Zheng; Xinlei Zheng; Youzhu Yuan. *ACS Catal.* **2015,** 5, 2659-2670.

29. Yuran Wang; Stijn Van de Vyver; Krishna K Sharma; Yuriy Román-Leshkov. *Green Chem.* **2013,** 16, 719-726.

30. Anup Tathod; Tanushree Kane; E.S. Sanil; Paresh L. Dhepe. *J. Mol. Catal. A: Chem.* **2014,** 388–389, 90–99.

31. Sari Rautiainen; Petra Lehtinen; Marko Vehkamäki; Klaus Niemelä; Marianna Kemell; Mikko Heikkilä; Timo Repo. *Catal. Commun.* **2016,** 74, 115–118.

32. Megías-Sayago C.; Ivanova S.; López-Cartes C.; Centeno M.A.; Odriozola J.A. *Catal. Today* **2017,** 279, (148–154).

33. Mathias Ibert; Francis Marsais; Nabyl Merbouh; Christian Bruckner. *Carbohydr. Res.* **2002,** 377, 1059–1063.

34. Grigor'eva I. A.; Chernaya S. S.; Trusov S. R. *Russ. J. Appl. Chem.* **2001,** 74, 2021–2026.

35. Nabyl Merbouh; Jean Francois Thaburet; Mathias Ibert; Francis Marsais; James M. Bobbitt. *Carbohydr. Res.* **2001,** 336, 75–78.

36. Tyler N. Smith; Kirk Hash; Cara-Lee Davey; Heidi Mills; Holly Williams; Donald E. Kiely. *Carbohydr. Res.* **2012,** 350, 6–13.

37. Jacques M. H. Dirkx; Hessel S. Van Der Baan; Jan M. A. J. J. Van Den Broek. *Carbohydr. Res.* **1977,** 59, 63-72.

38. Deshan Bin; Hong Wang; Jianxin Li; Hui Wang; Zhen Yin; Jianli Kang; Benqiao He; Zhenhuan Li. *Electrochim. Acta* **2014,** 130, 170–178.

39. Mathias Ibert; Patrick Fuertès; Nabyl Merbouh; Catherine Fiol-Petit; Christian Feasson; Francis Marsais. *Electrochim. Acta* **2010,** 55, 3589–3594.

40. Mathias Ibert; Patrick Fuertès; Nabyl Merbouh; Christian Feasson; Francis Marsais. *Carbohydr. Res.* **2011,** 346, 512–518.

41. Xin Jin; Meng Zhao; Muzzammil Vora; Jian Shen; Chun Zeng; Wenjuan Yan; Prem S. Thapa; Bala Subramaniam; Raghunath V. Chaudhari. *Ind. Eng. Chem. Res.* **2016,** 55, 2932−2945.

42. Thomas R. Boussie; Eric L. Dias; Zachary M. Fresco; Vincent J. Murphy; James Shoemaker; Raymon Archer; Hong Jiang. Dec. 16, 2010, 2010.

43. Vincent J. Murphy; james Shoemaker; Guazg Zhu; Raymon Archer; George Frederick Salem; Dias E. L. Dec. 15, 2011, 2011.

44. Jechan Lee; Basudeb Saha; Dionisios G. *Green Chem.* **2016,** 18, 3815–3822.

45. Jian L.; Qiuhua Z.; Aimin H.; Oscar G.; Steven L. S. *Inorg. Chem.* **1999,** 38, 6106-6113.

46. Shannon R. D. *Acta Cryst. A* **1976,** 32, 751-767.

47. Zheng-Rong T.; Yuan-Gen Y.; Steven L. S. *Chem. Mater.* **1997,** 9, 1126-1133.

48. Shannon R. D. *Acta Cryst.* **1976,** A32, 751–767.

49. Shen Y. F.; Suib S. L.; Young C. L. *J. Am. Chem. Soc.* **1994,** 116.

50. Romero-Sarria; Penkova A.; Martinez L. M.; Centeno T. M. A.; Hadjiivanov K.; Odriozola. J. A., *Appl. Catal., B* **2008,** 84.

51. Chen H. T.; Chang J. G.; Chen H. L.; Ju S. P. *J. Comput. Chem* **2009,** 30.

52. Darrah Thomas T.; Weightman P. *Phys. Rev. B* **1986,** 33, 5406–5413.

53. Haijun Zhanga; Naoki Toshima. *Catal. Sci. Technol.* **2013,** 3, 268-278.

54. Jothiramalingam R.; Viswanathan B.; Varadarajan T., *J. Mol. Catal. A: Chem.* **2006,** 252.

55. Nohman A.; Ismail H.; Hussein G., *J. Anal. Appl. Pyrol.* **1995,** 34.

Chapter 6

Summary and Conclusions

6.1. Summary and Conclusions

The present thesis reports development of various catalysts and process conditions for partial oxidation of petroleum and biomass derived molecules to industrially valuable chemical intermediates. The thesis is divided into 6 chapters which includes a chapter on summarization of the work carried out for this dissertation.

Chapter 1 gives a brief introduction to the significance of sustainable development, petroleum and biomass-derived feedstock for the synthesis of fuels and chemicals. Brief information is provided on renewable and non-renewable sources for manufacture of chemical intermediates and the utility of those materials. First part of the chapter deals with partial oxidation of petroleum derivatives to value added chemicals such as selective oxidation of PX PTA, followed by oxidation of BzOH to BzH. Subsequently, an introduction to the partial oxidation biomass derived glucose is given. Glucose is one of the main feedstock molecule from which many valuable chemicals can be obtained. In addition, sources of industrially important oxidized products like PTA, BzH, GA and GCA is highlighted. Some of the catalytic oxidations processes, oxidants used at industrial scale were discussed briefly. A detailed description of a variety of catalyst supports such as porous metal oxides, carbon materials, nitrogen-doped carbons, carbon nitrides and metal oxides is also discussed. Finally, the objectives of the thesis are outlined briefly.

Chapter 2 describes the catalyst preparation methods and experimental techniques used for their characterization. Preparation procedure of CNNT catalysts, prepared at different sintering temperatures is given in detail. In addition, preparation procedures of manganese oxides and different hetero metal doped manganese oxides are described. Some of these oxides were prepared by co-precipitation method. Microporous manganese oxides (Mg-OMS-1 and K-OMS-2) are prepared by hydrothermal methods. Precious metals were deposited on to these Mg-OMS-1 and K-OMS-2 supports. The second half of the chapter deals with were characterization of catalyst materials using various physico-chemical techniques including XRD, N_2 sorption, SEM, TEM, solid state NMR, XPS, TPD of O_2, NH_3 and CO_2, TPR in H_2, ICP-OES, *etc*. Theory and experimental procedures of each of these techniques is outlined in this chapter.

Chapter 3 starts with detailed introduction and a literature review on the conversion of PX to PTA, followed by the present work on development of alternate catalysts for production of

PTA. This reaction is carried out in batch mode using CNNT catalysts in presence of molecular O_2. Results of characterization of catalysts using XRD, TGA, UV-DRS, FTIR, XPS, SEM and NMR to study their structure, textural properties and morphology are discussed. The results obtained by using NMR and XPS are discussed in detail to for characterization of various types of nitrogen present in CNNT. The catalytic activity in PX oxidation using different CNNT samples and optimization of reaction conditions is also given in this part.

The present study shows that CNNT can be prepared at lower temperatures (~350 °C). But, with increasing temperature, CNNT formed undergoes structural change which does not help in its performance as catalyst. The structural change is attributed to the type of nitrogen present. With increasing CNNT formation temperature, the basic monomer units changed from s-triazine ring to tri-s-triazine rings. The presence of s-triazine ring as building block with a tubular morphology in the catalyst was crucial in achieving superior catalytic activity. Under the optimized reaction conditions, 49.1 mol% PTA yield at 93.5 mol% PX conversion was obtained after 18 h. The use of initiator (NHPI) enhanced the activity of the catalyst and no 4-CBA impurity was observed in the product. Use of 10 mol% NHPI initiator led to PX conversion of 92.3 mol% with 73.9 mol% of PTA yield. This catalyst was recyclable without any noticeable loss in activity. Used initiator can always be recovered and reused for large scale applications. This novel catalytic system can be translated to develop a large scale petrochemical process, as it used a metal free catalyst. Similarly, this process does not use any corrosive solvent like acetic acid.

Chapter 4 describes synthesis and characterization results of manganese oxides and Mn_3O_4 spinel type oxides, doped with Cu and Co cations. These oxides were characterized using XRD, N_2 sorption, XPS, NH_3-TPD, CO_2-TPD, O_2-TPD, *etc*. Subsequently, it describes catalytic activity of these catalysts in partial oxidation of BzOH to BzH.

Continuous fixed bed flow reaction was carried out for achieving selective oxidation of BzOH to get BzH over different manganese oxides. Among the manganese oxides, Mn_3O_4 was found to be highly active to give good BzH yields. However, its activity dropped over a period of time. Hence, performance of Mn_3O_4, doped with Co and Cu cations was studied. Among these, copper doped catalyst ($Cu_{0.25}Mn_{2.75}O_4$) was found to be most active. During the reaction, presence of copper plays vital role in the stabilization of activity while being highly selective to BzH. Formation of over oxidation products like benzoic acid, benzyl ether are found to be

responsible for the rapid deactivation of the catalyst. The presence of copper in optimum concentration ($Cu_{0.25}Mn_{2.75}O_4$), helps in desorption of the products formed in the form of esters. Under optimized reaction conditions, $Cu_{0.25}Mn_{2.75}O_4$ catalyst gave 84.5% BzOH conversion and 98.0% selectivity to BzH. The long term stability was checked with this catalyst, by evaluating it time on stream (TOS) for 24 h at WHSV-10 h^{-1}. The characterization results were correlated with the catalytic performance at the end of the chapter.

Chapter 5 begins with introduction and detailed literature review on the oxidation of glucose to GCA in a two step process. The present work focused on the partial oxidation of glucose to GA and subsequent step of GA to GCA over supported metal catalysts using molecular O_2. This chapter is divided into two parts. Part 5A deals with partial oxidation of glucose to GA. This part contains discussion on characterization of supported Au catalysts using XRD, N_2 sorption, SEM, TEM and XPS, *etc*. The catalytic activity in selective oxidation of glucose to GA is also discussed in this part. Part 5B deals with partial oxidation of GA to GCA using metal oxide supported Pt catalysts. The characterization of Pt catalysts was carried out using various physico-chemical techniques. It also describes the catalytic activity of these catalysts in the conversion of GA to GCA.

Catalyst 2wt% Au/Mg-OMS-1 shows very good activity and high GA selectivity (94%) under mild reaction conditions (70 °C, 5 bar O_2). The observed high catalytic activity and selectivity were attributed to basic support on which catalytically active nanoparticles of Au are dispersed. Instead of Mg-OMS-1, if K-OMS-2 or H-OMS-2 supports are used, the catalysts are not that active. This decrease in the activity is related to the basic metal constituting the support. These studies reveal that the presence of a basic metal on the support is necessary for the better activity. The 2wt% Au/Mg-OMS-1 could be recycled many a times, without any loss in activity or GA selectivity.

Part 5B deals with discussion on Pt on K-OMS-2, used for the partial oxidation of GA to GCA. Catalyst 2wt% Pt/K-OMS-2 displayed superior activity and good GCA selectivity (53.6%) and yield (20.6%). It was observed that the basicity of K-OMS-2 and the structural morphology play a crucial role for getting good activity by facilitating the adsorption of GA and thereby leading to good catalytic activity and GCA selectivity.

It is mandatory at the end of all chapters in a dissertation to summarize the research work undertaken for the advantage of the reader. Therefore, this chapter summarizes the conclusions reached based on the experimental results during these investigations. Initially it describes the content of each chapter in detail with outline of results at the end. This section also offers some suggestions for further research work in given areas and scope of their translation into industrial applications.

6.2. Suggestions for future research

The aim of the present investigation is to develop processes which are environmental friendly in partial oxidation of hydrocarbons and biomass derived compounds. Hence, this thesis dealt with the preparation and characterization of heterogeneous catalysts that are useful for green oxidation reactions. In order to commercialize any hydrocarbon oxidation process, achieving maximum yield of the desired product is an important criterion. It should also be accomplished in an environmentally benign way.

It is also important to convert the above discussed catalytic processes into commercially viable ones by scaling up to the desirable levels. Currently, chemical industry is keen to practice green processes that have no environmental impact, preferably using renewable raw materials. At the same time, the process should be low cost and inexpensive to establish a new plant or to convert the existing plant. In the commercial heterogeneous catalyst based processes, leaching of metal from the catalyst is a major drawback for the longevity of the catalyst life. Also, one should keep in mind about the elemental sustainability. Present industrial process for the oxidation of hydrocarbons (p-xylene) utilizes homogeneous metal catalyst, acetic acid as solvent and an inorganic initiator. Acetic acid is corrosive and inorganic generates by-product which is not environment friendly. The process also produces impurities which have to be separated for utilization of the product. Moreover, these processes constitute multiple steps. Because of the high industrial growth, majority of elements of the periodic table, which act a catalysts are depleting. Hence, it is highly desirable to design a metal free catalyst for various catalytic applications. For the present thesis, a metal free carbon nitride nanotube catalyst (CNNT) was prepared and applied for selective oxidation of p-xylene. The advantages of this catalyst is that it does not contain any metal, hence no problem of leaching during the reaction. These catalysts are sustainable, recyclable and inexpensive. These CNNT catalysts can successfully overcome the

disadvantages of present industrial process because there is no usage of metals, corrosive solvents, and single step process. Because of the above advantages, the CNNT catalysts can replace the present existing industrial catalysts. Hence, more work need to be carried out to use these catalysts for improving their activity and selectivity in partial oxidation of hydrocarbons.

The selective oxidation of benzyl alcohol to benzaldehyde under continuous process conditions is very important, as product benzaldehyde has a variety of commercial uses. Though the developed catalyst was tested for long duration of 24 h, it has to be monitored for much longer as in a commercial reactor it has to be stable for thousands of hours. Then only this process can be scaled up to a pilot plant level. Since, the catalyst used was spinel type mixed oxide without any precious metal, it should be further explored. These catalysts will be easy to prepare, inexpensive and the key metals required to prepare these catalysts are abundant. In addition, there are great opportunities to test different kinds of hydrocarbon oxidations with these catalysts.

Researchers are focusing on technologies that can facilitate the conversion of renewable biomass into fuels and chemicals, due to its easy availability and distribution. Utilization of biomass to make chemicals can be regarded as best alternative for producing chemicals in a sustainable manner. Oxidative transformation of biomass to chemicals (corresponding acids) is a major pathway to produce renewable chemicals. However a major drawback in the reported biomass oxidations is the use of high equivalents of external base, which makes the process not so environmentally benign. Hence it is highly recommended to design and develop processes that do not require addition of a base. Gold exchanged Mg-OMS-1 bifunctional catalyst was designed and base free oxidations of glucose to gluconic acid were conducted. Platinum exchanged K-OMS-2 bifunctional catalyst was designed and base free oxidations of gluconic acid to glucaric acid were carried out. These experiments demonstrated high yield of corresponding acids even in the absence of external base as the support contains Mg which acts as base. The catalysts were found to be recyclable. We believe metal exchanged OMS catalyst could be tested for many other biomass oxidations like glycerol and other hexoses. This work is progressing well presently in the group.

By and large, this study advances the knowledge on the oxidative conversion of hydrocarbons and biomass components to value added chemicals. It describes an eco-friendly, sustainable and green methodology by means of using heterogeneous catalysts and greener

oxidants (oxygen) for the conversion of hydrocarbons and biomass. Although, more research and process optimization is still needed, this study on designing green process is a huge step forward towards establishing sustainable chemical processes. The processes involving these catalysts will surely find industrial application in the very foreseeable future.

PUBLICATIONS

1. Hydrogenation of Cinnamaldehyde to Hydrocinnamaldehyde over Pd nanoparticles deposited on nitrogen-doped mesoporous carbon.
*Atul S. Nagpure, **Lakshmiprasad Gurrala**, Pranjal Gogoi and Satyanarayana Chilukuri*
RSC Advances, (2016), 6, 44333-44340.

2. Spinel based mixed oxides for improved benzaldehyde selectivity and stable activity in partial oxidation of benzyl alcohol
Lakshmiprasad Gurrala, Atul Nagpure and Satyanarayana V. Chilukuri.
Communicated.

3. Base free selective oxidation of glucose to gluconic acid on octahedral molecular sieve supported catalysts.
Lakshmiprasad Gurrala, Dherendra singh and Satyanarayana V. Chilukuri.
Communicated.

4. A metal-free catalyst for selective oxidation of SP^3 C-H activation of p-xylene to yield terephthalic acid.
Lakshmiprasad Gurrala, Venkatesh Piradi, Narasimha Rao Kanna and Satyanarayana V. Chilukuri.
To be communicated,

PATENT APPLICATIONS

1. Oxidation catalyst, the process for the preparation thereof and green process selective aerobic oxidation.
C. V. V. Satayanarayana, Narasimharao Kanna, Ganesh Dattatreya Kokate, ***Lakshmiprasad Gurrala.***
US 9302255 B2.

2. Selective aerobic oxidations using carbon nitride nanotubes.
C. V. V. Satayanarayana, Narasimharao Kanna, ***Lakshmiprasad Gurrala*****.**
WO2015083185 A1.

3. A Novel Metal free Catalyst for Selective Oxidation of Hydrocarbons.
C. V. V. Satayanarayana, Narasimharao Kanna, ***Lakshmiprasad Gurrala***.
IN. patent application no: 3490/DEL/2013, filing date 27/11/2014.